UNIVERSITY OF COPENHAGEN
FACULTY OF SCIENCE

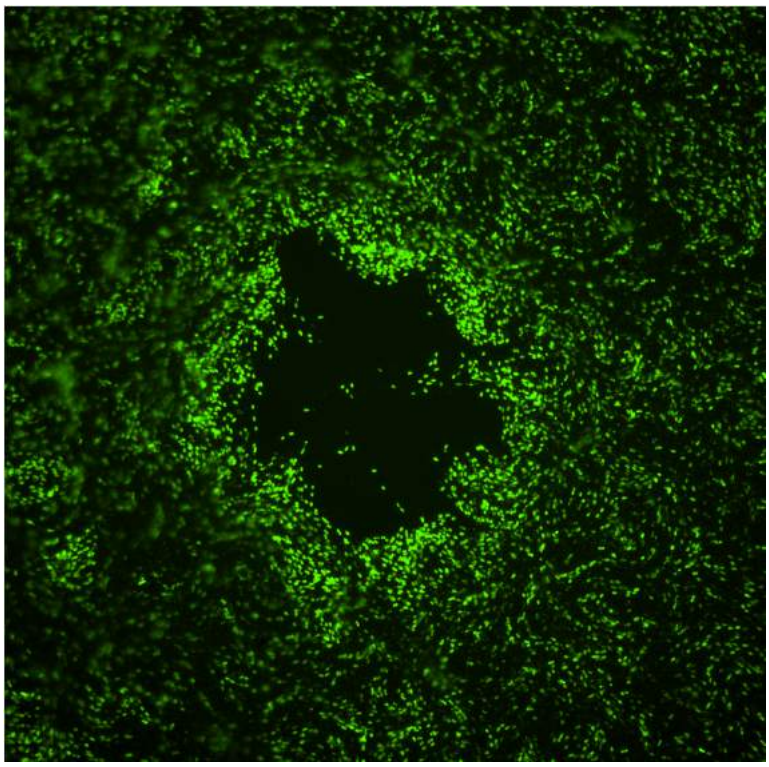

Ph.D. thesis

Population dynamics of phage-bacteria ecosystems under challenging conditions

Anastasios Marantos

Advisor: Prof. Kim Sneppen

Submission Date: October 13, 2023

This thesis has been submitted to the PhD School of The Faculty of Science, University of Copenhagen

To Litsa, Yannis, Orestis and Stavroula.
The 4 pillars of my life.

Ithaka

BY C. P. CAVAFY
TRANSLATED BY EDMUND KEELEY

As you set out for Ithaka
hope your road is a long one,
full of adventure, full of discovery.
Laistrygonians, Cyclops,
angry Poseidon—don't be afraid of them:
you'll never find things like that on your way
as long as you keep your thoughts raised high,
as long as a rare excitement
stirs your spirit and your body.
Laistrygonians, Cyclops,
wild Poseidon—you won't encounter them
unless you bring them along inside your soul,
unless your soul sets them up in front of you.
Hope your road is a long one.
May there be many summer mornings when,
with what pleasure, what joy,
you enter harbors you're seeing for the first time;
may you stop at Phoenician trading stations
to buy fine things,
mother of pearl and coral, amber and ebony,
sensual perfume of every kind—
as many sensual perfumes as you can;
and may you visit many Egyptian cities
to learn and go on learning from their scholars.

Keep Ithaka always in your mind.
Arriving there is what you're destined for.
But don't hurry the journey at all.
Better if it lasts for years,
so you're old by the time you reach the island,
wealthy with all you've gained on the way,
not expecting Ithaka to make you rich.
Ithaka gave you the marvelous journey.
Without her you wouldn't have set out.
She has nothing left to give you now.
And if you find her poor, Ithaka won't have fooled you.
Wise as you will have become, so full of experience,
you'll have understood by then what these Ithakas mean.

Abstract

Bacteria and their viruses, bacteriophages (or phages), are arguably the most representative biological organisms on planet Earth. Apart from being amongst the most ancient entities, they are unparalleled in sheer numbers, biomass, and diversity. Ubiquitous in nature, their interactions profoundly affect their environments and, consequently, humans. This thesis offers a study into the ecosystems of this host-parasite pair, focusing on population dynamics.

Laboratory studies of phage-bacteria dynamics predominantly operate under optimal conditions. However, in nature, phages and bacteria often face suboptimal conditions, ranging from limited resources to intense pressure from competition or predation. This thesis delves into phage-bacteria ecosystems under such challenging conditions, employing a spectrum of scientific methodologies. These methodologies range from data-driven theoretical analysis and collaborative work with experimentalists to purely experimental research.

Chapter 1 introduces the foundational terms and ideas necessary for a reader to navigate this work. Chapter 2 dives deep into the dynamics between phages and bacteria in the ocean's upper layers. Through a theoretical modeling approach, it elucidates mechanisms that can sustain diversity under intense competition for resources. Additionally, this chapter deciphers the underlying dynamics of infection patterns observed in previous field studies. Our research reveals patterns of network self-organization that promote specialization, thereby reducing competition between strains. Notably, even slight deviations from perfect specialization can profoundly benefit slower-growing bacteria. These bacteria, although growing at a reduced rate, can outcompete and potentially eliminate even the fastest-growing strains, through shared phage interactions. Our results challenge the notion of using growth rate as a definitive metric for fitness, hinting instead at an evolutionary process that proceeds in waves.

Chapter 3 delves into the phenomenon of bacterial dormancy, particularly under suboptimal conditions for growth and pressure from viruses. This work combines both experimental and theoretical methods to study sporulation in *Bacillus Subtilis*, which serves as a model for dormancy in Gram-positive bacteria. Apart from the widely accepted starvation-trigger for sporulation, this chapter reveals that the presence of viruses can also induce sporulation. Our findings suggest that susceptible cells can turn into dormant as a response to a molecular signal released upon cell lysis. In spatial environments, this leads to a collective defense in *Bacillus Subtilis* communities, which helps contain the spread of the viruses. This work is the first to document virally induced sporulation in *Bacillus Subtilis* and its significant role in offering protection at the population level by restricting the spread of viral infections.

Chapter 4 is devoted to a purely experimental study of how a host's metabolic state affects phage infection. Initial results resonate with previous findings, suggesting that phages might be selective, choosing not to infect *Escherichia coli* cells in a low metabolic state—an often characteristic state of cells facing challenging environmental conditions in nature. The primary goal of

this research is to assess the prevalence of this behavior across various phage-bacteria systems.

In summary, this thesis underscores that suboptimal conditions commonly found in natural systems can profoundly influence phage-bacteria dynamics.

Dansk Resumé

Bakterier og deres vira, bakteriofager (eller fager i kort form), er sandsynligvis de mest repræsentative biologiske organismer på planeten Jorden. Som nogle af de ældste enheder dominerer de i ren antal, biomasse og diversitet. Allestedsnærværende i naturen påvirker deres interaktioner dybt deres miljøer og, som en konsekvens, mennesker. Denne afhandling tilbyder en undersøgelse af økosystemerne af dette vært-parasitpar med fokus på befolkningsdynamik.

Laboratoriestudier af fage-bakteriedynamik opererer overvejende under optimale forhold. I naturen står fager og bakterier dog ofte over for suboptimale forhold, der spænder fra begrænsede ressourcer til intens konkurrence- eller rovdyrstryk. Denne afhandling går dybt ind i fage-bakterie økosystemer under sådanne udfordrende forhold og bruger et spektrum af videnskabelige metoder. Disse metoder spænder fra datadrevet teoretisk analyse og samarbejde med eksperimentatorer til rent eksperimentelle bestræbelser.

Kapitel 1 introducerer de grundlæggende termer og ideer, der er nødvendige for en læser for at navigere i dette arbejde. Kapitel 2 undersøger dybt dynamikken mellem fager og bakterier i havets øverste lag. Gennem en teoretisk modelleringsmetode belyser den mekanismer, der kan bevare diversitet under intens konkurrence om ressourcer. Desuden afkoder dette kapitel den underliggende dynamik i infektionsmønstre observeret i tidligere feltstudier. Vores forskning afslører netværks selvorganisationsmønstre, der fremmer specialisering, og dermed reducerer konkurrence mellem stammer. Bemærkelsesværdigt er, at selv små afvigelser fra perfekt specialisering kan drage stor fordel af langsommere voksende bakterier. Disse bakterier, selvom de vokser med en reduceret hastighed, kan udkonkurrere og potentielt eliminere selv de hurtigst voksende stammer gennem delte fage interaktioner. Vores resultater udfordrer forestillingen om at bruge vækshastighed som en afgørende målestok for fitness, antyder i stedet en evolutionær proces, der skrider frem i bølger.

Kapitel 3 går dybt ind i fænomenet bakteriedvalitet, især under suboptimale vækstforhold og tryk fra vira. Dette arbejde kombinerer både eksperimentelle og teoretiske metoder for at studere sporulering i *Bacillus Subtilis*, hvilket tjener som en model for dvale i gram-positive bakterier. Bortset fra den almindeligt accepterede sultudløser for sporulering afslører dette kapitel, at tilstedeværelsen af vira også kan inducere sporulering. Vores resultater tyder på, at modtagelige celler kan blive dvale som et svar på et molekylært signal frigivet ved cellelysis. I rumlige miljøer fører dette til et kollektivt forsvar i *Bacillus Subtilis* samfund, hvilket hjælper med at indeholde spredningen af vira. Dette arbejde er det første til at dokumentere viralt induceret sporulering i *Bacillus Subtilis* og dens betydelige rolle i at tilbyde beskyttelse på befolkningsniveau ved at begrænse spredningen af virale infektioner.

Kapitel 4 er viet til et rent eksperimentelt studie af, hvordan en værts metaboliske tilstand påvirker fageinfektion. Indledende resultater genlyder med tidligere fund, hvilket antyder, at fager kan være selektive og vælge ikke at inficere Escherichia coli-celler i en lav metabolisk tilstand - en ofte karakteristisk tilstand af celler, der står over for udfordrende miljøforhold i naturen.

Hovedmålet med denne forskning er at vurdere udbredelsen af denne adfærd på tværs af forskellige fage-bakteriesystemer.

Sammenfattende understreger denne afhandling, at suboptimale forhold, som ofte findes i naturlige systemer, kan have en dybtgående indvirkning på fage-bakteriedynamikker.

Acknowledgements

There is a list of people that I wish to thank for their contribution to my PhD journey:

Kim Sneppen: First and foremost I want to thank my mentor and principal supervisor Kim Sneppen. I don't think I can count the amount of times that me and my good friend and former colleague Jan Fabio have discussed how lucky we are to have Kim as a supervisor. His qualities both on an academic and on a personal level were the main reason that made my PhD experience exceed my highest expectations. I will be forever grateful to him for his support and compassion, for urging me to play and for helping me unlock my creativity.

Namiko Mitarai: It has been a privilege to be co-supervised by Namiko Mitarai. She is not just a great scientist, but also a really well-rounded person, a combination that I aspire to. I am thankful for her guidance during my PhD studies.

Stanley Brown: It is rare to meet a person as helpful and selfless as Stanley Brown. The past eight months that I have been working with Stanley in the lab I've gained a wealth of knowledge in microbiology that I will cherish forever. I want to wholeheartedly thank him for his sincere interest and for being so patient with me in the lab.

Joshua Weitz: I visited Joshua Weitz's lab in Georgia Tech, Atlanta, US for four months during the last year of my PhD and I have been working under his supervision since, on a project that ended up being a major part of my thesis. I would like to thank him for his hospitality, his guidance and for making me feel like part of his group since day one.

Jacopo Marchi: Jacopo has had every role possible during my stay at Georgia Tech. Co-supervisor, collaborator, office-mate, friend. I want to thank him for everything.

Andreea Măgălie: Andreea has been one of my closest collaborators during the past year. I grew a lot during this collaboration both on an academic and on a personal level and I want to sincerely thank her for that and for the nice times during my stay in Atlanta.

Jay Lennon and Daniel Schwartz: For the stimulating discussions and their guidance and feedback during our collaboration over the last year of my studies.

Frede Thingstad, Sandeep Krishna and Ala Trusina: I would like to thank Frede Thingstad, Sandeep Krishna and Ala Trusina for accepting to being part of my thesis defence committee. It is a great honor since their work has been very influential to mine.

Jan Fabio Nickels: My PhD started with Jan Fabio as my office-mate and finished with him as one of my closest friends and collaborators. Our countless, endless discussions on any possible topic has been among the most precious parts of my PhD experience. I want to thank him for his support and friendship through these years.

Alessandra Lucchetti: Alessandra and I started our PhD program on the exact same day. We've been together through that and I will always be grateful for her support and friendship.

The Biocomplexity group: I want to thank everyone in the Biocomplexity group for creating such an amazing working environment. Sharing time and space with you, seeing how you

work, think and behave has been the most transforming experience of my PhD program. I want to especially thank **Bente Markussen** for everything she has done for the group and for me personally during my studies. Also I want to thank **Mogens Jensen** who is the father of this group, for his support on multiple levels and for everything that he taught me during my time as a teaching assistant in his Dynamical Systems course. Finally I wish to thank my colleagues **Julius Bier Kirkegaard, Bjarke Frost Nielsen, Mathias Heltberg, Andreas Eilersen, Gustav Halvorsen, Mikkel Skjoldan Svenningsen, Yusuke Himeoka, Thuan Pham, Rasmus Skytte Eriksen** and **Xiaochan Xu** for being the greatest source of inspiration I could have asked for.

The Weitz lab: For making me feel part of the group from the first day and for wanting to give me the best experience possible during my stay in the US. I want to especially thank **Gabi Steinback** for everything that she did for me to make this visit possible and **Tapan Goel** for our stimulating discussions, for his advice and support during these past few months and for being a real friend.

The CREW: My closest friends. I want to thank them from the depth of my heart for being next to me even when we are far from each other. I wish to especially thank my best friend **Angelos Spyropoulos** for his help on every aspect of my life during the last period of my PhD.

Extended circle of family and friends: For their love and support and for making my life more beautiful during this period.

My 4 closest people: My partner, **Stavroula Menenakou**, my brother **Orestis Marantos** and my parents **Ioannis Marantos** and **Garyfalia Konstantopoulou** have been on my side on every single day and on every single aspect of this journey. There are no words in my vocabulary to express my gratitude. This work is dedicated to them.

Table of content

1 Introduction

1.1 Bacteria and bacteriophages

This thesis has two "heroes": **bacteria** and **bacteriophages**. **Bacteria** are prokaryotic unicellular organisms, which means they lack a defined nucleus and other membrane-bound organelles that are typically found in eukaryotic cells (e.g. mitochondria and chloroplasts) [1]. Bacteria comprise one of the two main subdomains of Prokaryotes (the other being Archaea) [2]. Central to their anatomy (see Figure 1) is the cytoplasmic membrane, a phospholipid barrier that encloses the cell's contents and regulates the passage of substances [1, 3]. Within this membrane lies the cytoplasm, a mixture of macromolecules (like proteins, lipids, nucleic acids, and polysaccharides), small organic molecules (primarily the building blocks for macromolecules), ribosomes, which are responsible for protein synthesis, and the bacterial genetic material [3]. The genetic material, typically a circular chromosome, is situated in an irregularly shaped area of aggregated DNA, RNA and proteins known as the nucleoid [4].

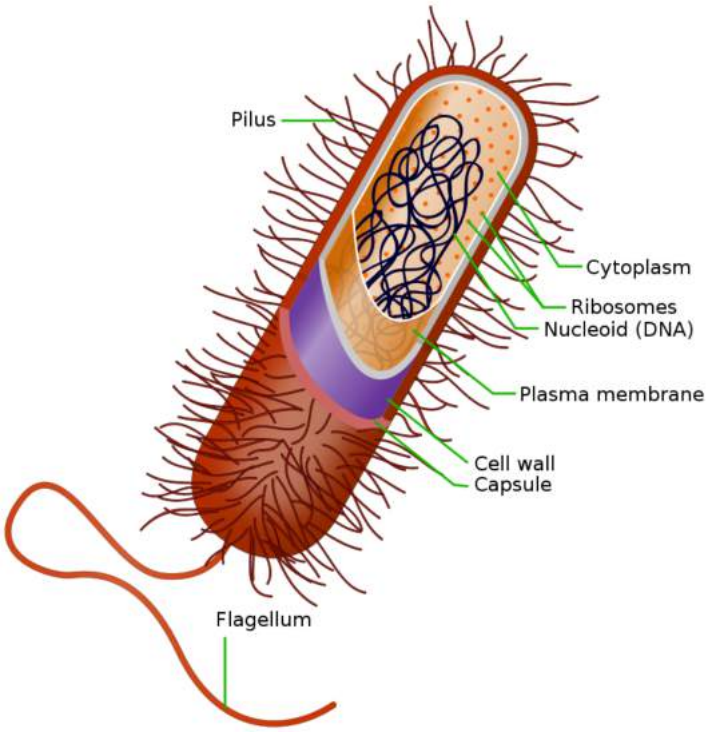

Figure 1: **Schematic representation of bacterial anatomy.** The illustration showcases the basic morphological features of bacteria. It should be noted that not all bacteria possess all of these features. (Adapted from the Wikipedia page on "bacteria" and credited to Ali Zifan).

Apart from these features that are common to all bacteria, a cell can also contain plasmids, small circular DNA fragments separate from the main chromosome, often carrying genes that confer unique abilities, like antibiotic resistance [5]. Furthermore, many bacteria feature structures like flagella for movement, and pili or fimbriae for attachment and interaction with their environ-

ment [6, 7, 8, 9]. Most bacterial cells possess a rigid cell wall which provides structural strength and prevents the cell from bursting due to osmotic pressure. This cell wall, primarily made of peptidoglycan, is external to the cytoplasmic membrane and is more robust than the membrane itself [1].

The structure and composition of the cell wall, particularly the amount of peptidoglycan, can differentiate bacteria into two primary categories based on the Gram stain method (see Figure 2): Gram-positive and Gram-negative [10]. Gram-positive bacteria have a cell wall that is predominantly made up of peptidoglycan, sometimes constituting as much as 90% of the wall [1]. This thick layer of peptidoglycan (or even multiple layers of peptidoglycan stacked upon one another) provides the cell with structural strength and rigidity [11, 1]. Conversely, Gram-negative bacteria possess a more intricate cell wall [1]. While they do contain peptidoglycan, it forms only a thin layer [12]. The majority of their cell wall is composed of an outer membrane, known as the lipopolysaccharide layer (LPS) [13, 14]. In the Gram stain method, cells are initially stained with crystal violet, then decolorized and counterstained with a pink stain [1, 15]. Gram-positive cells, with their thick peptidoglycan layer, retain the crystal violet dye and appear purple (see Figure 2). In contrast, gram-negative cells, due to their thinner peptidoglycan layer and outer membrane, do not retain the dye and instead take up the counterstain, resulting in a pink appearance [1, 15].

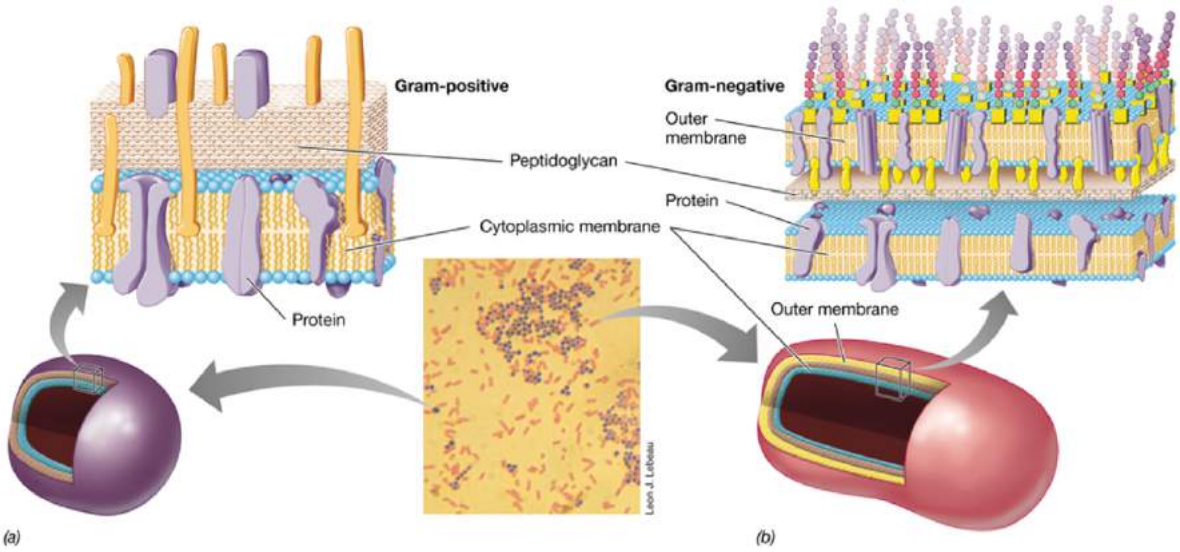

Figure 2: **The Gram stain method.** At the center of the figure, an example of the results of this fundamental microbiological method is displayed. The method classifies bacteria into two categories based on the properties of their cell walls, resulting in distinctive colors: (a) Gram-positive and (b) Gram-negative. (Adapted from [1]).

A significant characteristic of certain Gram-positive bacteria is their ability to form endospores [16, 17]. These specialized, dormant structures offer remarkable resistance to adverse environmental conditions, ensuring bacterial survival during challenging periods [18]. When conditions become favorable again, endospores can germinate and return to their active, vegetative state [16]. This characteristic is exemplified in *Bacillus subtilis*, a model organism for Gram-positive bacteria [19], and the subject of Chapter 3, which delves into its sporulation process. In contrast, the model

organism for Gram-negative bacteria is *Escherichia Coli* [1], and is the central topic of Chapter 4.

Bacterial morphological diversity is not limited to differences in cell wall structure and Gram-type classification. Bacteria exhibit great diversity in their size ranging from 0.15–0.2 μm in diameter to as much as 700 μm long [1]. They also come in a great variety of shapes [20, 21]. Bacteria can be cocci (spherical), bacilli (rod-shaped), or vibrio, which are slightly curved, resembling a comma (see Figure 3). Some bacteria adopt a spiral shape, known as spirilla, while others take on a more tightly coiled form called spirochaetes. There are even rare instances of star-shaped bacteria. Furthermore, the way bacteria arrange themselves post-division can vary. Cocci might form elongated chains, as seen in Streptococcus, or assemble in cube-like structures like Sarcina. Others, like Staphylococcus, group in grape-like clusters. Bacterial diversity is also reflected in their growth rate: the rate at which a population increases in number over time, primarily driven by their mode of reproduction, binary fission [3]. In this asexual process, a single bacterial cell duplicates its genetic material and splits into two identical daughter cells [3]. However, growth rates can vary widely among bacterial species, influenced by environmental factors and specific metabolic characteristics. Bacteria also display a vast range of metabolic capabilities [1]. For example, some bacteria are aerobic, relying on oxygen for their metabolic processes. In contrast, anaerobic bacteria thrive in environments devoid of oxygen. Facultative anaerobes are particularly versatile, capable of living in both oxygen-rich and oxygen-poor conditions, adjusting their metabolic pathways accordingly.

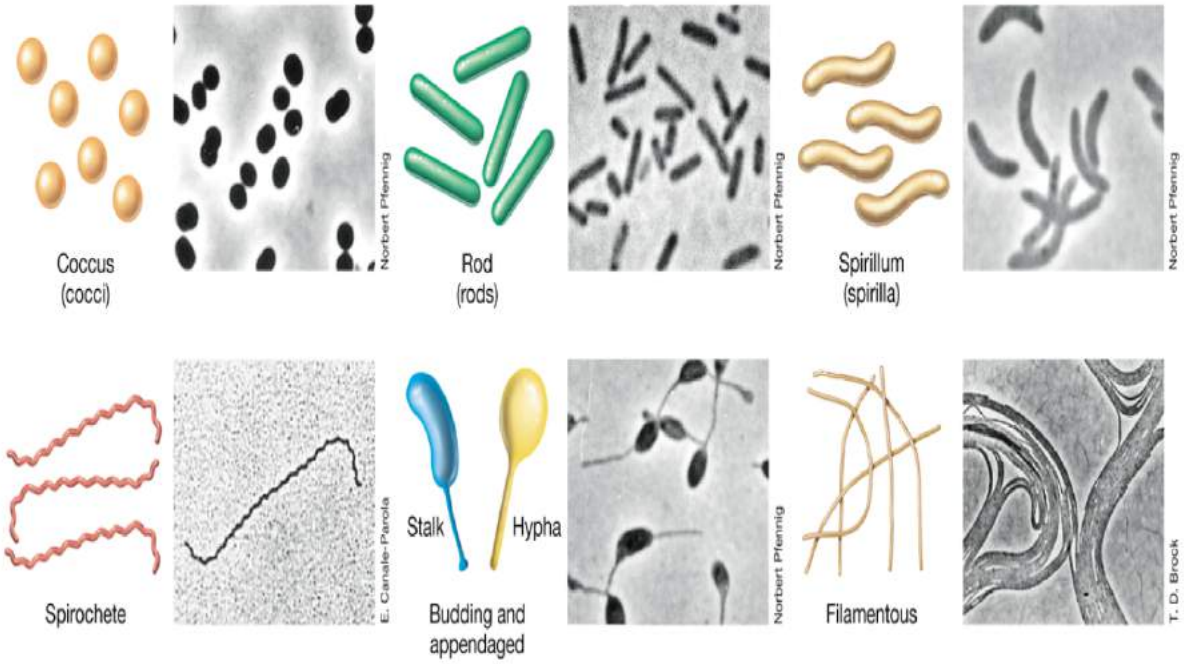

Figure 3: **Morphological diversity of bacteria.** Bacteria are among the most diverse living organisms. This figure depicts photomicrographs and drawings of the most characteristic types of bacteria. (Adapted from [1]).

Bacterial diversity, spanning their morphological, metabolic, and reproductive characteristics, is a testament to their adaptive capacities and the vast range of environments they inhabit

[22, 23, 24, 25]. This diversity is not a mere coincidence but a reflection of their genetic adaptability tailored to specific ecological niches. The field of microbial ecology, which studies microorganisms in their natural habitats, underscores the profound influence of the environment in shaping microbial characteristics [1].

Microorganisms, predominantly bacteria, are ubiquitous, populating every conceivable environment on Earth [22, 23, 24, 25]. From the deepest ocean trenches to the highest mountain peaks, from the human gut to the polar ice caps, bacteria have cemented their ubiquitous presence. Their sheer numbers are staggering, with an estimated 10^{30} microbial cells on Earth, dwarfing even the estimated 10^{22} stars in the universe [26, 1]. Not only do they constitute a significant fraction of the Earth's biomass, but they also hold vast reservoirs of essential nutrients, with their combined nitrogen and phosphorus content surpassing that of all plant and animal cells combined [1]. Such vast numbers and genetic diversity have allowed them to colonize even the most extreme environments, with extremophiles defining the physiochemical boundaries of life [22, 23, 24, 25].

This vast diversity necessitates significant time for its development. Bacteria, being among the most ancient life forms on Earth (as shown in Figure 4A), have had the luxury of this extensive timescale [27]. Originating approximately 3.5 billion years ago, while most plant and animal phyla have emerged in the last 600 million years, bacteria have had billions of years to evolve, experiment, and diversify. This prolonged evolutionary journey has enabled bacteria to not only adapt to a myriad of environments but also to profoundly influence and shape them [1]. Their pivotal role in global processes, from nutrient cycling to shaping climate patterns, highlights their enduring ecological importance [28, 29, 30, 31].

Given their omnipresence, bacteria naturally exert a profound influence on human environments and are integral to many human activities [1]. In agriculture, bacteria assist plants through symbiotic relationships, facilitating processes like nitrogen fixation, thereby reducing the reliance on synthetic fertilizers [1]. Within the rumens of animals such as cattle and sheep, microbial communities break down cellulose, allowing these animals to extract nutrients from otherwise indigestible plant matter [1]. The food industry heavily depends on bacterial fermentation, which enhances both the shelf life and flavor of products, including dairy, baked goods, and beverages [32]. Beyond food production, bacteria play central roles in pharmaceuticals and biofuel production[1, 32]. Additionally, they have a pivotal role in environmental management, notably in bioremediation, where they help cleanse environments of pollutants [33].

While the majority of bacteria are beneficial [34], some can pose threats to human health [35]. Diseases caused by pathogenic bacteria, such as tuberculosis or cholera, have historically been significant health concerns and major factors of human mortality [36] (see Figure 4B). It was, in fact, the devastating impacts of these diseases that spurred early scientific investigations into bacteria, leading to the discovery of their ubiquitous presence and diverse roles [1].

To combat pathogenic bacteria, the primary weapon in our arsenal has been antibiotics [32]. These antimicrobial agents, naturally produced by certain bacteria and fungi, target essential

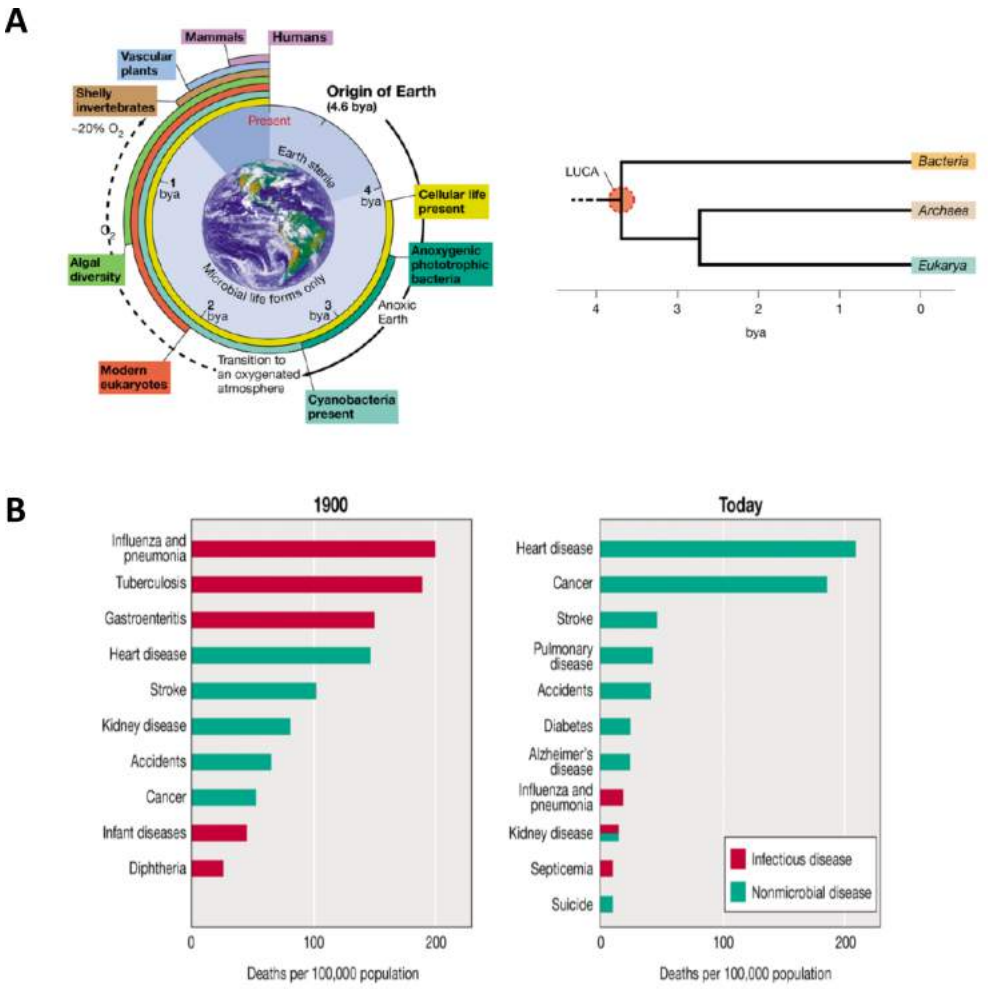

Figure 4: **The history of bacteria.** **A** Bacteria are one of the earliest life forms on Earth. The illustration in the left subpanel displays a timeline of bacterial presence on Earth compared to other life forms. The right subpanel depicts the estimated timepoints of divergence between the three domains of life on a billion-year scale. The divergence of bacteria from the Last Universal Common Ancestor (LUCA) is estimated to have happened around 3.7-3.8 billion years ago [1]. **B** Bacteria profoundly impact their environments, including humans. This diagram highlights the primary causes of death per 100,000 people in the US at the beginning of the 20th and 21st centuries. As illustrated, infectious diseases caused by pathogens were the primary cause of death in humans at the start of the 20th century. Today, thanks to advances in microbiology and medicine, this trend has reversed, significantly improving human health and longevity. (Both figures are adapted from [1]. The data in panel B come from the United States National Center for Health Statistics and the Centers for Disease Control and Prevention).

molecular processes in bacterial cells [3]. For example, antibiotics like penicillin and its derivatives specifically inhibit the synthesis of peptidoglycan, a crucial component of the bacterial cell wall [37, 1]. Due to this specificity, some antibiotics are effective only against certain bacteria; for instance, vancomycin is potent against Gram-positive bacteria but leaves Gram-negative pathogens unaffected [1]. Beyond the cell wall, other antibiotics target vital processes such as DNA replication, RNA synthesis, and protein translation [1]. The overarching strategy is to harness the weapons of one microbe against another. Historically, even before the advent of antibiotics, there was an approach that employed bacterial viruses, known as bacteriophages, to combat bacterial infections [38, 39, 40, 41].

Bacteriophages (meaning "bacteria eaters" in Greek), or simply phages, are viruses that specifically target and infect bacteria [39, 40, 41]. Viruses, including bacteriophages, are not tra-

ditionally considered living organisms because of their obligatory parasitic nature, which requires a host cell for their reproduction [42]. Given their dependence on bacteria, phages can be found in virtually every environment where bacteria exist from aquatic environments, soils and the human body, to geothermal hot springs and the acidic environments of sulfuric lakes [1].

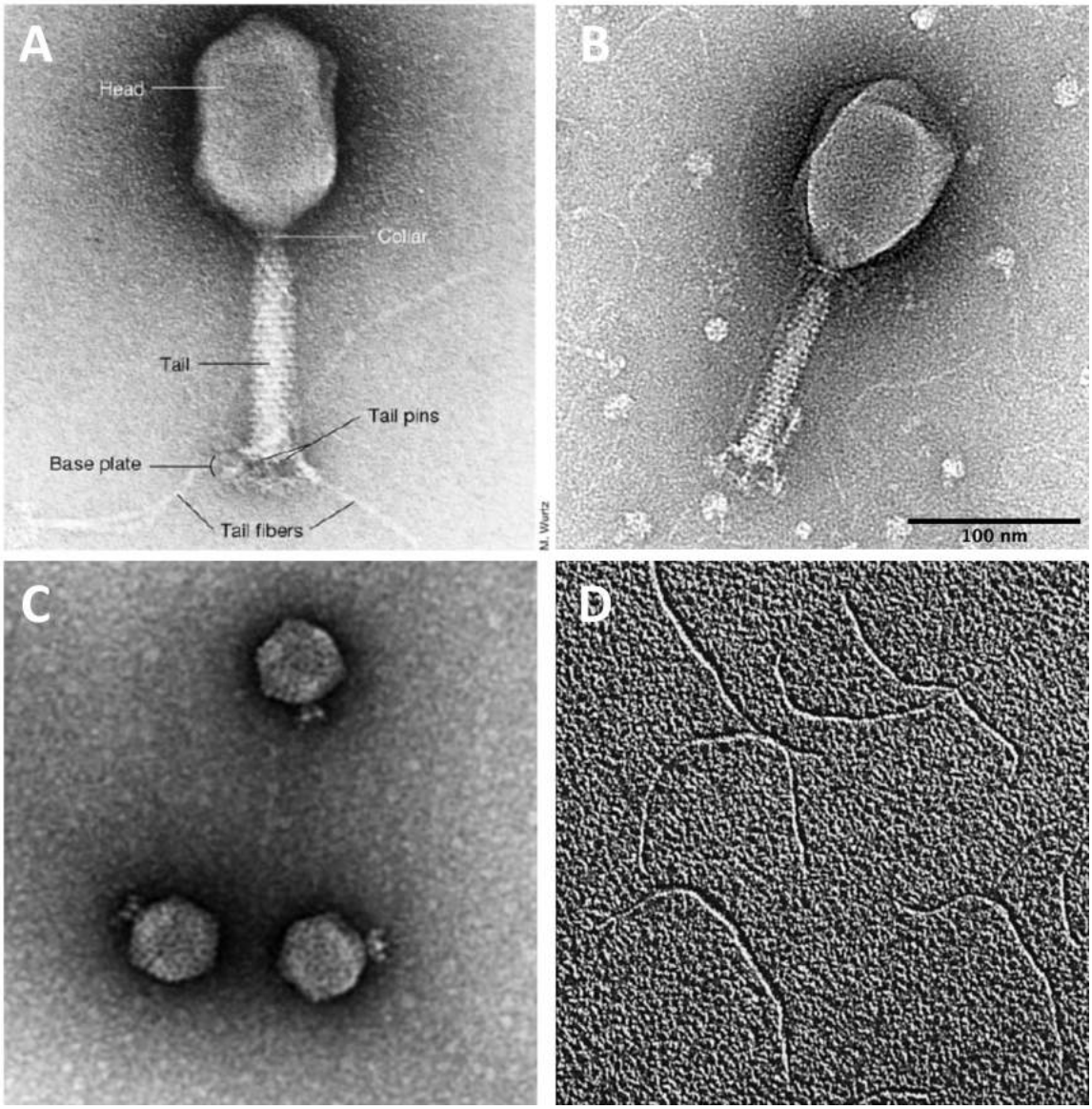

Figure 5: **Bacteriophage anatomy and morphological diversity.** Transmission electron micrographs of bacteriophages **A** T4, **B** T2, **C** P22, and **D** fd. Panel A displays the basic morphological features of a phage. Nevertheless, as panels B-D show, bacteriophages, being the most diverse organisms on Earth, do not necessarily share all of these features. (The electron micrograph of panel A is adapted from [1] and credited to M. Wurtz. The remaining electron micrographs are adapted from Wikipedia pages for "bacteriophages" and "filamentous bacteriophages", with credits to Sherwood Casjens and Elaine Lenk (panels B and C), and to Marvin and Hoffmann (panel D).)

Their ubiquity is also reflected in their staggering sheer numbers [43]. Bacteriophages are estimated to outnumber all other organisms combined, including bacteria. In many environments, phages can be found in quantities up to ten times greater than bacteria [43]. Their numbers combined with their presence across diverse habitats, contribute to their unparalleled genetic

diversity, most of which remains elusive [1]. Particularly, viral metagenomic studies, which analyze the sum total of all viral genes in a given environment, reveal that approximately 75% of the gene sequences identified have no known counterparts in existing viral or cellular gene databases. In contrast, bacterial metagenomes typically contain only about 10% of such unknown genes [1].

One of the primary indicators of this diversity is the variation in their sizes [40]. While a typical phage might range between 50 to 200 nanometers, there are instances of phages as small as 20 nanometers and jumbo phages that exceed 500 nanometers [44]. This size variation often correlates with the complexity of their genetic content, with larger phages generally possessing more extensive genomes. Morphologically, phages exhibit a wide array of structures [42, 40]. The tailed bacteriophages, characterized by their icosahedral head capsids, and their tails, are perhaps the most recognized due to their prevalence and association with well-studied bacterial species such as Escherichia coli [42, 40] (see Figure 5A). The head capsids engulf their genome (DNA or RNA) and the tails (whenever present) facilitate the attachment and injection of genetic material in the host. However, the phage world encompasses a broader spectrum of shapes, from filamentous forms to those that are more spherical or amorphous [42, 40] (see Figure 5B-D). Each morphological type, determined by evolutionary pressures, often signifies a specific mode of interaction with its bacterial host. The specificity of phages in terms of host range is another dimension of their diversity. Many phages are highly specific, targeting a single bacterial strain with remarkable precision [42, 40]. This specificity arises from the interactions between the phage and specific receptors on the bacterial surface (see Figure 6), which can range from proteins and carbohydrates to complex structures like flagella or pili [1]. However, some phages exhibit a broader host range, capable of infecting multiple bacterial strains or even different species [45]. This variability in host specificity not only impacts bacterial population dynamics but also plays a role in bacterial evolution, especially through processes like horizontal gene transfer [46, 47, 48].

Post-infection, bacteriophages exhibit complex reproductive strategies which are pivotal to the understanding of their interactions with bacterial hosts [42, 40, 46, 49]. Upon successful attachment and injection of their genetic material into a bacterial cell, phages commit to one of two primary life cycles: lytic or lysogenic [50, 51, 52, 53, 54, 55, 56, 57, 58, 59, 60, 61, 62].

In the lytic cycle (see Figure 7), the phage hijacks the host's cellular machinery to replicate its genetic material and synthesize phage-specific proteins. This process results in the assembly of new phage particles within the host cell. Eventually, the bacterial cell undergoes lysis, a process facilitated by phage-produced lytic enzymes that break down the bacterial cell wall, in a burst that releases a multitude of new phages, often referred to as progeny, that are ready to infect other susceptible bacterial cells. This cycle is typically rapid and results in the destruction of the host bacterium. In the lysogenic cycle (see Figure 7), rather than immediately replicating and producing progeny, the phage integrates its genetic material into the host's genome, becoming what is known as a prophage. In this state, the phage remains inactive, replicating in tandem with the bacterial chromosome. During lysogeny, the host, now known as a lysogen, can acquire new properties from

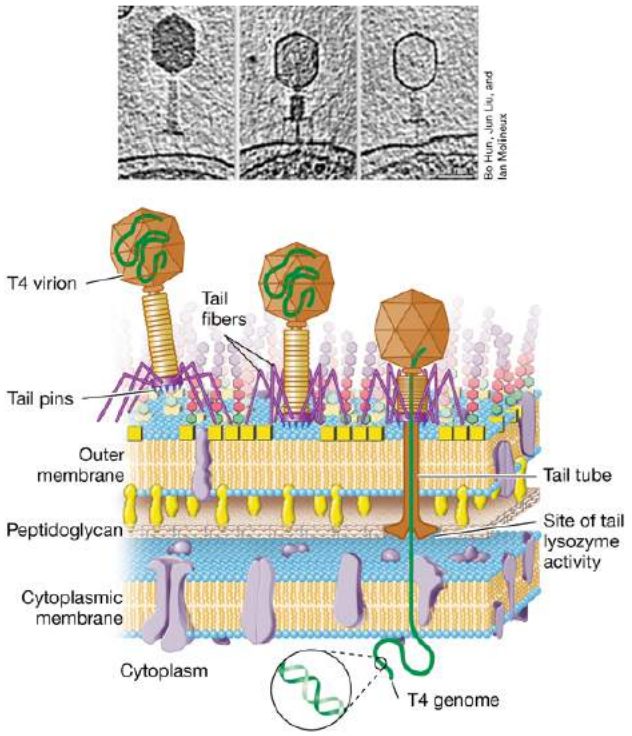

Figure 6: **Genetic material injection during phage infection.** Bacteriophages infect their bacterial host cells by binding to a surface receptor and then injecting their genetic material into the host. The details of the receptor and the injection process are highly specific to each host-parasite pair. This figure displays a top image and a bottom illustration depicting the genetic material injection process for the bacteriophage T4. (Adapted from [1]).

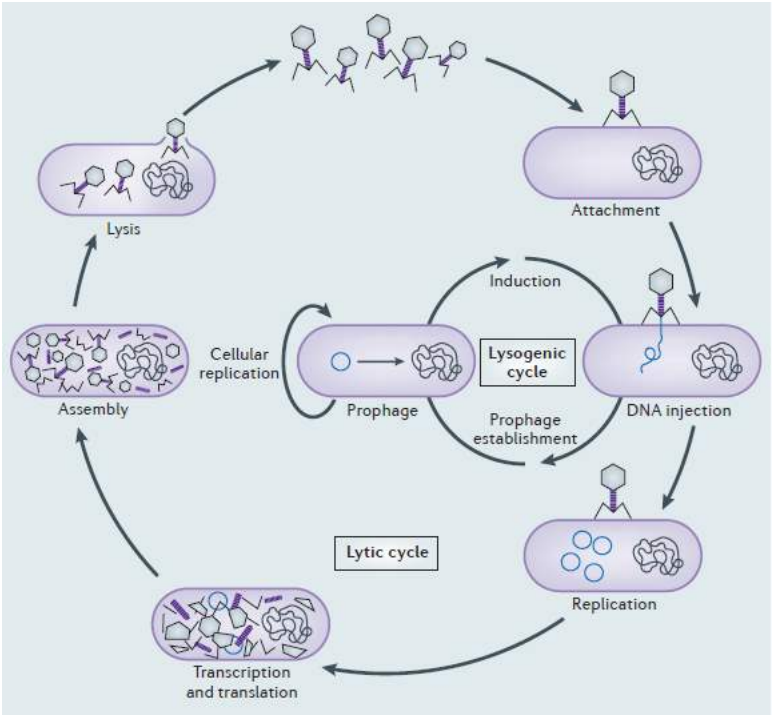

Figure 7: **The lytic and lysogenic life cycles of bacteriophages.** This illustration depicts the key steps of both processes. It's important to note that not all phages can undergo both life cycles. (Adapted from [63]).

the prophage which might even be beneficial. However, under specific environmental triggers (or sometimes even spontaneously), the prophage can be prompted to exit the lysogenic state and transition into the lytic cycle, leading to active phage replication and eventual lysis of the host cell. Certain bacteriophages, such as the T-even phages or the SPO1 phage, are exclusively lytic [1]. These phages, also known as virulent phages, are the central subjects of chapters 2 and 3. In contrast, lysogenic phages, also termed temperate phages, have the capability to opt between a lytic and a lysogenic life cycle[50]. While this decision-making process is stochastic, it is not entirely random [56, 62]. Numerous factors, including environmental conditions, the presence of co-infecting phages, the metabolic state of the host, and even cell volume, play a role in influencing this choice [61]. For instance, under optimal conditions, the λ phage, which is the main subject of chapter 4, predominantly opts for the lytic pathway, with over 90% of infections resulting in lysis [49]. However, this propensity shifts dramatically under less favorable conditions [49]. Nutrient scarcity or high multiplicities of infection increase the probability of lysogeny, highlighting the phage's adaptability in response to environmental signals [49].

Bacteria are not merely passive targets for phage infections. They have evolved a plethora of strategies to counteract phage invasions [49, 64, 65]. Some bacteria acquire resistance through mutations, rendering them devoid of the surface receptors necessary for phage attachment. Others have developed immunity mechanisms that prevent phage development once they've entered the cell. This includes the Restriction Modification systems, which degrade foreign DNA, and the CRISPR-Cas system, offering adaptive immunity against specific phage sequences [49, 64, 65]. Additionally, Toxin-antitoxin systems can induce cell death upon phage infection, and abortive infection mechanisms can halt phage replication [49, 64, 65]. They have developed their own countermeasures to bypass or neutralize these bacterial defenses, ensuring their propagation. This dynamic interplay has given rise to a relentless microbiological "arms race" centered on cellular survival and viral proliferation [49].

This dynamic relationship between bacteria and bacteriophages is manifested across a wide range of scales. In this thesis, we adopt a coarse-grained approach, focusing on phage-bacteria ecology at the level of population dynamics.

1.2 Phage-bacteria ecology and population dynamics

This thesis delves into the intricate world of **phage-bacteria ecosystems** on the scale of interactions of their populations [66, 46]. A foundational framework often employed to study such systems is the **Lotka-Volterra system of equations** [67, 68]. Originally conceptualized to describe predator-prey interactions in ecological systems, Lotka-Volterra equations, are pivotal for the field of **microbial ecology** [66, 46, 1]. At its core, ecology is the study of the relationships between living organisms and their environments [69, 46, 70]. To study phage-bacteria ecology within a **population dynamics** framework, we need to define on a population level, a few vari-

ables that are related to the characteristics of an organism's life cycle and influence its reproductive success. These are known as **life history traits** [46] and include:

- **Growth rate:** The rate at which a population increases in size.
- **Decay rate:** The rate at which a population decreases due to natural causes.
- **Infection rate:** The frequency at which phages successfully infect bacterial cells.
- **Latent period:** The time interval between the infection of a bacterium by a phage and the release of new phage particles.
- **Burst size:** The number of new phage particles released from a bacterium post-infection.

Each of these traits plays a crucial role in shaping the dynamics of the phage-bacteria system and will be mentioned recurrently throughout this work. The following system of equations constitutes a simple example of Lotka-Volterra equations utilizing life history traits to describe phage-bacteria population dynamics [49].

$$\frac{dB}{dt} = \underbrace{kB}_{bacterial\ growth} - \underbrace{\alpha B}_{bacterial\ decay} - \underbrace{\eta PB}_{infection\ rate}$$

$$\frac{dP}{dt} = \underbrace{\beta\eta PB}_{viral\ lysis} - \underbrace{\delta P}_{viral\ decay}$$

where B and P are the population densities of bacteria and phages respectively. The bacterial population grows with growth rate k, while there is also some natural decay at rate α. In the absence of hosts, the viral population decays at a rate δ. However, when both bacteria and phages are present, phages infect bacteria at an infection rate η, and utilize bacterial resources to replicate inside the host. For the sake of simplicity in this example, we neglect the latency period during which phages multiply inside the host (see chapter 3 for inclusion of latency time). Eventually, the infected bacteria burst, releasing new phages in a process characterized by a burst size β. This results in an increase in phage numbers and a corresponding decrease in bacterial populations. This example lays the foundational framework for the approach we will adopt in the subsequent chapters.

1.3 Chapter overview

The overall theme of the thesis is population dynamics of phage-bacteria ecosystems under challenging conditions. Presented below is a concise overview of the primary content and focus of each chapter.

Chapter 1: The current chapter is an introduction to the fundamental terms and ideas needed for a reader to follow this thesis.

Chapter 2: A study on the eco-evolutionary dynamics of phage-bacteria in the upper layers of the ocean. This theoretical study delves into the dynamics that allow for the steady coexistence of phage-bacteria ecosystems in environments characterized by high competition for limited resources. It also addresses the infection patterns observed in previous studies providing new insights about the underlying mechanisms and network structure. Our research shows that in order to reach stability, the infection network self-organizes to increase specialization and decrease competition. In a such a system, slow growing strains can outcompete and eliminate faster growing strains by sharing a phage strain with it. This work was conducted under the supervision of Prof. Kim Sneppen and co-supervised by Assoc. Prof. Namiko Mitarai, leading to two publications.

Chapter 3: This chapter is devoted to the study of dormancy, focusing specifically on the interplay between sporulation in *Bacillus Subtilis* and virus-host interactions, and the consequent effects on the spatial dynamics of phage-bacteria communities. This work was initiated during my visit to the Weitz lab at Georgia Tech, in Atlanta, Georgia, USA, and spanned the entirety of my program's final year. It incorporates both experimental and theoretical findings, demonstrating for the first time that sporulation in *Bacillus Subtilis* can be virus-induced, offering collective protection to cell populations. Experiments were conducted by Dr. Andreea Măgălie as part of her thesis work in collaboration with Dr. Daniel Schwartz and under the supervision of Prof. Jay Lennon at Indiana University, Bloomington, Indiana, USA. I was responsible for spatial model development, parameterization, and analysis in collaboration with Dr. Măgălie and under the supervision of Dr. Jacopo Marchi and Prof. Joshua Weitz (currently faculty at the University of Maryland, College Park, Maryland, USA). The research is now essentially complete and is awaiting submission after minor editorial work.

Chapter 4: In this chapter, we experimentally explore the effect of the host's metabolic state on phage infections. Our results replicate previous findings, showing that the λ phage can opt not to infect Escherichia coli hosts that are in a low metabolic state. Our study aims to explore the generality of this viral feature. This research is conducted under the supervision of Prof. Kim Sneppen and Assoc. Prof. Namiko Mitarai and with the help of Prof. Stanley Brown. The work is currently in progress.

2 Phage-bacteria dynamics in the Ocean

2.1 Introduction

Until recently, unpolluted seawater was considered an environment with an unimportant viral presence. Although electron microscopy was invented in the 1930s, it took over five decades before anyone undertook a comprehensive survey of uncultured natural seawater for microbial life. This perception shifted dramatically in 1989 with a study by Bergh et al. [71]. Their research demonstrated that the density of viruses in the upper layers of the sea was between 10^3 and 10^7 times higher than previously estimated. But how do viruses manage to sustain populations of that size? Which are their hosts, and what is the diversity of such an ecosystem? Moreover and even broadly, how and to what extent does such a ubiquitous and abundant ecosystem interact with other ecosystems, marine or not, that were previously considered independent? The subsequent efforts to answer such questions established this discovery as a seminal moment, with implications far beyond the study of microbial ecosystems alone.

Today we know that the number of microbial entities in the oceans is astronomical. Bacteriophages are the most abundant of them all, with their number estimated to be on the order of 10^{31}, corresponding to approximately a trillion phages for every grain of sand in the world [43, 41]. Bacteria follow in numbers with estimations suggesting that the world's oceans contain 10^{30} individual bacteria cells [26].

Apart from dominating in sheer numbers, this host-parasite pair plays a central role in oceanic ecosystems. Bacteria are one of the most dominant contributors to marine biomass [72, 73]. They play a critical part in global biogeochemical cycle and exert influence on other ecosystems, thereby molding the overall microbial genomic diversity [74, 75, 76, 77, 78, 79, 80, 81, 82, 83]. Furthermore, they are linked to diseases affecting a wide range of species – from coral reefs and marine plants to animals and humans – impacting both individual organisms and entire populations [1, 84].

Remarkably, many of these bacteria inhabit environments characterized by scarce resources and intense predation from bacteriophages. It is believed that bacteriophage predation accounts for the decimation of half the oceanic bacterial population daily [85, 86, 1]. Yet, in the face of such adversity, this host-parasite tandem continues to coexist within stable and diverse ecosystems. This chapter aims to delve into the dynamics that underpin such resilient ecosystems.

2.2 Ecosystems of phages and bacteria in the upper layers of the Oceans

Unlike deeper ocean zones, the epipelagic zone, which spans from the sea's surface to a depth of 200 meters, generally lacks natural barriers that would insulate local ecosystems from external influences [87, 88]. It is, therefore, an open ecological environment for microbes, meaning that

new strains of phages or bacteria can enter local patches of the sea that were not present before. Furthermore, the amount of available resources for bacteria is relatively limited. Consequently, one could logically deduce that this would not be a favorable environment for the rich and diverse phage-bacteria ecosystems. After all, the bacteria face a dual pressure: they're exposed to predation due to the absence of hideouts and must compete with other bacteria for limited resources. In striking contrast to that, there is an abundance of viruses and bacteria that coexist in stable and diverse ecosystems over many such local patches across the oceans [89, 90, 71, 91, 92, 93, 94, 45]. The question therefore is; what is the structure of the phage-bacteria interaction network that shapes and maintains the diversity in such ecosystems?

To answer this question, Moebus and Nattkemper [95] embarked on an expedition to the Atlantic Ocean and collected water samples from various stations in many different locations. Based on their field and laboratory investigations, they reconstructed the largest to-date network of phage-bacteria interactions for marine ecosystems. More recently, Kauffman et al. [96] revisited this study, employing state-of-the-art genomics techniques to assess a network of an equivalent magnitude of bacterial strains, phage strains, and interactions.

Figure 8: **The epipelagic zone.** This chapter focuses on phage-bacteria ecosystems in local patches at the epipelagic (photic) ocean zone, which spans the upper 200m of the ocean.

Their analyses revealed that the overarching structure of the phage-bacteria interaction network is nested-modular, characterized by a preponderance of one-to-one interactions between parasite-host pairs [97, 98] (see main panel in Figure 9). These modules suggest that there is a geographic element behind this specificity. However, the effect is not strong enough to exclusively suggest local eco-evolutionary adaptations since there are phage strains that can infect hosts that are thousand of kilometers away [95, 49, 46].

Examining individual local stations, as in the study by Haerter et al. [99], reveals a balance between the number of phage and bacterial strains (see subpanel in Figure 9). However, the total strain count can differ considerably between stations. To simulate these local ecosystems, Haerter and colleagues treated them as open systems where bacteria fully share resources. It is a well-established theoretical concept that two species that fully share resources cannot coexist, as they would occupy the same biological niche. This idea is encapsulated in the "competitive exclusion" principle. Though the principle was finalized and named by Hardin in 1960, elements of it can be traced back to the works of Darwin [100, 101, 68, 102, 103, 104].

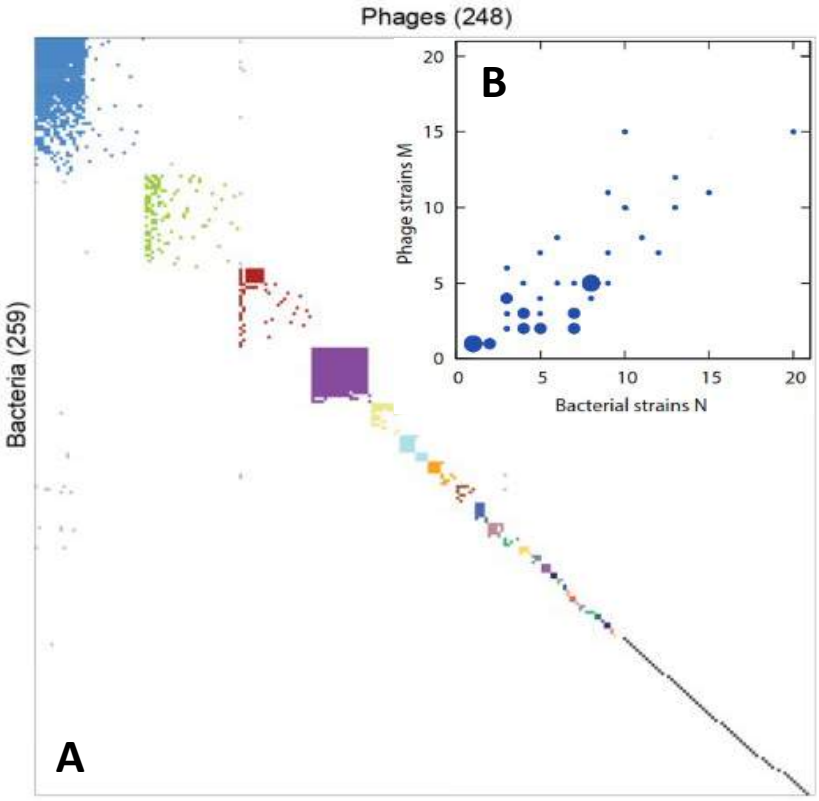

Figure 9: **Data on phage-bacteria ecosystems at the epipelagic zone of the Atlantic Ocean. A)** By repeating the study of Moebus and Nattkemper [95] and the analysis of Flores et al. [97], Kauffman et al. validated that the infection network of phages and bacteria across all stations has an overall nested-modular structure with abundant one-to-one interactions [96]. Here, every row corresponds to a specific bacterial strain, and every column to a phage strain. The order of the rows has been reshuffled similarly to Flores et al. to unravel the nested-modular pattern [97]. **B)** As demonstrated by Haerter et al. [99], an analysis of the data at each local station reveals balanced diversity between phages and bacteria. This panel comes from the work of Haerter et al. [99] on the data of Moebus and Nattkemper [95]. Each dot corresponds to data on the number of phage and bacteria strains from a different local station, while the size of the dot represents the observed frequency of each combination.

According to the principle, the system should not be able to sustain more than one bacterial strain. The fastest-growing strain would simply out-compete the other. However, this balance shifts with the introduction of phages [105, 106]. If a phage strain enters the system by attacking the slower-growing strain, then it would just accelerate its demise. But, by suppressing the population of the faster-growing host strain, the phage can alleviate competition for the slower-growing strain, freeing up resources and enabling all three strains to coexist [49]. The concept can be extended by sequentially adding slower and slower-growing bacteria paired up with bacteriophages that suppress their number to allow the new slower-growing bacterial strain to enter. This predator-mediated stable coexistence is known as the "Kill the Winner" hypothesis [92, 107] and has been one of the main mechanisms that show how predators can foster stable and diverse ecosystems.

Similarly to bacteria, phages are also subject to the competitive exclusion principle when they fully share their hosts. In such a predator-prey system, Haerter et al. showed that the recorded balanced diversity stems from these two levels of competitive exclusion at play [99]. By generalizing the principle, they showed that prey strains can outnumber predator strains at most by as much

as the number of shared resources. Therefore, a simplifying assumption of one common resource leads to a system that can be stable only if the number of prey is either equal to or exceeds the number of predators by one. As diversity builds up sequentially with new bacterial strains needed to support the entrance of new phage strains, the parameter space that allows for stable coexistence of all the species becomes progressively narrower, setting in effect an upper limit to the total amount of species that one can have in an ecosystem like that.

2.3 From Kill the Winner to Eliminate the Winner

2.3.1 Model description

In the study of Haerter et al., the infection networks are either fully nested (meaning that every bacterium is resistant to any phage that preexisted its entrance in the system and susceptible to all the rest) or fully diagonal (absolute specialization with each phage infecting only one bacterial strain) by design. These constitute theoretical limit cases not typically encountered in natural ecosystems. There are several other possibilities for network structures (like modular or random interaction networks), and every such structure typically manifests itself as a distorted pattern under the random noise of the environment [45].

In our study [108], we extend the work of Haerter et al. by generalizing the constraints on network structures. Our models allow for interactions to be either completely random between strains (designated as Model R in Figure 10) or nested but with some randomness in the realization of each interaction (Model N in Figure 10). This approach allows us to test the widely-reported nested structure of such ecosystems in existing literature [95, 96, 99, 97, 109, 110, 45]. We simulate a well-mixed ecosystem in which new phage and bacterial strains are introduced stochastically and equiprobably. Our simulations start with a single bacterial strain, and new strains are introduced sequentially in an event-based algorithm, where every time point corresponds to a new species invasion attempt in a system at steady state. Therefore, after the addition of the new strain, we let the system evolve dynamically until it reaches equilibrium. If the invasion attempt is successful, the diversity (measured as the number of species in the system) increases by one. If not, the system is rendered unstable, leading to the extinction of one or more species as the ecosystem evolves toward a new steady state. A new strain is allowed to attempt invasion only after the system has reached equilibrium, and this cycle is then repeated.

The dynamics of our system are described by the following generalized Lotka-Volterra system of equations [67, 68, 105, 109, 99] for a set of bacteria and phage strains, with population densities that are given by B_i and P_k respectively and with implicit resources that are fully shared between

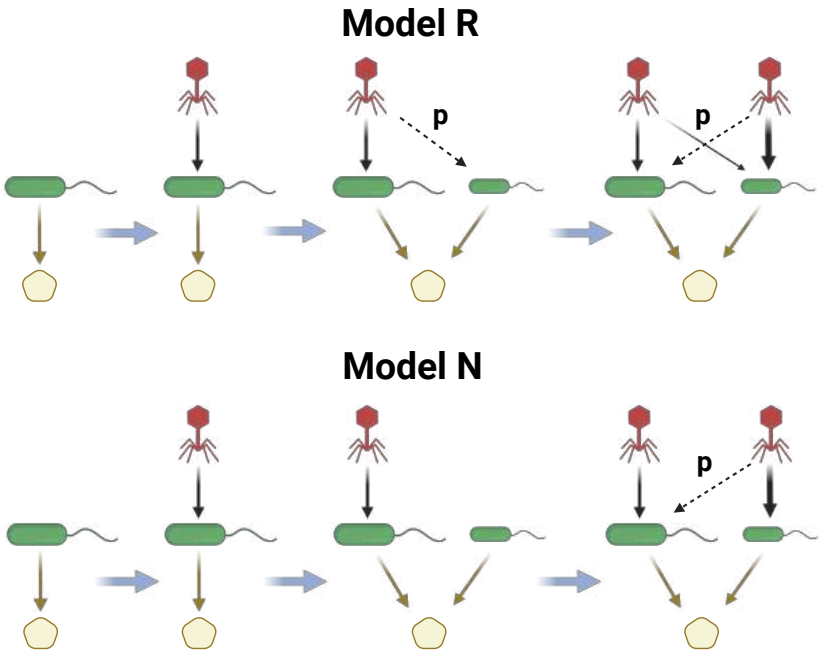

Figure 10: **Schematic depiction of Models R and N.** The arrangement of the schematics is based on their chronological introduction into the system, going from left to right. The arrows indicate a new event. It is worth noting that in Model R, a newly introduced phage might target a bacterium that was not the most recently added. Phages target any bacteria that is not already under attack by other phages, although only one bacterial strain can be in this "free" state. On the contrary, Model N's assumption of resistance as a prerequisite for entrance dictates that the most recently introduced bacteria will necessarily be free of phages. For the rest of the text green circles will symbolize bacterial strains, while red circles will represent phage strains. The resources will be omited since the bacteria share them fully. (Created with BioRender).

the bacterial strains:

$$\frac{dB_i}{dt} = k_i B_i \left(1 - \sum_{j=1}^{N} p_{ji} B_j\right) - \alpha B_i - B_i \sum_{k=1}^{M} \eta_{ki} P_k$$

$$\frac{dP_k}{dt} = P_k \sum_{m=1}^{N} \beta_k \eta_{km} B_m - \delta P_k$$

The population density parameters are quantified in units of the environment's carrying capacity, while parameters relevant to rates are quantified in terms of the maximum possible bacterial growth rate. These parameters are derived from referenced oceanic studies and include the bacterial growth rate of strain i, k_i, which is of the order of 2/day [85], the bacterial death rate, $\alpha = 0.1$ [85] and the phage decay rate $\delta = 1$ [86]. η_{ki} and β_k represent the infection rate of bacterial strain i by phage strain k and the burst size of the phage strain k, respectively. For our simulations we assume uniformly distributed $k_i \in [0, 1]$, $\eta_{ki} \in (0, 1)$ and $\beta_k \in [1, 50]$, characteristic of each strain or, in the case η_{ki}, characteristic of each strain-strain interaction. Finally, bacteria j and i are assumed to interact only purely competitively in a struggle for a fully shared resource ($p_{ji} = p_{ij} = 1$).

Since the data from local stations correspond presumably to phage-bacteria ecosystems at equilibrium, we focus on systems at steady-state, similarly to Haerter et al. [99]. This sets a time-

scale for the dynamics that justifies our latency omission simplification. Therefore, our model ecosystem evolves under the following algorithm: Every newly introduced strain has a population density of 10^6. We evaluate whether the linear equations at a state corresponding to $\frac{1}{B_i}\frac{dB_i}{dt} = 0$ and $\frac{1}{P_k}\frac{dP_k}{dt} = 0$ lead to non-degenerate and feasible (positive) solutions. If so, the system moves to a new steady-state that includes this strain. If not, we identify the strains that are driven to extinction before acquiring a new system that can attain a steady state. To do this, we start from the conditions at the time of invasion (conditions of the previous steady state and the new strain that attempts to establish itself) and let the system evolve by integrating with the fourth-order Runge-Kutta method. We consider as extinct every strain with population density below a minimal threshold (10^{-20}) [108].

We assume that new phage-bacteria interactions can only be established at the introduction of each strain in the system and, once settled, remain unchanged. In our Model R (see Figure 10), we relax any presumptions regarding phage-bacteria interaction networks by introducing randomness in the materialization of interactions upon entrance. More specifically, any invading bacterial strain can get infected by a preexisting phage strain with probability $p \in [0, 1]$. Similarly, newly introduced phage strains infect bacterial strains without predators with probability 1 and any other strain with probability $p \in [0, 1]$. Thus, for $p = 0$, Model R produces a fully diagonal network similar to the one from [99], while $p = 1$ results in a fully connected phage-bacteria network.

Given the repeatedly reported nestedness of marine phage-bacteria networks in literature [95, 92, 97, 45, 109, 99, 110, 96], we constructed a second model, named Model N. This model is intentionally nested to serve as a comparative framework against Model R (Figure 10). Model N is built on the assumption that invasions can only happen by bacterial strains that are resistant to all existing phages. As in Model R, new phage strains infect with probability 1 any phage-free bacteria and with probability $p \in [0, 1]$ every other bacterial strain. However, unlike Model R, only bacteria fully resistant to all preexisting phages can enter the system. This leads to a historical organization of the phage-bacteria network, where newer bacterial strains are attacked only by the most recent phage strains, thus typically having fewer and newer predators than the older bacterial strains. As a result, the extreme cases $p = 0$ and $p = 1$ of Model N correspond to the network structures studied by [99], namely a diagonal and a fully nested network respectively [99]. In the following subsection, we will present a summary of our results (for a more detailed approach, see the manuscripts included in the end of the current chapter [108, 111]) and showcase that emergent patterns make the two models converge in the parameter region of interest for our system.

2.3.2 Results and Discussion

Our modeling approach has been guided by the reported balanced diversity at the local stations [99]. As corroborated by the upper panel of Figure 11 and Figure S1 of the supplementary material

from [108], our models can replicate the reported diversity both in terms of the total number of species and in terms of equivalence between the number of phage and bacteria strains.

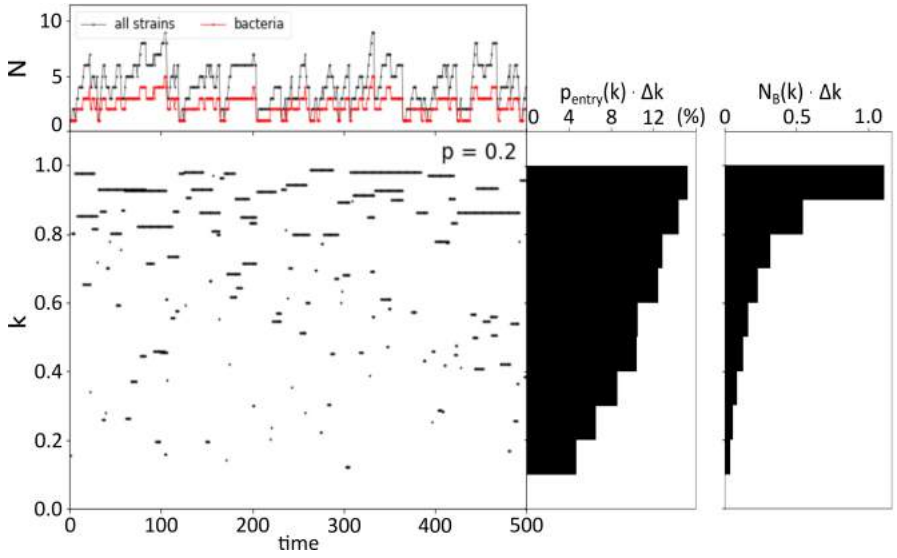

Figure 11: **The evolutionary dynamics of Model R.** The central panel shows the growth rates of the system's bacteria at each time-point for a short but representative period of 500 time-steps, corresponding to 500 consecutive stable ecosystems and invasion events. The selection of $p = 0.2$ for a cross-link probability is just indicative of the parameter region that we expect to be based on the analysis from [99]. Each horizontal line signifies a distinct bacterial strain, and its position on the y-axis corresponds to its growth rate. Therefore, the bigger the bacteria line, the longer the survival time of this bacterial strain. The upper panel illustrates the evolution of the number of all strains (phages and bacteria as a black curve) and of the bacterial strains (red curve) with time, with the bacteria curve being practically a vertical projection of the central plot. The number of bacterial strains is about half the number of the "all strains" curve as in the observations at the local stations [99]. An important feature of the combined information of the central and upper plot is the extinction events that can reach system-size magnitudes and affect even the fastest-growing strain. The right side panels are effectively a horizontal projection of the central plot over 10000 time-steps. The inner histogram displays the distribution of the invasion probability of a bacterial strain as a function of its growth rate $p_{entry}(k)\Delta k$. The outer histogram shows the average number of bacterial strains distribution in the system at each time-step as a function of their growth rate $N_B(k)\Delta k$. The bin size for both histograms is $\Delta k = 0.1$. The combined information from the central and right side panels is a manifestation of the inherent advantage in invasiveness and survival that comes with a high growth rate. (Reprinted from [108]. The qualitative features are similar to the one of Model R as shown in the supplementary figure S1 of Marantos et al. [108])

Interestingly, even though the net growth rate at steady-state is zero, a significant advantage emerges from a high basal Malthusian growth rate. This is illustrated in the central as well as in the right side panels of Figure 11, demonstrating that higher bacterial growth rates increase the likelihood of successful invasions and prolonged survival within the system. Despite that, and even more interestingly, we show that we can have extinctions of even system-size magnitudes and that having a higher growth rate does not guarantee protection (showcased at the central and the upper panel). The repeated observation that even the fastest-growing strain can get eliminated by a slower-growing strain prompted a more in-depth examination of the network structure and dynamics in order to decipher the underlying mechanisms behind these extinction events.

A closer examination of the network dynamics revealed an infection network that self-organizes toward a "Kill the Winner" structure. Recognizing this pattern requires focusing not only on the presence of a phage-bacteria strain link but also on its strength, defined as the magnitude of $\beta\eta$ (see Figure 12 and Figure 13A). This analysis illuminates a pattern of emergent specialization (see Figure 13A). In order to reach stability, each phage strain needs to predominantly live off

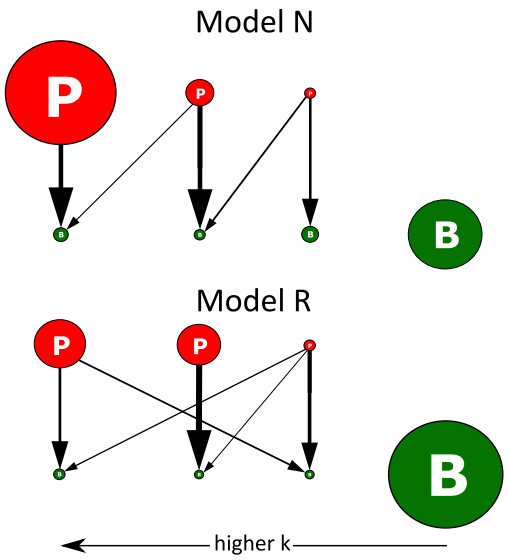

Figure 12: **Indicative representations of infection networks for both models.** These schematics illustrate exemplary ecosystems of phages and bacteria, with the top part of the figure corresponding to the nested model (Model N) and the bottom part to the random model (Model R) when simulated with cross-link probability $p = 0.5$. The key difference between the two models is that Model N requires phages to target only the bacteria that existed at the time of their introduction. The sizes of the circles are proportional to the population density of the corresponding strains, while the arrow widths reflect the $\beta\eta$ value of their respective interactions. Notably, the bacterial historical assembly typically coincides with their growth rate ordering since older bacteria tend to have higher k. Conversely, older phages can prey on newer bacteria in the Model R, leading to a more stochastic structure. Finally, this figure has a feature of high importance that is common for both models. The specialization indicated by the strong parallel infection links that result in one-to-one phage-bacteria pairs regarding dominant interactions. (Reprinted from Marantos et al. [108]).

the bacterial strain that is the most vulnerable to their attacks while being the most successful at invading this strain compared to all other phage strains in the system. This arrangement fosters system stability and robustness as specialization minimizes competition and the likelihood of competitive exclusion.

Furthermore, as demonstrated in Figure 13B, C, Model N, and Model R converge as p $\to$ 0. Since the analysis of [99] showed a correspondence of 1.4 bacterial strains for every phage strain, we expect to be at the region of low p. Therefore, we show that the assumption for bacterial resistance to all existing phage strains as a prerequisite for bacterial invasion is not only plausible but not even necessary to be imposed as a condition since it is an emergent property of the system. Consequently, we have an emergent nested yet close to being diagonal network resulting from dynamics that lead to higher stability and robustness only when competition is minimized.

Therefore, we have a one-to-one network [45] with a few additional weaker links. These weaker links, though, prove to be quite crucial for the eco-evolutionary dynamics as they favor the slow-growers significantly. In Figure 13D, we show that even the slightest chance of an extra weak link disturbs the traditional one-to-one "Kill the winner" organization substantially by increasing the chance of elimination of the faster-growing strain and by distributing the resources more evenly between bacterial strains with different growth rates.

Ultimately, as illustrated in Figure 14, this weaponization of a common phage-predator by a slower-growing but resistant bacterial strain against a faster-growing but susceptible strain has been identified as the main mechanism that drives the extinction of even the fastest growing strains. These extra links allow for predator sharing through formations of Susceptible bacteria-Resistant bacteria-Phage triplets that consequently lead to a generalized version of the dynamics observed in three species systems with two prey and one common predator [106, 49, 90]. As a consequence, we go from self-organized "Kill the Winner" dynamics where the presence of phage-predators allows for coexistence of fully competing bacterial strains through suppression ("killing")

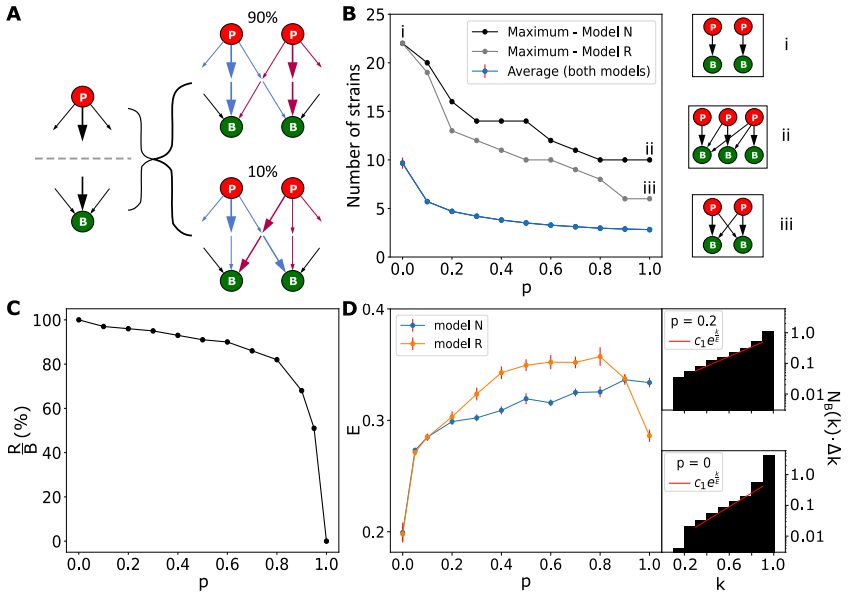

Figure 13: **Network structure analysis in relation to cross-link probability p.** A) Each strain possesses a number of infection links with other strains, the "strength" of which is denoted by $\beta\eta$. Here, we show that in $\sim$ 90% of all stable ecosystems, the strongest links (highlighted as bold arrows) between phages and bacteria align, leading to pairwise specialized predatory connections that resemble a "Kill the Winner" organization. Here, each arrow color corresponds to a different phage. Such a prevalence of the "Kill the Winner" structure was observed in both models (with a slight decline from roughly 90% at $p \sim 0.1$ to 80% at $p \sim 1$). This indicates that ecosystem stability requires predominantly phages that are optimally adapted to infect the bacterial strains that are the most susceptible to them. B) This Figure shows the average and maximal diversity over 10000 time-steps as a function of p. The trend is that diversity increases as cross-links (and therefore niche similarity between phages) decrease. At $p = 0$, the infection matrix becomes diagonal, and both models are indistinguishable and similar to the schematics of sub-panel i. As in the "Kill the Winner" model, the role of phages is limited to nullifying bacterial competition, thus resulting in peak diversity. As p increases and approaches unity, the two models progressively diverge, driven by the "resistance for entry" assumption difference that is manifested significantly given enough cross-links. The maximum and total diversity are also decreasing as extra links increase the similarity between strains and, therefore, competition. Model N will be able to sustain more strains since its assembly rules result in fewer and more hierarchically ordered links than Model R, where competitive exclusion depends much more on the varying strength of the infection link $\beta\eta$. Subpanels ii and iii show the differences in network structure for the limiting case $p = 1$ for Model N and Model R, respectively. C) This is an analysis of Model R, which shows the fraction R/B of bacteria that successfully invade and contribute to the system's diversity while being resistant to all preexisting phages. Interestingly, even for relatively large p-values, Model R's assembly rules become essentially equivalent to Model N's. Therefore, the inherent principle of bacterial resistance for successful entry in Model N emerges in Model R as a prerequisite condition for establishing a large, stable, and robust ecosystem. D) Here, we plot the Elimination Factor E of fast from slow growers, defined as the least squared fit of the time-averaged number of bacteria in relation to growth rate $N_B(k) \propto \exp\left(\frac{k}{E}\right)$, as a function of the cross-link probability. The right-hand side sub-panels demonstrate examples (for Model R but similar to Model N) on the derivation of the Elimination Factor from the scaling relationship between steady-state diversity and the growth rate k. The two side panels are related to model R. For $p = 0$, our model behaves like the classic "Kill the Winner" model. As shown, even the slightest increase in the chance for a cross-link has a significant effect on the value of the Elimination Factor. A higher E-value translates to smaller differences between the faster and the slower growers in representation in the system. The same effect can be seen in the chance of entering the system (see supplementary Fig S2 in Marantos et al. 2022). Therefore, even a few additional links suffice to increase the risk of elimination for fast growers significantly and distribute the resources among bacteria of different growth rates more equally. (Adapted from Marantos et al. [108])

of the population size of the most competent competitor to an actual elimination of the winner. This result sets limits on connections between fitness and reproductive rate maximization since having a higher growth rate can result in higher fitness only for the time-windows where common predators are absent or have an unimportant effect. The presence of shared predators intermits the growth rate maximization evolutionary "game" by altering it with the introduction of resistance as a key factor.

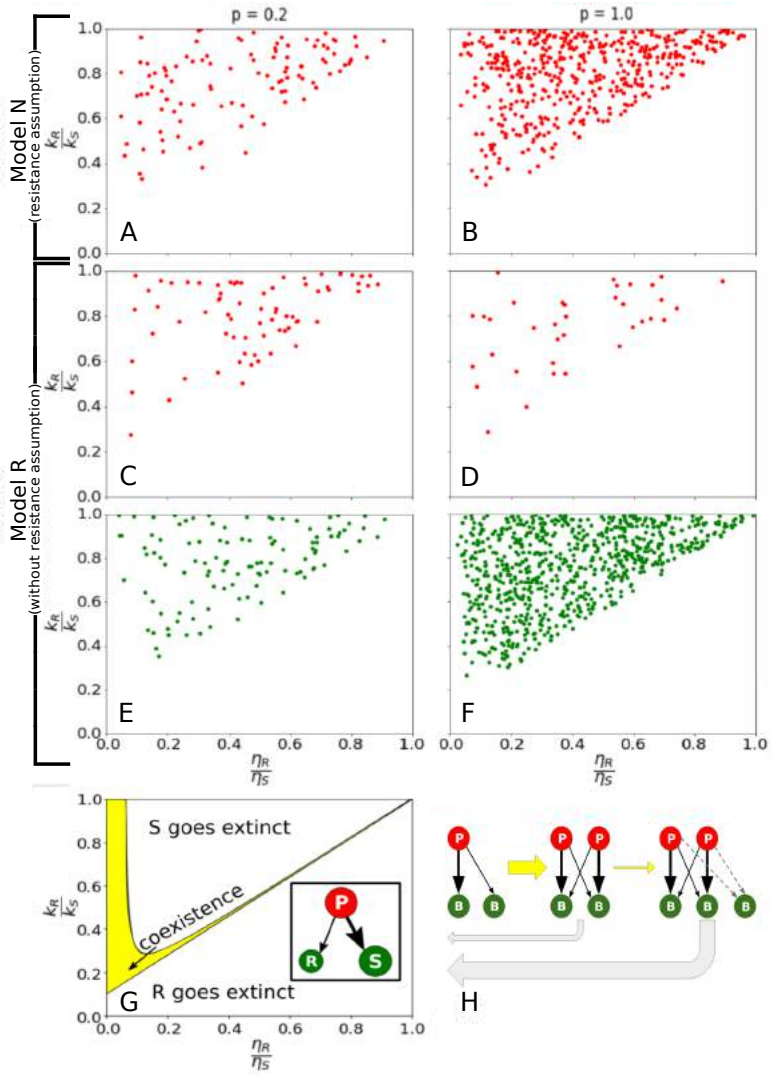

Figure 14: **Extinction events.** A-F) Events where faster growing yet more susceptible to phage attacks strains (S) are eliminated by slower growing but more resistant ones (R). Each dot represents such an event that occurs only when a phage infects both S and R. The x-axis displays the infection rate ratio η_R/η_S, and the y-axis shows the growth rate ratio k_R/k_S. Each dot signifies an event instigated by the introduction of a new strain. The color distinction clarifies the invasive strain type: red for phages and green for bacteria. In Model N (A-B), only phage introductions lead to extinctions, as new bacteria are always resistant to all existing phages, and slower growers cannot out-compete their faster counterparts without assistance. Conversely, in Model R, fast-growing bacterial extinctions can be triggered by both phage and bacteria invasions (C-F). G) We have analytically identified the regions of coexistence and extinction of a simplified system with two fully competing bacteria and a common phage-predator (see Supplementary S1 Appendix). The inner panel shows the triplet-motif, where growth rates are symbolized by circle sizes, and susceptibility is depicted by arrow thickness. Therefore, a larger circle labeled 'S' indicates faster growth but higher phage susceptibility, and a smaller circle labeled 'R' denotes slower growth but greater resistance. Coexistence occurs (yellow region) within a specific parameter set where the slower-growing bacterium is less susceptible to the phage than its faster-growing counterpart. [106, 49]. Notably, an even broader parameter range exists where the slower bacterium can out-compete and eliminate its faster counterpart. (H) These schematics depict the network's progression as new strains are introduced. As the system expands, the coexistence parameter region shrinks, and extinctions, indicated by grey arrows, become increasingly likely. (Adapted from Marantos et al. [108]).

2.4 Conclusion

Our study delves into the complex relationships between phages and bacteria in the upper layer of the ocean, an ecosystem with significant ecological, biogeochemical, and even public health ramifications [74, 75, 76, 77, 78, 79, 80, 81, 82, 83, 1]. It is a theoretical investigation into a potential mechanism that can describe previous experimental findings. Specifically, we focus on the observations of an overall nested-modular infection network with an abundance of one-to-one interactions and on the balanced diversity between phage and bacterial strains in local oceanic patches [95, 99, 96].

In these patches, limited resources lead to intense competition among bacteria, challenging the maintenance of diverse microbial communities. Several mechanisms have been proposed as a solution to this paradox [111, 89]), including the cross-feeding of metabolites among different species [112, 113, 114], a variability in preference for slightly different resources [115], and spatial in-homogeneity [116, 117]. In this study, we have approached this problem with the concept of predator-mediated diversity [105, 106, 92, 99, 49]. Using models that consider random bacterial or phage invasions and shared food sources, we were able to replicate the observed diversity in these communities. Our analysis reveals that despite the benefits of rapid growth, faster-growing bacterial strains are still vulnerable to extinction events that can even reach system-size. By focusing on the "strength" of the interactions, we show emergent specialization. The system tends to self-organize into a "kill-the-winner" structure, where phages target the most susceptible bacterial strains, reducing competition and increasing overall stability.

Our model diverges from the classic "kill-the-winner" model by introducing additional links that give an edge to slower-growing bacterial strains. We identified a specific mechanism, a triplet motif of susceptible fast-growing strain, resistant slower-growing strain, and a phage that allows the slower growers to out-compete their faster counterparts (see Figure 15).

Although our model is based on an open system where newly added species' properties are chosen independently of existing species, it successfully recreates real-world observations and points to how ecosystems self-organize for stability and robustness. Despite that, we acknowledge that the new species with properties that correlate with existing species may appear due to mutation [118]. Prior research has demonstrated that co-evolution within a closed system can lead to nested-modular interaction networks [118] and increased specialization [119]. Nevertheless, previous findings indicate that the occasional influx of external phages to a subsystem accelerates local adaptation by introducing greater genetic variation [120]. Integrating elements of mutation and external invasions in one model could provide a more comprehensive understanding of these complex phage-bacteria ecosystems.

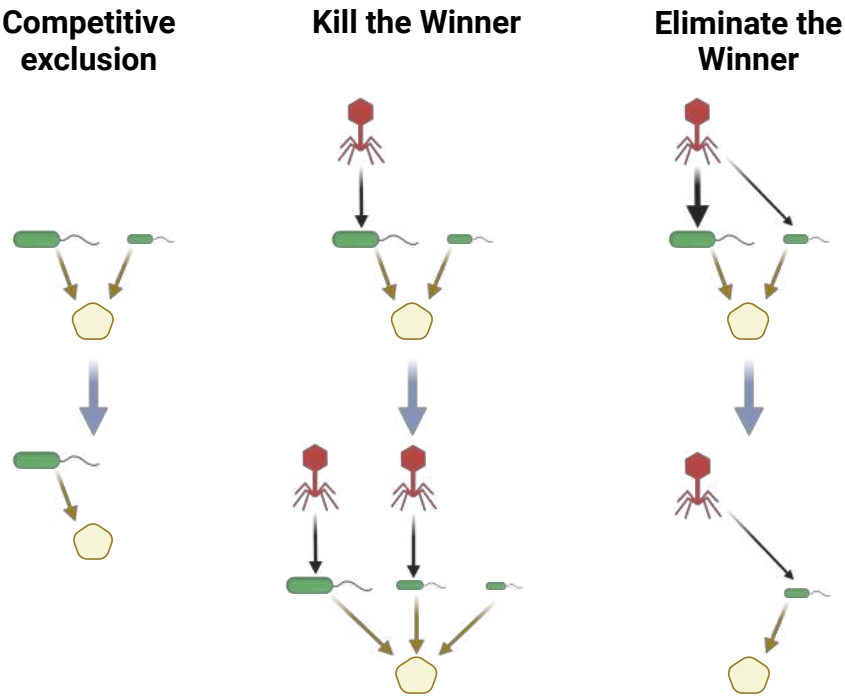

Figure 15: **From Competitive exclusion to Eliminate the Winner** According to the Competitive exclusion principle, two bacterial strains that fully share their resources cannot coexist; the faster-growing strain will eventually outcompete and drive the other to extinction. If a phage infected the slower-growing strain, this would merely expedite the process. However if the phage targets the dominant (or "winning") strain, coexistence between the two bacterial strains becomes feasible, thereby fostering ecosystem diversity. Our study indicates that in our phage-bacteria ecosystem, a "Kill the Winner" dynamic naturally emerges, as this minimizes competition between bacterial strains. Interestingly, if phages are permitted to infect multiple bacterial strains, a slower-growing yet more resistant strain can outcompete a faster-growing strain, if the latter is more susceptible to their shared parasite. (Created with BioRender.com)

2.5 Manuscript: From Kill the Winner to Eliminate the Winner in Open Phage-Bacteria Systems

Authors: Anastasios Marantos*, Namiko Mitarai*, Kim Sneppen*

Affiliations: *Center for Models of Life, Niels Bohr Institute, University of Copenhagen, Copenhagen, Denmark

My contribution: I contributed to the development of the model, to the associated computational work, to the production of figures and data processing, and to the writing of the article both at the initial stage and at the reviewing/editing phase.

Supervision: I worked under the supervision of Prof. Kim Sneppen and co-supervision of Assoc. Prof. Namiko Mitarai.

Publication status: Published in PLOS Computational Biology

DOI: 10.1371/journal.pcbi.1010400

PLOS COMPUTATIONAL BIOLOGY

RESEARCH ARTICLE

From kill the winner to eliminate the winner in open phage-bacteria systems

Anastasios Marantos, Namiko Mitarai, Kim Sneppen*

Center for Models of Life, Niels Bohr Institute, University of Copenhagen, Copenhagen, Denmark

* ksneppen@gmail.com

Abstract

Phages and bacteria manage to coexist and sustain ecosystems with a high diversity of strains, despite limited resources and heavy predation. This diversity can be explained by the "kill the winner" model where virulent phages predominantly prey on fast-growing bacteria and thereby suppress the competitive exclusion of slower-growing bacteria. Here we computationally investigate the robustness of these systems against invasions, where new phages or bacteria may interact with more than one of the resident strains. The resulting interaction networks were found to self-organize into a network with strongly interacting specialized predator-prey pairs, resembling that of the "kill the winner" model. Furthermore, the "kill the winner" dynamics is enforced with the occasional elimination of even the fastest-growing bacteria strains due to a phage infecting the fast and slow growers. The frequency of slower-growing strains was increased with the introduction of even a few non-diagonal interactions. Hence, phages capable of infecting multiple hosts play significant roles both in the evolution of the ecosystem by eliminating the winner and in supporting diversity by allowing slow growers to coexist with faster growers.

Author summary

We demonstrate that in an open system of phages and bacteria with very limited resources, a bacterial strain that has a high growth rate can still be outcompeted by a slower-growing strain if they have a common phage. The impact of this on ecosystem structure is significant as soon as there is a small probability to have a common phage among bacterial strains. Furthermore, by analysing the structure of the interaction network we show that it self-organizes into a network with strongly interacting specialized predator-prey pairs, in order to reduce phages competition. Nevertheless, the presence of the remaining links is very important for the network dynamics since even a few of them significantly enhance the frequency of slower-growing strains.

Citation: Marantos A, Mitarai N, Sneppen K (2022) From kill the winner to eliminate the winner in open phage-bacteria systems. PLoS Comput Biol 18(8): e1010400. https://doi.org/10.1371/journal.pcbi.1010400

Editor: Mercedes Pascual, University of Chicago, UNITED STATES

Received: February 28, 2022

Accepted: July 17, 2022

Published: August 8, 2022

Data Availability Statement: All code and data are available at GitHub: (https://github.com/TassosMar/Eliminate-the-Winner).

Funding: AM and KS have received funding and salary from the European Research Council (ERC) under the European Union's Horizon 2020 research and innovation program under grant agreement No. 740704 https://erc.europa.eu/ and NM has received funding from the Novo Nordisk Foundation (NNF21OC0068775). https://www.novonordisk.com/ The funders had no role in study

Introduction

The epipelagic oceanic zone (0–200 meters depth) is an open environment with sub-parts that have some influx of new phage and bacterial strains. Such an environment makes it very hard

design, data collection and analysis, decision to publish, or preparation of the manuscript.

Competing interests: The authors have declared that no competing interests exist.

for bacteria to hide from phages, exposing them to direct predation. In fact, it has been estimated that phages kill 15–40 % of the ocean's bacteria every day [1]. Despite that, phages and bacteria manage to coexist. This was quantified e.g. by the colossal work of Moebus and Nattkemper [2], where they collected water samples from many different locations in the Atlantic ocean and reconstructed a large microbial network of interacting phages and bacteria. An updated version of the study has been recently conducted by [3], confirming the patterns found in Moebus and Nattkermper data and further revealing additional information on the ecosystem from genome sequencing. Yet, how the phage-bacteria system can maintain diversity in such an open environment is still a standing question in ecology [4–9].

Two strains of bacteria (or phages) that fully share their resources (hosts) cannot coexist. This statement is known as the competitive exclusion principle [10–15], and more generally, the number of consumers that coexist cannot exceed the number of resources [16]. This principle reflects a detrimental competition between the fastest-growing strain and any slower-growing ones. Survival of the fastest grower and its tempting connection to the survival of the fittest [10] lead Fisher and his followers to use net growth rate as a measure of fitness [17]. This view was challenged by the "kill the winner" scenario of Thingstad [8] where steady-state populations are maintained by predators independent of their Malthusian growth rates. In steady state the net growth rate of all the species is zero, suggesting a neutral selection without fitness bias for further evolution. In this work we will augment this perspective, and show that basal Malthusian growth rate still plays a role for the long term survival.

The "kill the winner" scenario considers a system of multiple specialist phage-bacteria relations where all bacteria are limited by the same resource. In this scenario, the fastest-growing bacteria will be preferentially targeted by phage predation due to their large biomass and by suppressing their biomass, they leave space for slower-growing bacteria to enter the system and coexist.

This concept was extended to the sufficient condition for the coexistence of diverse bacteria strains and virulent phage strains by Haerter *et al.* [18]. They showed that irrespective of the phage-bacteria interaction network structure, the number of bacteria strains can exceed the number of phage strains at most by the number of independent resources for bacteria. As diversity increases the remaining resources diminish due to consumption by an increasing number of marginally abundant susceptible bacteria, resulting in "a narrowing staircase" of coexistence [18, 19]. To increase the diversity with a limited number of resources, the system needs to evolve with keeping the balanced diversity of phages and bacteria, which was in agreement with the experimental data [2, 20].

The above works revealed the conditions for the phage-bacteria interaction networks that allow coexistence. As example systems that satisfy the conditions, analyses in [18, 19] focused on the diagonal and nested organization of the phage-bacterial network. However, there are different networks that satisfy these conditions. It may be diagonal as in the "kill the winner model" [8], it may be nested [9, 20–22], or it may be more randomly organized. The actual ecosystem realized in nature should depend on the history of species assembly [21–24]. Having the phage-bacteria ecosystem in an open oceanic condition in mind, we here explore how the ecosystem assembles with a stochastic invasion of phages and bacteria by using dynamic models of a well-mixed microbial ecosystem. In particular, we quantify the importance of the bacterial growth rate as their fitness and how the phages can mediate the successful invasion of slow growers. We find that although the classical "kill the winner" suppression of the fastest grower is the norm, the fastest-growing bacteria typically exist longer than the slower grower. Despite that, occasionally a slow-growing bacteria completely eliminates a faster grower, reflecting true "kill the winner" events. These types of events also limit the lifetime of the fastest-growing bacteria without the need of assuming extinction by fluctuations in small population numbers [25].

Methods

Model

In our model, we analyze how the ecosystem naturally assembles in an open system where new bacteria and phage strains are introduced occasionally. For simplicity, we consider a well-mixed ecosystem of bacteria and virulent phages [8, 18, 20]. We assume that the resources are fully shared between all bacterial strains, i.e. if there are no phages, there will be only one bacterial strain that can stably exist in the environment; the fastest growing one. We consider macroscopic populations of strains and ignore latency as we focus on systems that reach steady-state before each new addition of a phage or bacterial strain. More specifically, for a given set of strains, the dynamics of bacterial (B_i) and phage (P_k) population densities are assumed to be governed by a set of generalized Lotka-Volterra equations [12, 18, 21, 26, 27]:

$$\frac{dB_i}{dt} = k_i B_i \left(1 - \sum_{j=1}^{N} p_{ji} B_j\right) - \alpha B_i - B_i \sum_{k=1}^{M} \eta_{ki} P_k$$

$$\frac{dP_k}{dt} = P_k \sum_{m=1}^{N} \beta_k \eta_{km} B_m - \delta P_k$$

The rate parameters are measured in units of the maximal possible bacterial growth rate and all the density parameters in units of the carrying capacity of the environment. k_i is the bacterial growth rate of strain i reported to be of order 2/day [28]. $\alpha = 0.1$ is the universal death rate of bacteria (e.g. due to protist predation that is expected to amount to half bacterial death in the oceans [28]) and $\delta = 1$ is the decay rate of phages (phage decay rates in the ocean is about 2/day [29]). p_{ji} represents interactions between bacterial strain j and bacterial strain i, and is here assumed to be purely competitive ($p_{ji} > 0$). η_{ki} is the infection rate of bacterial strain i by phage strain k whereas β_k is the burst size of the phage strain k.

We start our simulation with a system of only one bacteria strain with a growth rate selected uniformly $\in [0, 1]$ in the steady-state of non-zero population size (this requires the growth rate bigger than α). Then, at each update step, we allow either a phage strain or a bacterial strain to invade the system. These additions are arbitrarily set to be equiprobable, but the qualitative messages of our work do not change substantially if invasion rates are asymmetric. A new strain is only allowed to invade when the population sizes are stabilized, which represents our next updating step. Thus our timescale corresponds to a series of events that lead to coexisting steady states of phage and bacteria strains.

We assign each bacterial strain a growth rate k_i selected uniformly $\in [0, 1]$. Moreover, $p_{ji} = p_{ij} = 1$ which reflects bacteria that interact directly by competing for a shared resource. $\eta_{ki} \in (0, 1)$ is sampled randomly and is considered to be a characteristic of every phage-bacterial strain interaction, while $\beta_k \in [1, 50]$ and is uniformly distributed and is a characteristic of each phage strain. Every new strain that is introduced to the system starts with a population density of 10^{-6}.

In the actual computation of the steady-state of a given strain combination, we follow Haerter et al. [18] and consider linear steady-state equations ($\frac{1}{B_i}\frac{dB_i}{dt} = 0$ and $\frac{1}{P_k}\frac{dP_k}{dt} = 0$) to evaluate whether these linear equations provide non-degenerate and feasible (positive) solutions. If the system with a newly added strain yields a feasible steady-state solution, the strain is added and the system is updated to this new steady state. Each time an added strain implies that solutions do not fulfil these criteria, at least one strain is bound to go extinct. When this happens in our computational models, we need to identify which strains should be dropped out of the system. To do this we start from the steady-state populations of the previous time step and integrate

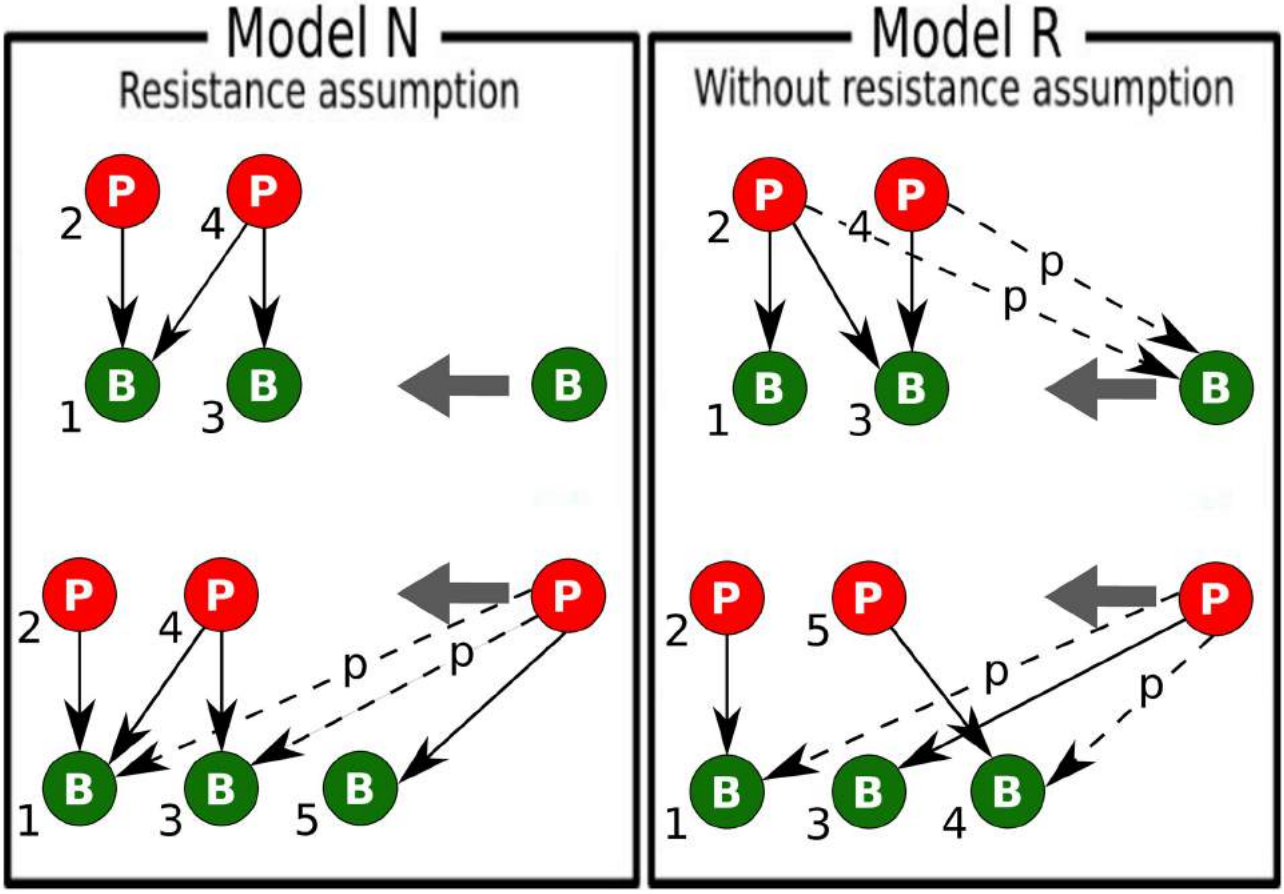

Fig 1. Schematic representation of Models N and R. The green (red) circles correspond to bacteria (phage) strains, hierarchically ordered from oldest to newest in the system (numbers). Notice that in model R, the new phage may attack a bacteria that is not the latest added. It just attacks whoever of the bacteria are not attacked by other phages (there can only be one of these). In model N the last added bacteria will automatically be the phage free one.

https://doi.org/10.1371/journal.pcbi.1010400.g001

the equations with the Runge–Kutta fourth-order method until one strain population falls below a very small threshold (10^{-20}).

We consider two models for the possible phage-bacteria interactions with a newly added strain (Fig 1). Model N (nested by construction) is based on the assumption that only bacterial strains resistant to all existing phages can enter the system. The phages that try to invade the system attack the bacterial strain that does not have a phage predator and in addition every other bacteria with probability $p \in [0, 1]$. This choice reflects the dominant population of the "phage-free" bacteria.

Model N will organize the bacteria historically, with the oldest being potentially infected by all phages, while the younger are only exposed to recently introduced phages. The model N will produce a diagonal network when $p = 0$ and a fully nested network when $p = 1$, the two extremes of nested networks that were studied in [18]. Here we generalize by further allowing for any value of p which will again yield sustainable interactions for balanced diversity. One of the main reasons for the study of model N is that there is a general consensus in the community that marine phage-bacteria networks exhibit significant nestedness [2, 3, 8, 9, 18, 20–22].

In Model R (random assignment of attack) we relax the rule about nested order of attack. Thus here we allow any of the already existing phages to attack the newly introduced bacteria with some probability $p \in [0, 1]$. Further, as in model N, a new phage is set to attack a bacterial

strain that doesn't have predators with probability 1 and every other bacteria with probability $p \in [0, 1]$. The model R will produce a network with all possible bacteria-phage pairs connected when $p = 1$.

Results

Fig 2 illustrates the dynamics of model R in time units of subsequent bacteria or phage invasion trials (see S1 Fig of the parallel plot for model N, which shows similar features). The central plot show existence of individual bacteria in terms of their growth rate.

The upper panel presents the vertical projection of the central plot in terms of the number of bacteria strains (red) and the total number of bacteria and phage strains (black). The fact that the total number of the strains is up to two times larger than the number of bacteria is in line with the balanced diversity manifested in the observational data analyzed by [18]. Also, the total number of strains is in agreement with the expectation from the narrowing staircase of the evolving "kill the winner" scenario of [18]. Furthermore, it is seen that even system's size extinction events are possible, reflected in occasional collapses to only one strain.

The right-hand side panels constitute a horizontal projection of the central figure. The first one (starting from the left) shows the growth-rate dependent probability density $p_{entry}(k)$ of bacteria to enter the system, while the second plot shows the average number density $N_B(k)$ of

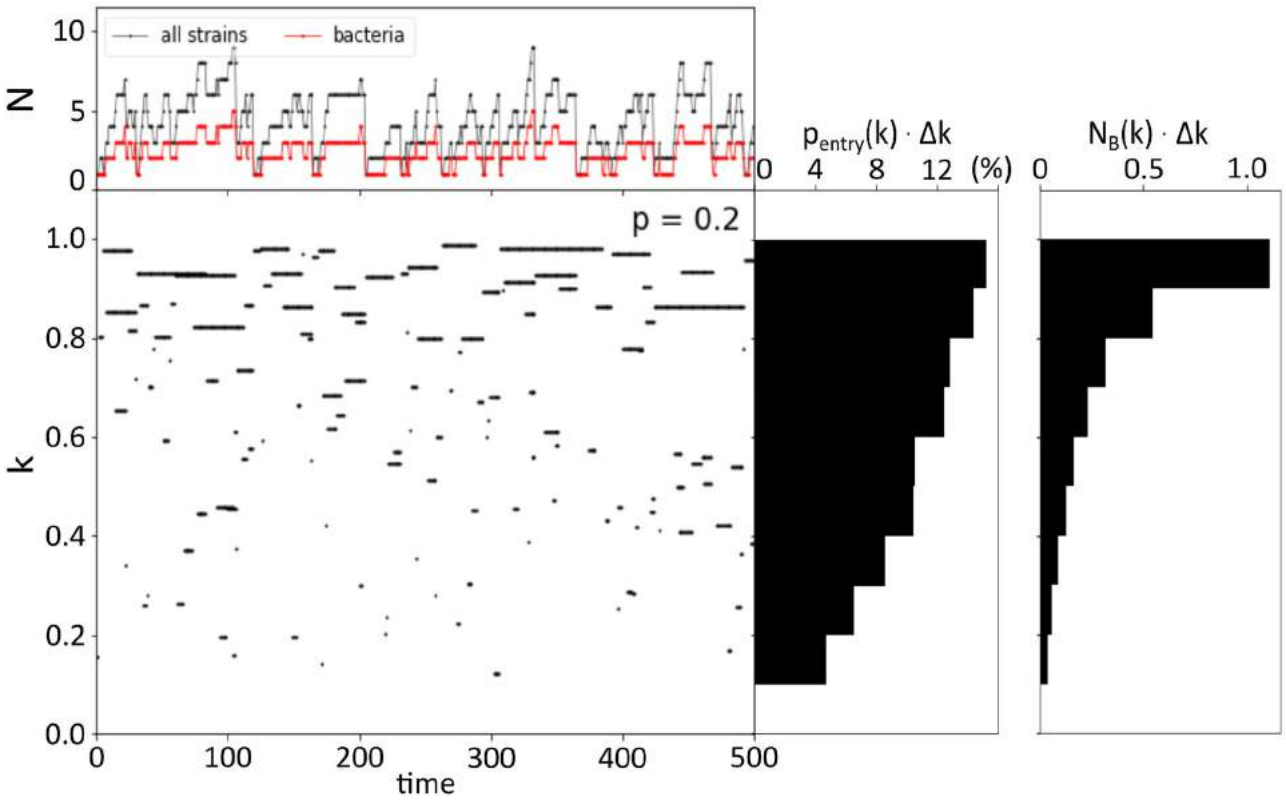

Fig 2. Evolutionary dynamics in Model R. The central plot shows the dynamic replacements of bacterial strains with time (cross-link probability $p = 0.2$). Each horizontal line corresponds to a bacterial strain, with the ordinate indicating its maximal growth rate. The top panel captures the number of bacterial strains (red line) and the total number of phages and bacteria (black line). The first right-hand panel displays $p_{entry}(k)\Delta k$, the distribution of the probability of a bacterial strain to enter the system as a function of its growth rate sampled over 10000 time-steps. The second right-hand panel shows $N_B(k)\Delta k$, the distribution of the average number of bacteria that exist at each time-step in the system as a function of their growth rate over 10000 time-steps. The bin size for sampling in k-space is taken to be $\Delta k = 0.1$.

https://doi.org/10.1371/journal.pcbi.1010400.g002

bacteria that exist at every time-step as a function of their growth rate. It is immediately apparent that there is a systematic tendency to favour a high growth rate. The central plot corroborates that result, as one can see that bacteria with high growth rates tend to live longer. Thus, although "kill the winner" is at play on a population level, with populations of fast growers being suppressed by phages, there is some long term advantage to being a fast-growing strain. However, there are situations where the fastest growing strain can be driven to extinction by a slower-growing one.

In order to understand the dynamics that govern those extinctions, we explore the network structure around strain extinction events. In Fig 3 we examine events where the fastest-growing bacteria (S) is replaced by a slower grower (R). We found that, when there is such an event, there is always a phage that infects both S and R. Therefore, the events are characterized by the ratio of the growth rate of the slow grower to the fast grower k_R/k_S in the vertical axis and the ratio of the common phage's infection rate to each strain η_R/η_S in the horizontal axis. Each of these events is marked by a dot and was triggered by the invasion of a new strain in the system. The colour of the dots indicates the type of these invasive strains (red for phages and green for bacteria). In Model N (Fig 3A and 3B), it is always the introduction of a phage that initiates the extinction because a slow-growing bacteria cannot eliminate any faster-growing bacteria without help. In contrast, in model R, extinctions of fast growing bacteria can be initiated by both a phage or a bacteria that support an already present phage (Fig 3C–3F).

These patterns can be easily understood when we consider the simpler system of only two competing bacteria and see how the system's diversity could possibly increase as a new strain is added to the system. In our single food source scenario, a faster and a slower-growing bacterium can only coexist with the help of a phage. Coexistence is then possible for a rather narrow set of parameters, provided that the slower grower is less exposed to the common phage than the faster grower (therefore represented as a bigger circle with S for faster-growing but more susceptible to phage attacks and a smaller circle with R for slower-growing but more resistant). This set of parameters is illustrated by the yellow area in Fig 3G [30, 31]. Remarkably, there is an even bigger range of parameters where the slower grower can out-compete the fastest grower and dominate the system. And of course, there is the biggest range of parameters where the fast-growing bacteria eliminates the slow grower (see S1 Appendix for the analytical calculation of these parameter regions). The striking similarity of the region where the faster growing but susceptible to the common phage goes extinct, between the Fig 3A–3F and 3G, constitutes a strong indication that the main mechanism through which a slower growing but resistant bacterial strain can out-compete a faster-growing yet susceptible to the common predator strain is through this triplet motif.

However, model N and R differ in the invasions that drive such extinctions. In Model N (Fig 3A and 3B), it is always the introduction of a phage that initiates the extinction, because of the assumption that the bacteria just entering the system are resistant to all existing phages. Therefore, the triplet with common phage can only be formed with the introduction of a phage strain that attacks both the faster-growing strain and the free, slow-growing bacteria that entered the system last before it.

On the other hand, extinctions in model R can be initiated by both a phage and a bacteria (Fig 3C–3F). When the probability p for connecting to existing strains is small, phages and bacteria invasions are equally likely to cause extinctions (see Fig 3C and 3E). However as p increases the extinction of the fastest grower is increasingly triggered by the invasion of a bacteria (Fig 3D and 3F). This reflects triplets formed by the bacteria that invade while having a link to an existing phage that is already preying on another bacteria. In a fully connected network as obtained for $p = 1$ in Model R, the probability for the formation of these triplet motifs is 1 already for total number of strains N = 3 and their number grows with the number of

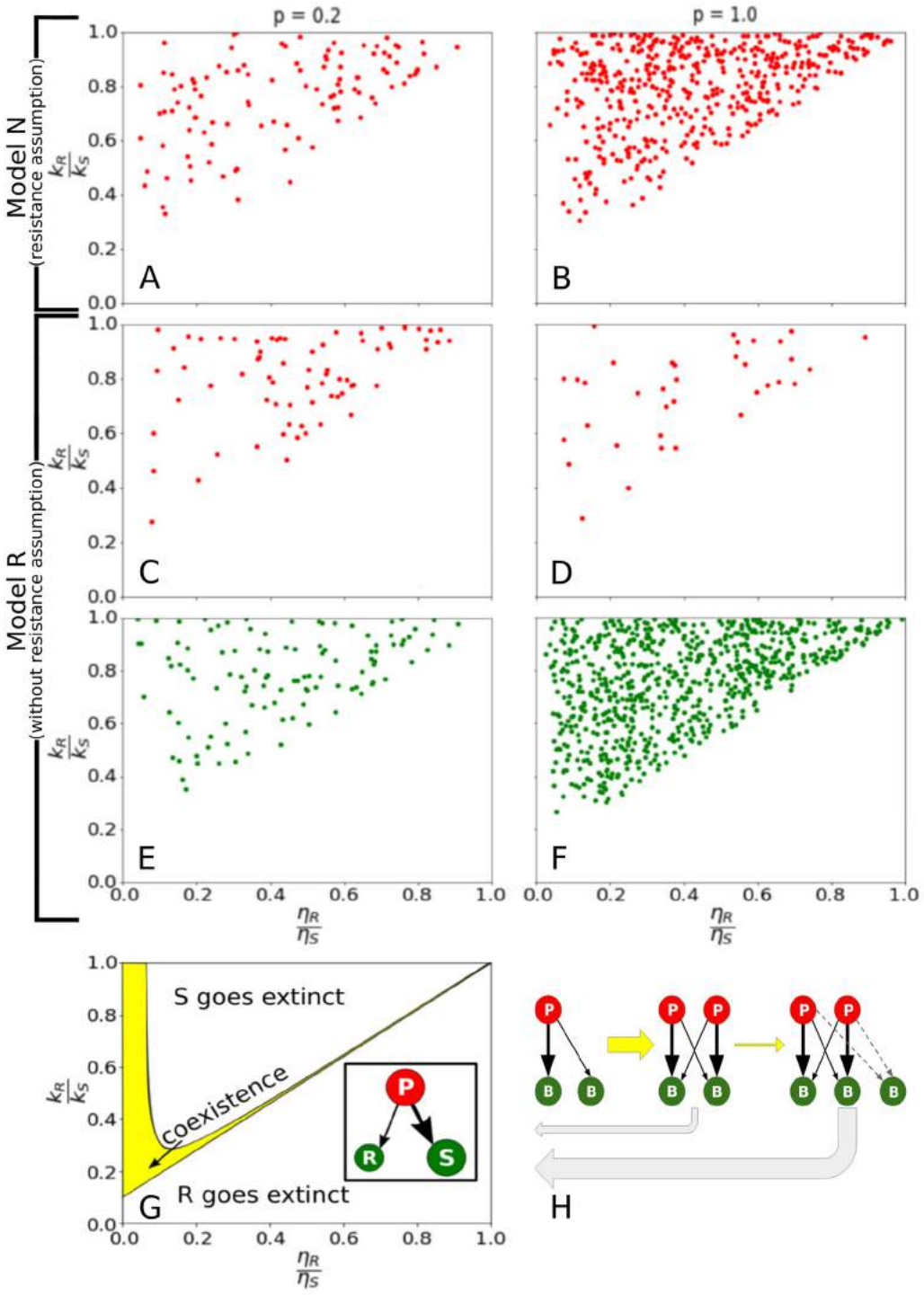

Fig 3. Extinction events. (A-F) Elimination of the fastest grower (S) by a slower-growing bacterial strain (R), using one common phage. The x-axis show ratio η_R/η_S of infection rates to the bacterial strain, while y-axis marks the ratio k_R/k_S of growth rates. Red dots mark events initiated by a phage while green dots mark events initiated by new a bacterial strain. (G) Analytically calculated regions of coexistence and extinctions for the above system (see S1 Appendix). The insert shows the motif with growth rates marked by circle size and susceptibility by the thickness of arrows. The yellow region marks the coexistence of all three strains. (H) Illustration of the evolution of the network as strains are added. Extinctions (grey arrows) are more likely as the system grows.

https://doi.org/10.1371/journal.pcbi.1010400.g003

bacteria strains $N_{bacteria}$ as $N_{bacteria}^2$ for $N > 3$. Therefore the closer our network is to the fully connected one, the higher the number of triplets that should be sustained (Fig 3H). As a result coexistence region becomes progressively narrower, setting practically an upper limit to the system's size and an increase in the number of extinction events of the fastest growing bacterial strain.

In addition to the replacement of the fastest grower, the detailed study of the network structure illuminates some interesting patterns in phage-bacteria ecology. In Fig 4, we show example networks from model N and model R at $p = 0.5$. Here, the link width is proportional to $\beta\eta$, which signifies the importance of the link. We see that both networks exhibit parallel strong links forming phage-bacteria pairs, even though a phage can infect multiple hosts and a host can be attacked by multiple phages. In other words, the predator-prey pairs are fairly specialized, reflecting a return to the "kill the winner" organization (where each strain had only one link).

We quantified how often this specialization is seen in our model (Fig 5A). We found that in about 90% of all stable ecosystems, all the strains form pairwise specialized predatory links that resemble the "kill the winner" structure. This means that stable ecosystems typically require phages that are disproportionately more adapted to infect the bacterial strain which is the most vulnerable to their attacks. This high prevalence of emergence of "kill the winner" systems was seen for both the N and the R model, decreasing from about 90% at $p \sim 0.1$ to 80% at $p \sim 1$. This close to the diagonal organization of predatory links in the bacteria-phage interaction matrix reflects a selection that minimizes similarity between phages and thereby reduces the competitive exclusion between the phages.

Fig 5B illustrates how the diversity decreases as the probability p of predatory links increases. In the $p = 0$ case where the interaction matrix is diagonal (See the subpanel Fig 5Bi), diversity is the highest because the role of the phages is limited to neutralizing bacterial competition. Hence, model N and model R are indistinguishable. As p increases the diversity decreases, reflecting a gradual change toward a system where all phages share the same resource (at $p = 1$) and competitive exclusion is only limited by different predation strengths of different phages (the $\beta\eta$'s). Furthermore, for larger p that maximal diversity in model N increasingly differs from that predicted by model R. This reflects the difference of the network structure at $p = 1$ for model N (subpanel Fig 5Bii) and model R (subpanel Fig 5Biii): more hierarchical predation increases phages' differences, which in turn decrease competitive exclusion. This tendency can also be seen in Fig 4, where phages in model N have a clear hierarchy of population sizes, while in model R phages have similar population sizes to each other due to competition.

Competitive exclusion implies that a system with more phage strains than bacterial strains is unstable [18]. Therefore, a growing diversity needs an introduction of a new bacterial strain. Subsequently, such a new bacteria makes it relatively easy for a new phage strain to invade, provided that it is the main predator of that last bacterial strain. Fig 5C demonstrates that model R effectively behaves as model N, in the sense that successful invading bacteria that add to the diversity nearly always are resistant to all existing phages. Fig 5C shows the fraction R/B of such events where the invader is resistant to all phages. For small and moderate p values one sees that increase in diversity almost always relies on invaders having such universal resistance, i.e. $R/B \sim 1$. First, for p exceeding 0.8, this fraction decreases. At $p \sim 1$ any invading bacteria are set to be attacked by all phages in the system, and thus R/B is forced to be 0. This suggests that the "bacterial resistance as a prerequisite for entrance" assumption that was intrinsic to model N emerges as a consequence of also the more relaxed assumptions in model R. This also suggests that the results from the nested model simulations from Ref. [18] would be recapitulated by model R although with a smaller overall diversity.

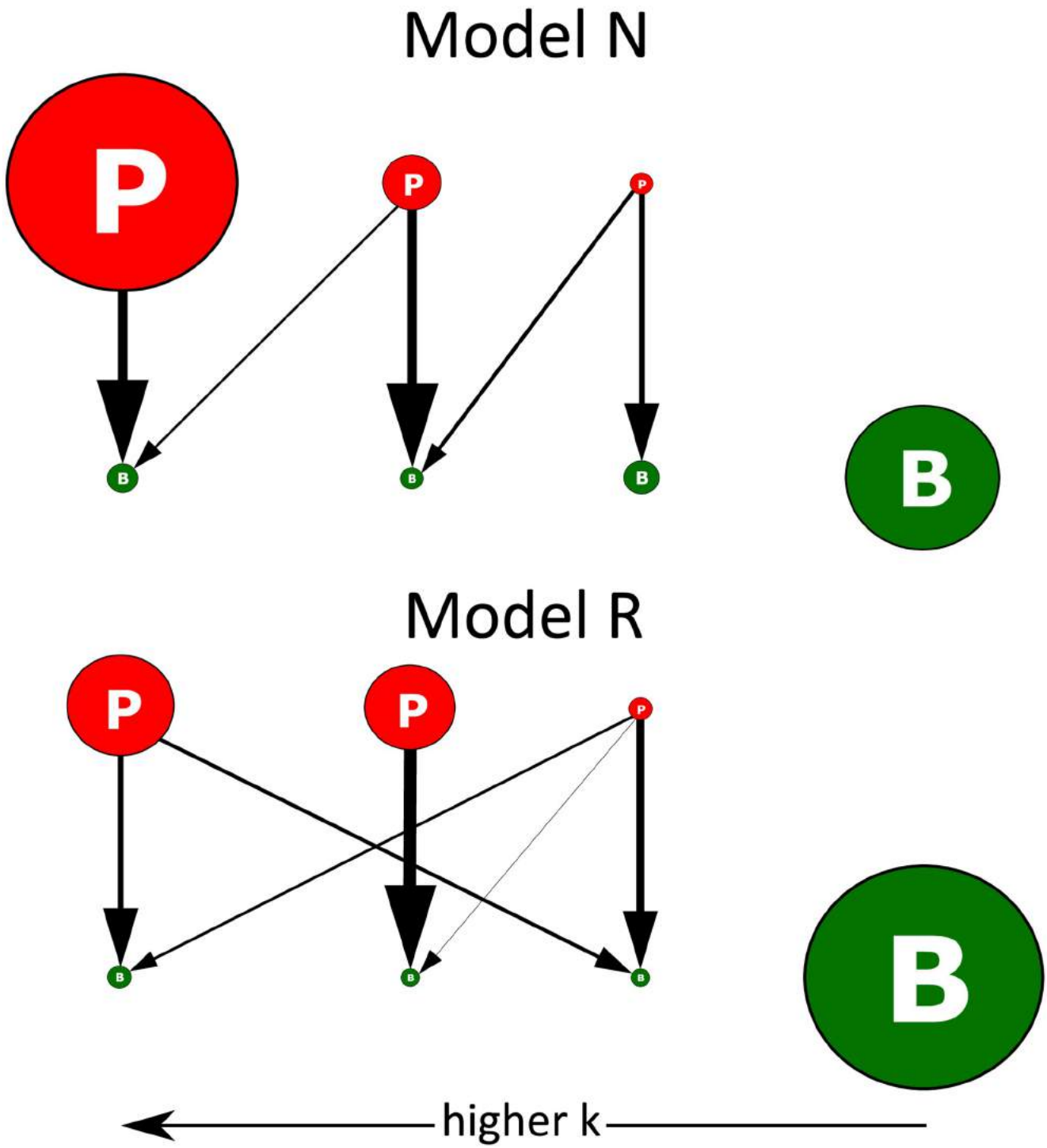

Fig 4. Example of interaction networks. The upper and lower panels show ecosystem examples for respectively the nested (N) and the random model (R). In model N the phage can only prey on bacteria that were present when the phage was introduced. This often concurs with the ordering after growth k, as older bacteria typically have larger k. In the model R an old phage can (with probability p) prey on a new bacteria which opens for the more random organization. Simulation is done with $p = 0.5$ and the sizes of the circles are proportional to the population. The width of the arrows is proportional to $\beta\eta$ of the corresponding interaction. Notice the parallel strong links that give rise to phage-bacteria pairs regarding dominant interactions.

https://doi.org/10.1371/journal.pcbi.1010400.g004

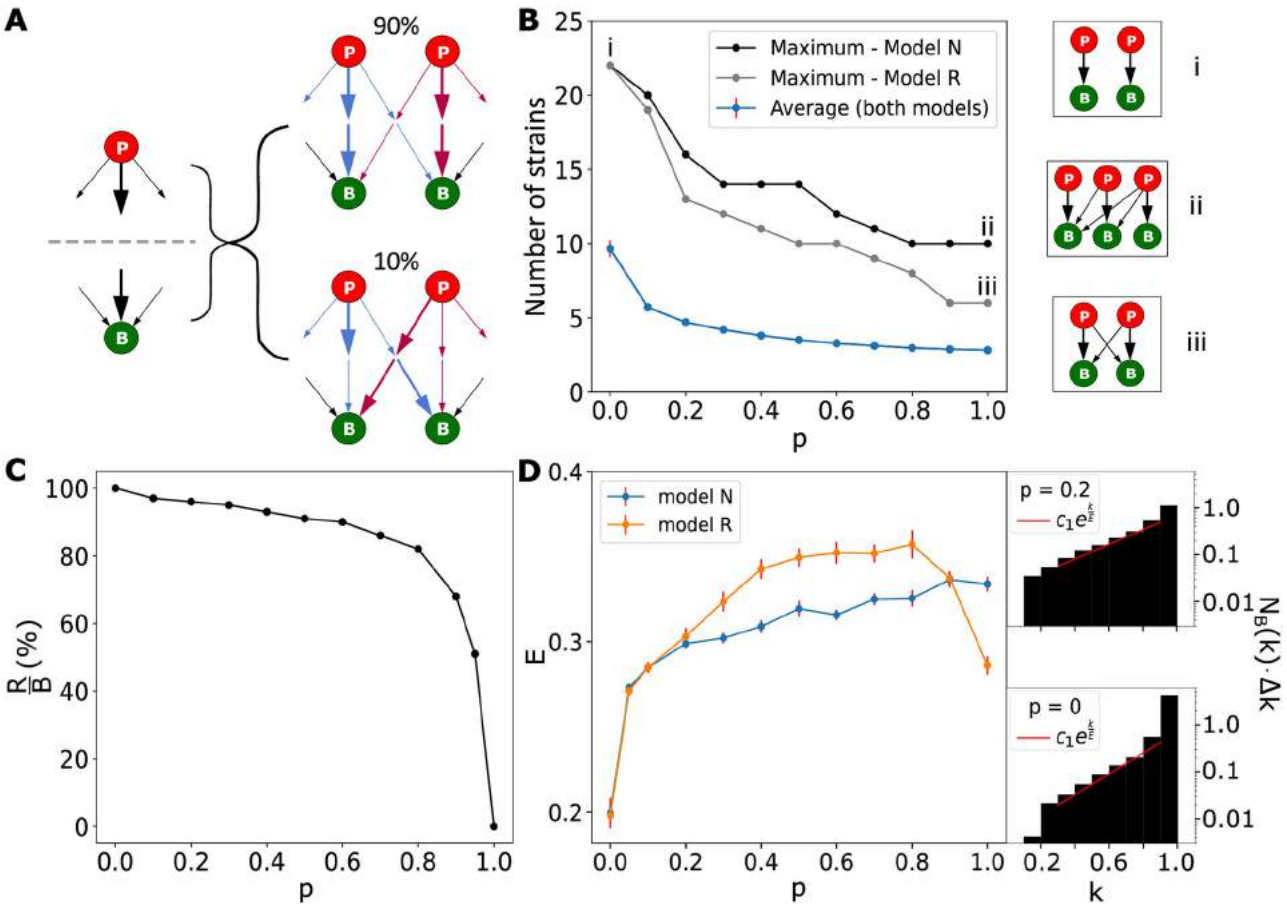

Fig 5. Analysis of evolved networks as a function of cross-link probability *p*. (A) Each phage (bacteria) has a number of links of different "strength" $\beta\eta$. In ∼90% of stable ecosystems, the strongest links (bold arrows) from phage and to bacteria coincide for all strains, forming pairs. Different arrow colors correspond to different phages. (B) Average and maximal diversity obtained for 10000 additions to the system. The sub-panels show characteristic networks at the corresponding points. (C) Analysing events in Model R where a new bacterial strain leads to increased diversity. The panel show the fraction of these events where the new bacteria are resistant to all preexisting phages. (D) The Elimination factor E of fast to slow growers as a function of p. The side panels show how the elimination factor is obtained from the scaling of steady-state diversity with the growth rate k. Both side panels correspond to model R.

https://doi.org/10.1371/journal.pcbi.1010400.g005

Overall we have seen that the two models are indistinguishable for small p: They have the same upper diversity limits, and their diversity increases with the successful addition of a new bacterial strain, which subsequently allows for the addition of a new phage strain and the extinctions of their fastest-growing bacteria obey the same rule. Their difference only emerges for larger p, where invading bacteria to a larger extent drives diversity down, resulting in increased relative diversity for model R as p increases beyond 0.2.

The most interesting aspect of varying p is the fact that it modulates the classical "kill the winner" scenario associated with $p = 0$ to a situation where the slow-growing bacteria do even better when p is just slightly above 0. This is quantified in Fig 5D where we plot the elimination factor E of the fastest grower compared to the slower-growing bacterial strains. This is defined by the least square fit of

$$N_B(k) \propto \exp\left(\frac{k}{E}\right)$$

for $k \in [0.3, 0.9]$, where $N_B(k)$ is the time-averaged number of bacteria as a function of the growth rate (see the right panels of Fig 5D for examples). A higher value of E represents relatively less diversity of faster bacteria compared to slower growers and correspondingly to a larger risk to be eliminated. Thus higher E represents an increased effect of eliminating the winner, while a low $E \sim 0.2$ at $p = 0$ reflects the traditional "kill the winner" model. We see that already for $p = 0.05$, a sharp rise of $E \sim 0.28$ is observed. This leads to a much more equal distribution of resources between bacteria with different sizes of growth speeds. This sharp mitigation of the advantage of the fastest growers with the slight probability for cross-link can also be seen in the entry to the system characterized by $p_{entry}(k)$ (cf. Fig 2), which is analyzed in the S2 Fig.

For $p \gtrsim 0.8$ Model R has markedly different behaviour from model N. This is seen in Fig 5C and 5D and S2 Fig. At such high p values the invading bacteria are attacked by most of the resident phages, and the few gains in diversity are often caused by invading bacteria that are susceptible to resident phages (Fig 5C). This makes differences between phages small and most parameters lead to eliminations by competitive exclusion. Furthermore, the phage load among bacteria becomes similar, and bacteria to a larger extent compete through their growth rate. As a consequence the maximal diversity decreases (Fig 5B) and the slope E drops (Fig 5D) for p above 0.8.

Discussion

This work investigated open systems of phages of bacteria, mimicking a small patch of the ocean exposed to meandering phages and bacteria from outside the patch. Such sub-systems were sampled in the Atlantic ocean by [2, 32] and analyzed in [20] and [18]. Flores et al. [9, 20] highlighted the nested structure of the overall interaction network, while Haerter et al. [18] emphasized the balanced diversity of phages and bacteria at each local patch. By considering each patch as an open dynamical system we here studied the emerging structure and robustness of the local microbial networks.

Our model considers subsequent random invasions of individual phage strains or bacterial strains. We observe dynamics where any strain is exposed to extinctions; even the fastest-growing bacteria (Fig 2). Hence diversity of the developing one patch system occasionally collapses to one, thereby mimicking the wide range of diversities reported from a number of samples from the Atlantic ocean (see [2, 18, 33, 34]).

The elimination of even the fastest grower by a slower-growing strain separates our model from the standard "kill the winner" model. The growth speed of the fastest grower is not monotonic in time [18] or requires small populations eliminated by noise as suggested by [25]. Furthermore, the term "kill" by Thingstad [8] refers to repression in numbers that leads to coexistence, while our analysis demonstrates the pronounced effect of occasional elimination of the fastest grower. In other words, while the growth rate-based fitness measure in the Fisher sense [17] is dynamically driven to a maximum value, this optimal is punctuated when a common predator exposes the system to extreme consequences of apparent competition [5]. Fig 3 demonstrated the basic motif for this elimination of fast growers [5, 30, 31], highlighting the requirement of a weaker phage exposure (lower η) for becoming a winner in spite of being a slower grower.

The concept of using phages as a weapon has been investigated previously by [35], where an immune strain with a prophage was using phages from spontaneous induction events to invade a sensitive strain. Thereby a temperate phage was able to lead to a population redistribution that only could be maintained if lysogens of the two strains had the same growth rate. In fact, even if the sensitive strain was always lysed by infections one would typically end in a

"kill the winner" type coexistence between a slower-growing lysogen and the faster growing sensitive strain.

Our evolving systems with virulent phages exhibit lower diversity when the apparent competition is increased (larger p in Fig 5B). This is what naively should be expected because higher p tends to diminish differences between predators, thereby increasing competitive exclusion. Remarkably, an increase in the frequency p of phage-bacteria interactions still leads to systems where each phage has a dominant host, and the host in turn is mainly predated by this same phage. In effect, the observed systems self-organise to resemble the diagonal "kill the winner" network supplemented with weaker cross-links (Fig 5A and 5C). This specialization emerges in order to minimize the competition between the phages and avoid competitive exclusion. This is different from the reasoning in classic trade-off theory, where specialization in interaction arises because it is costly for bacteria to sustain resistance to past phages and for phages to attack rare hosts [36, 37].

Perhaps the most remarkable aspect of cross-links is that they greatly favour the weak growers. Allowing phages to have more hosts, the pressure on the fast grower enhances and leads to a substantially larger diversity of the slow growers (Fig 5D and S2 Fig). The robustness of this effect is seen by the change in relative abundance when changing the model from the "kill the winner" scenario [8] with an implicit $p = 0$ to an "Eliminate the winner" model with a remarkably small but finite $p \sim 0.05$.

From a wider perspective, this paper investigated how the structure of microbial networks depends on the rules at which they are assembled [21–24]. We demonstrated that the dominant interaction structures in the obtained networks were robust to the assumption of whether additions were specialized, nested or random. We further found that the total diversity decreased with the likelihood that newly added species interact directly with resident species. Importantly, the most general model (R) obtained nested microbial networks as an indirect effect of competitive exclusion against invading bacteria. Nestedness and specialization may thus emerge in an open system, without the need for an evolution constrained by mutating genomes in a more closed system. That such evolutionary dynamics lead to similar network structures was demonstrated by [38].

Overall, predators are regulators of diversity already in the original "kill the winner" model [8], and mediators of competition already in the original "apparent competition" model [5]. But here they also put limits on any absolute measure of fitness in terms of reproductive rate. They are the mechanism for killing the winner at a new scale, where the winner is really eliminated and a new race for a new fastest grower can be restarted. Therefore evolution/replacement dynamics proceed in waves [39], often restarting when the fastest grower is replaced.

Supporting information

S1 Appendix. Analytical calculations of Fig 3G.
(PDF)

S1 Fig. Evolutionary dynamics in Model N. The central plot shows the dynamic replacements of bacterial strains with time (cross link probability $p = 0.2$). Each horizontal line corresponds to a bacterial strain, with the ordinate indicating its maximal growth rate. The top panel captures the number of bacterial strains (red line) and the total number of phages and bacteria, (black line). The first right hand panel displays the distribution of the probability of a bacterial strain to enter the system as a function of its growth rate sampled over 10000 time-steps. The second right hand panel shows the distribution of the average number of bacteria that exist at

each time-step at the system as a function of their growth rate over 10000 time-steps.
(TIF)

S2 Fig. Entry advantage related to growth rate. The central plot shows the relative entry advantage G_A of the fastest grower compared to the slower grower. The right subpanels display the definition of G_A as $G_A = \frac{slope}{P_{entry}(k=0.3)\Delta k}$ from the fitting of the distribution of the probability that a bacterial strain of growth rate k invades the system successfully. Both side panels correspond to model R but they would be practically the same for model N as one can see from the central panel.
(TIF)

Acknowledgments

The authors wish to thank Julius Bier Kirkegaard for the fruitful discussions on the computational method in this work.

Author Contributions

Conceptualization: Anastasios Marantos, Namiko Mitarai, Kim Sneppen.

Formal analysis: Anastasios Marantos.

Funding acquisition: Kim Sneppen.

Methodology: Anastasios Marantos, Namiko Mitarai, Kim Sneppen.

Project administration: Kim Sneppen.

Resources: Kim Sneppen.

Software: Anastasios Marantos.

Supervision: Namiko Mitarai, Kim Sneppen.

Validation: Anastasios Marantos, Namiko Mitarai, Kim Sneppen.

Visualization: Anastasios Marantos.

Writing – original draft: Anastasios Marantos, Namiko Mitarai, Kim Sneppen.

Writing – review & editing: Anastasios Marantos, Namiko Mitarai, Kim Sneppen.

References

1. Keen EC. A century of phage research: bacteriophages and the shaping of modern biology. BioEssays: news and reviews in molecular, cellular and developmental biology 37.1 2015; pp. 6–9.
2. Moebus K, Nattkemper H. Bacteriophage sensitivity patterns among bacteria isolated from marine waters Helgolander Meeresuntersuchungen 34.3 1981; pp. 375–385.
3. Kauffman KM, Chang WK, Brown JM, Hussain FA, Yang J, Polz MF, et al. Resolving the structure of phage-bacteria interactions in the context of natural diversity. Nature communications 13(1), 372, 2022. https://doi.org/10.1038/s41467-021-27583-z PMID: 35042853
4. Hutchinson GE. The Paradox of the Plankton. The American Naturalist 95.882, 1961; pp. 137–145. https://doi.org/10.1086/282171
5. Holt RD. Predation, apparent competition, and the structure of prey communities. Theoretical Population Biology 12, 1977; pp. 197–229. https://doi.org/10.1016/0040-5809(77)90042-9 PMID: 929457
6. Bergh Ø, Børsheim KY, Bratbak G, Heldal M. High abundance of viruses found in aquatic environments. Nature 340, 1989; pp. 467–468. https://doi.org/10.1038/340467a0 PMID: 2755508

7. Wilson JB. Mechanisms of species coexistence: twelve explanations for Hutchinson's'Paradox of the Plankton': evidence from New Zealand plant communities. New Zealand Journal of Ecology 13, 1990; pp. 17–42.
8. Thingstad TF. Elements of a theory for the mechanisms controlling abundance, diversity, and biogeochemical role of lytic bacterial viruses in aquatic systems. Limnology and Oceanography 45, 2000. https://doi.org/10.4319/lo.2000.45.6.1320
9. Weitz JS, Poisot T, Meyer JR, Flores CO, Valverde S, Sullivan MB, et al. Phage–bacteria infection networks. Trends in Microbiology 21.2, 2013; pp. 82–91. https://doi.org/10.1016/j.tim.2012.11.003 PMID: 23245704
10. Darwin C. On the Origin of Species by Means of Natural Selection, or The Preservation of Favoured Races in the Struggle for Life. John Murray, London, 1859.
11. Grinnell J. The origin and distribution of the chestnut-backed chickadee. The Auk 21, 1904; pp. 364–379. https://doi.org/10.2307/4070199
12. Volterra V. Variazioni e fluttuazioni del numero d'individui in specie animali conviventi. Memoria della regia accademia nazionale del lincei ser. 2, 1926; pp. 31–113.
13. Lotka AJ. The growth of mixed populations: Two species competing for a common food supply. Journal of the Washington Academy of Sciences 22(16/17), 1932; pp. 461–469.
14. Gause GF. The Struggle for Existence. Soil Science 41, 1936; p. 159. https://doi.org/10.1097/00010694-193602000-00018
15. Hardin G. The competitive exclusion principle. Science 131, 1960; pp. 1292–1297. https://doi.org/10.1126/science.131.3409.1292 PMID: 14399717
16. Levin SA. Community Equilibria and Stability, and an Extension of the Competitive Exclusion Principle. The American Naturalist 104, 1970; pp. 413–423. https://doi.org/10.1086/282676
17. Fisher RA. The Genetical Theory Of Natural Selection. The Clarendon Press, 1930.
18. Haerter JO, Mitarai N, Sneppen K. Phage and bacteria support mutual diversity in a narrowing staircase of coexistence. ISME Journal 8.11, 2014; pp. 2317–2326. https://doi.org/10.1038/ismej.2014.80
19. Thingstad TF, Våge S, Storesund JE, Sandaa R-A, Giske J. A theoretical analysis of how strain-specific viruses can control microbial species diversity. Proceedings of the National Academy of Sciences 111.21, 2014; pp. 7813–7818. https://doi.org/10.1073/pnas.1400909111 PMID: 24825894
20. Flores CO, Valverde S, Weitz JS. Multi-scale structure and geographic drivers of cross-infection within marine bacteria and phages. ISME Journal 7, 2013; pp. 1–13. https://doi.org/10.1038/ismej.2012.135 PMID: 23178671
21. Jover LF, Cortez MH, Weitz JS. Mechanisms of multi-strain coexistence in host-phage systems with nested infection networks. Journal of Theoretical Biology 332, 2013; pp. 65–77. https://doi.org/10.1016/j.jtbi.2013.04.011 PMID: 23608631
22. Jover LF, Flores CO, Cortez MH, Weitz JS. Multiple regimes of robust patterns between network structure and biodiversity. Scientific Reports 5, 2015. https://doi.org/10.1038/srep17856 PMID: 26632996
23. Gould SJ, Lewontin RC. The spandrels of San Marco and the Panglossian paradigm: a critique of the adaptationist programme. Proceedings of the royal society of London. Series B. Biological Sciences 205.1161, 1979; pp. 581–598.
24. Maynard DS, Servan CA, Allesina S. Network spandrels reflect ecological assembly. Ecology letters 21.3, 2018; pp. 324–334. https://doi.org/10.1111/ele.12912 PMID: 29377488
25. Xue C, Goldenfeld N. Coevolution maintains diversity in the stochastic "Kill the Winner" model. Physical review letters 119.26, 2017; p. 268101. https://doi.org/10.1103/PhysRevLett.119.268101 PMID: 29328693
26. Lotka AJ. Elements of Physical Biology. Williams and Wilkins, 1925.
27. Campbell A. Conditions for the Existence of Bacteriophage. Evolution 15, 1961; pp. 153–165. https://doi.org/10.1111/j.1558-5646.1961.tb03139.x
28. Fuhrman JA, Noble RT. Viruses and protists cause similar bacterial mortality in coastal seawater. Limnology and oceanography 40.7, 1995; pp. 1236–1242. https://doi.org/10.4319/lo.1995.40.7.1236
29. Noble RT, Fuhrman JA. Virus decay and its causes in coastal waters. Applied and Environmental Microbiology 63.1, 1997; pp. 77–83. https://doi.org/10.1128/aem.63.1.77-83.1997 PMID: 16535501
30. Levin BR, Stewart FM, Chao L. Resource-Limited Growth, Competition, and Predation: A Model and Experimental Studies with Bacteria and Bacteriophage. The American Naturalist 111, 1977; pp. 3–24. https://doi.org/10.1086/283134
31. Haerter JO, Sneppen K. Spatial structure and Lamarckian adaptation explain extreme genetic diversity at CRISPR Locus. mBio 3, 2012; p. 4. https://doi.org/10.1128/mBio.00126-12 PMID: 22807565

32. Moebus K, Nattkemper H. Taxonomic investigations of bacteriophage sensitive bacteria isolated from marine waters. Helgolander Meeresuntersuchungen 36.4, 1983; pp. 357–373. https://doi.org/10.1007/BF01983456

33. Wichels A, Biel S, Gelderblom H, Brinkhoff T, Muyzer G, Schütt C. Bacteriophage Diversity in the North Sea. Applied and environmental microbiology 64, 1998; pp. 4128–33. https://doi.org/10.1128/aem.64.11.4128-4133.1998 PMID: 9797256

34. Holmfeldt K, Middelboe M, Nybroe O, Riemann L. Large Variabilities in Host Strain Susceptibility and Phage Host Range Govern Interactions between Lytic Marine Phages and Their Flavobacterium Hosts. Applied and Environmental Microbiology 73.21, 2007; pp. 6730–6739. https://doi.org/10.1128/AEM.01399-07 PMID: 17766444

35. Brown SP, Le Chat L, De Paepe M, Taddei F. Ecology of microbial invasions: amplification allows virus carriers to invade more rapidly when rare. Current Biology 16.20, 2006; pp. 2048–2052. https://doi.org/10.1016/j.cub.2006.08.089 PMID: 17055985

36. Brodie ED III, Brodie ED Jr. Evolutionary response of predator to dangerous prey-reduction of toxicity of newts and resistance of garter snakes in island populations. Evolution 45.1, 1991; pp. 221–224. https://doi.org/10.1111/j.1558-5646.1991.tb05280.x

37. Bowen L, Van Vuren D. Insular endemic plants lack defenses against herbivores. Conservation Biology 11.5, 1997; pp. 1249–1254. https://doi.org/10.1046/j.1523-1739.1997.96368.x

38. Beckett SJ, Williams HTP. Coevolutionary diversification creates nested-modular structure in phage–bacteria interaction networks. Interface focus 3.6, 2013; p. 20130033. https://doi.org/10.1098/rsfs.2013.0033 PMID: 24516719

39. Maslov S, Sneppen K. Diversity waves in collapse-driven population dynamics. PLoS computational biology 11.9, 2015; e1004440. https://doi.org/10.1371/journal.pcbi.1004440 PMID: 26367172

2.6 Manuscript: Sustainable Diversity of Phage-Bacteria Systems

Authors: Namiko Mitarai*, **Anastasios Marantos***, Kim Sneppen*

Affiliations: *Center for Models of Life, Niels Bohr Institute, University of Copenhagen, Copenhagen, Denmark

My contributions: I contributed mainly to the first part of the paper which was based on our previous work titled "From Kill the Winner to Eliminate the Winner in Open Phage-Bacteria Systems" by producing and processing the data required for the new figure and in the writing/editing/reviewing part as well as by providing references to the literature. In the rest two parts my contribution was limited. I contributed to the writing/editing/reviewing part and by providing references to the literature.

Supervision: I worked under the supervision of Prof. Kim Sneppen and Assoc. Prof. Namiko Mitarai who were the main authors of this work.

Publication status: Published in Current Opinion in Systems Biology

DOI: 10.1016/j.coisb.2023.100468

Available online at www.sciencedirect.com

ScienceDirect

Current Opinion in Systems Biology

Sustainable diversity of phage-bacteria systems

Namiko Mitarai, Anastasios Marantos and Kim Sneppen

Abstract

Bacteriophages are central to microbial ecosystems for balancing bacterial populations and promoting evolution by applying strong selection pressure. Here, we review some of the known aspects that modulate phage–bacteria interaction in a way that naturally promotes their coexistence. We focus on the modulations that arise from structural, physical, or physiological constraints. We argue they should play roles in many phage–bacteria systems providing sustainable diversity.

Addresses

The Niels Bohr Institute, University of Copenhagen, Blegdamsvej 17, Copenhagen, 2100 Ø, Denmark

Corresponding author: Mitarai, Namiko (mitarai@nbi.ku.dk)

Current Opinion in Systems Biology 2023, **35**:100468

This review comes from a themed issue on **Systems Ecology & Evolution (2023)**

Edited by **Edu Kussell and Nobuto Takeuchi**

For a complete overview see the Issue and the Editorial

Available online 1 June 2023

https://doi.org/10.1016/j.coisb.2023.100468

Keywords

Virulent phage, Kill the winner, Colony, Spatial refuge, Dormancy.

Introduction

Bacteriophages play a critical role in balancing and sometimes reshaping microbial ecosystems, supporting the diversity of bacterial strains [1–4] and in facilitating the transmission of genes between different bacterial strains [5] and species [6]. Genetic engineering and gene-editing in modern biotechnology are by-products of the fitness gain of bacteria when they protect themselves from phages by restriction-modification enzymes [7,8] or CRISPR systems [8–11]. Future explorations in phage resistance mechanisms will likely unravel other aspects [12–16] of the aeon-long war between these dominating life forms [17,18] on our planet. Here, we will review parts of this vast area of research that modulate these interactions to make the system more sustainable in the long term (Figure 1), focusing on 1) phages' ability to reshuffle optimal bacterial growth, 2) the effect of spatial refuges against unlimited phage predation, and 3) implications of the phage lysis dependence on the physiological state of hosts.

Eliminating the winner: ongoing reshuffling of bacterial fitness

The resource competition and resulting exclusion make it hard for bacterial species to coexist when they require similar nutrients for growth [19,20]. This challenges the observation of diverse microbial communities. Several mechanisms have been proposed, including the cross-feeding of metabolites among different species [21–23], a variation of affinity to slightly different nutrient sources [24], and spatial in-homogeneity [25,26].

This situation changes dramatically once we consider bacteriophages [1,3,4,27–29]. Virulent phage specialized in predating on bacterial species keeps the bacterial species population down, and the growth rate of the bacteria is only reflected in the phage population size [30], making the nutrient available for more slowly-growing bacterial competitors that otherwise cannot coexist. This phenomenon is called 'Kill the Winner' [1], and it predicts that slow and fast-growing bacterial species stably co-exist. Notably, however, the slower-growing bacteria are exposed to elimination by invading faster-growing bacteria, provided these invaders sometimes have time without phage predators. An open system with an occasional invasion of new bacteria and phage species tends to evolve towards a state with faster-growing bacterial species intermittently [3,4,31].

However, if individual phage species can prey on several bacteria species, the long-term prediction deviates from this scenario. Such cross-interactions make the apparent competition [32] possible, where the slowly growing bacteria may out-compete the faster grower [4] by being less susceptible to the common phage, even when the bacterial species compete for the nutrient source. This is illustrated in Figure 2, where we follow the development of an open microbial ecosystem as a function of time counted as the number of bacterial or phage species that enter the system [4]. The model assumes *one* common food source for all species. It is simulated in the quasi-steady state approximation where new species are only added when the temporal dynamics of previous species are settled to a steady state. The interaction between the existing species and the newly added species is assigned

Figure 1

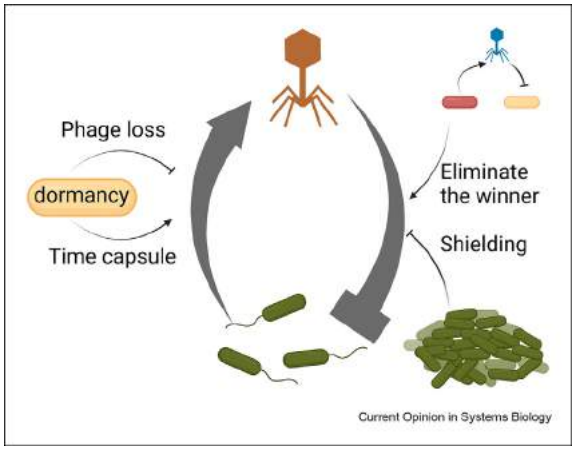

Modulation of phage–bacteria interactions for sustainable diversity. Created with Biorender.com.

randomly, with the possibility of cross-interactions (Figure 2). Figure 2 illustrates the growth rate for each co-existing bacteria, with a colour that marks the bacterial population in units of total carrying capacity.

Figure 2 shows that 1) even bacterial hosts with very high growth rates can be eliminated, 2) newly introduced bacteria often settle at relatively high populations soon after the introduction and subsequently tend to lose population with additions of other competing strains or phages, and 3) High populations of any particular strain are highly transient, while states with about 10% or lower population density stay longer without big changes.

While this model analysed a completely open system where newly added species properties are chosen independently of existing species, new species may appear due to mutation in a closed system. Hence, their properties are correlated with existing species [33]. Such a coevolution model gives a nested-modular structure to the resulting interaction network [34]. A recent study following a coevolving wild population has indicated a local adaptation, i.e., phages are best at infecting the co-occurring hosts [35]. Interestingly, it has been shown that occasional immigration of phages from outside of a subsystem accelerates the local adaptation by introducing more genetic variation [36]. For a quantitative understanding of phage-bacteria ecosystem data [37,38], a complete approach would be combining local co-evolution with invasion from outside of the system.

Space mediated defence: micro-colony and self-organised spatial refuges against phages

The above consideration of co-existence suffers from the classical limitations of ecosystem stability for well-mixed systems described by differential equations

Figure 2

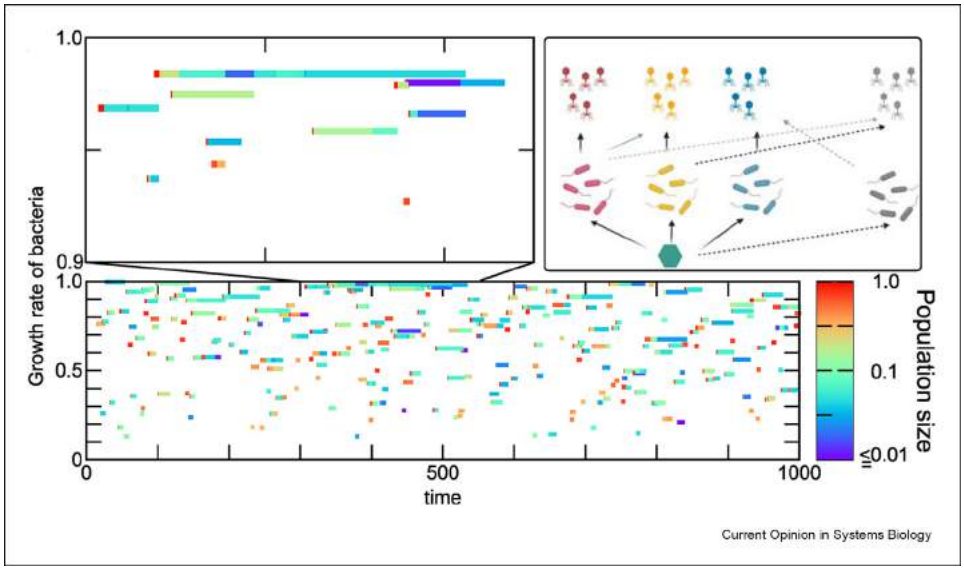

From Kill the winner to Eliminate the winner. The plot shows the time evolution of the coexisting bacterial species' growth rate (vertical axis) and population size (colour bar). The lower panel shows a long time course, and the upper panel shows the magnification of the indicated duration. The box figure shows a schematic description of the model (Created with Biorender.com). There is one nutrient source for bacteria feeding all the bacterial species, and phages can predate on one or more bacterial species with variable strength (solid allows). New phage or bacterial species are added to the system one by one randomly after the system reaches the steady state. The predation link between the newly added and existing species (dotted arrows) is drawn randomly. The details of the model are given in the study by Marantos et al. [4] as model R.

[39]. However, in real ecosystems, forming spatial refuges is crucial [25]. For example, coral reefs support a huge diversity of life by providing hiding places against larger predators. The diverse possibility of how a life form can provide hiding for some life forms from their competitors makes formal modelling difficult. One such toy model was to consider the non-transient interactions between lichen species on a rock surface [40], predicting the existence of stable states with high diversity when each species directly interfere only a fraction of other species and if the fraction is below a threshold.

Even a sub-millimetre scale of spatial heterogeneity is sufficient for a microbial system to provide a spatial refuge. Here we consider phages interacting with bacteria on a colony boundary [43,44]. In particular, we study bacterial colonies' survival when exposed to a virus [41,42]. One sees a plaque in Figure 3 formed on a bacterial lawn initially infected by a single virulent phage [41]. Here, a small number of phages were mixed with bacteria in a soft agar, cast on a hard agar with nutrients, and incubated. Subsequently, most single bacteria grew into small colonies since the agar was too viscous for bacteria to be motile. Some bacteria were attacked by the phage or by its progeny as phages grow and spread by diffusion between the growing microcolonies. Noticeably, increasing remnants of phage-attacked colonies are observed as one approaches the periphery of the plaque from the inside. This indicates that larger colonies upon phage attack provide some resistance against phage proliferation, and thus that bacteria inside a colony are partly protected.

In [42], we infected colonies of various sizes with a virulent mutant of the temperate bacteriophage P1. We found that colonies larger than $\sim 10^5$ cells at the first phage attack survived and grew under phage predation, while smaller colonies could not. The possible mechanism is illustrated in agent-based simulations in Figure 3. The phages are modelled as point particles that diffuse in space and infect a bacterial cell upon encountering it. As a result, cells on the colony surface are infected at high multiplicity [45], and phages cannot diffuse long inside a colony before they are adsorbed. The colony becomes surrounded by infected and dying bacteria while its non-infected inside grows. When the growth of the bacteria inside the 3-dimensional colony exceeds the death on the 2-dimensional surface layer, the colony can survive. Thus, a tipping point for colony survival primarily depends on phage adsorption and phage latency time relative to the bacterial growth rate [42].

The collective protection from phage attack in a colony is empowered further when the bacteria produce extracellular structures that constitute a large part of the biofilm [46]. For example, the collective protection by expression of curli polymer that can trap T7 phage enables matured enough *Escherichia coli* biofilm to keep growing under phage attack [47,48]; more complex collective protection has been reported recently in a multispecies biofilm [49]. A simulation study confirmed that the mobility of phage is the key when attacking a biofilm [50].

From a larger perspective, a medium with many colonies will naturally be able to sustain phage attacks and be much more robust than the homogeneously mixed system. While the dense colony appears as a large target for phage to encounter by diffusion, the overall adsorption rate will be reduced compared to all the cells being dispersed uniformly in the media [51,52]. The more the phage encounter is delayed, the larger the microcolony becomes, providing better collective protection. When effectively simulating the shielding of phage attack at the colony surface and the phage diffusion between

Figure 3

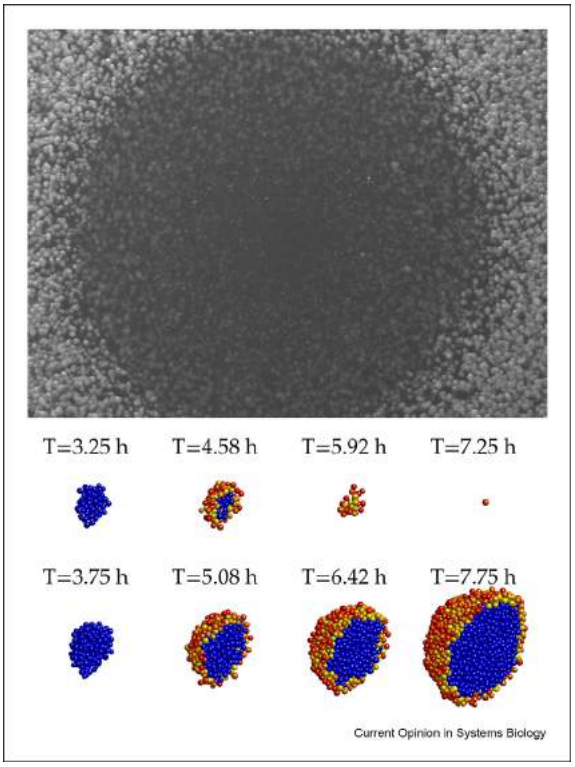

Role of microcolonies and space. The top image visualizes plaque formed by Cl^- mutant of the λ phage, which acts as a virulent phage when infecting a sensitive *Escherichia coli* cell (Image from the study by Mitarai et al. [41]). The white does are bacterial colonies. The killing zone by phage (plaque) appears as a darker region. The radius of the plaque is about one millimetre. The bottom panel shows a simulation of a microcolony attached by a phage from outside (Cross sections are shown, image from the study by Eriksen et al. [42]). Blue spheres are uninfected bacterial cells, and yellow to red spheres are the infected cells in the latency period. Phage particles are not visualised. When the first phage attack is early (i.e., the colony is small, top panel), all the cells can eventually be killed. In contrast, when the colony size upon the first phage attack is large enough, the colony can keep growing despite the continuous killing by the phage on the surface.

colonies, robust survival of bacteria and phage have been predicted when bacteria grow as microcolony [53].

How to deal with an inactive host: dependence on the host's physiological condition

Since the production of the phage depends on the infected host's ability to replicate genetic materials (DNA or RNA) and produce proteins (though some phages bring in genes for machinery), the phage growth inevitably depends on the host's physiological states. It has been demonstrated that phage production decreases as the bacterial growth rate slows down [54–59]. A mathematical analysis has demonstrated that such physiology dependence can support a new mode of coexistence between bacteria and virulent phage [60]. It is necessary to consider the phage production dependence on the bacterial growth rate to reproduce the plaque morphology and final size in a mathematical model [41]. However, it is worth noting that exceptions such as T7 can keep spreading in a stationary phase loan at a limited speed [61]. Since bacterial growth is limited in various natural environments, it is crucial to investigate the physiology dependence to fully understand the phage-bacteria ecosystem and evolution.

Interestingly, the host physiology dependence is not limited to the phage yield after infection. Recently, we found that a phage preferentially adsorbs to metabolically active bacteria [62]. More specifically, the wild type λ-phage adsorption dropped significantly when the host cell was metabolically inactive, possibly by detecting the hyperdiffusion of the receptor protein in growing *E. coli* [63] that ceases on energy depletion [64]. This phenomenon requires a particular design of the wild type λ-phage's tail protein that allows the virus to bind reversibly, which is lost in a λ host range mutant [65]. The preference to infect metabolically more active cells may increase overall phage growth in an environment where hosts with different physiological states are accessible.

Should a phage always avoid injecting its genetic material into a metabolically inactive host? Of course, infecting a dead host cell will be a pure waste for a phage. However, infecting a dormant but alive host [66,67] may have a long-term benefit. An interesting example is a phage which infects bacteria such as *Bacillus subtilis* that can form an endospore under certain stressed conditions. Endospores are metabolically inert but can survive under extreme stresses and germinate to regrow when the condition is right again after an immense period [68]. Many phages that infect spore-forming bacteria can form a 'virospore', i.e., an endospore where the phage genome is also encapsulated [69,70]. When a virospore germinates, the phage can undergo the lytic cycle to produce phage progeny. Another example is a phage infecting a dormant persister *E. coli* cell, where a lytic phage stayed silent while the host was in dormancy, but as soon as the host resumed its growth, phage replication also resumed to complete the lytic cycle [71]. It has been proposed [72–75] that survival in a very low host density environment is a possible selection pressure for phage to be temperate, i.e., a phage can enter the lysogeny [76] where it stays dormant, and its genetic material can be replicated with the host replication. Even though the 'pseudolysogeny'-like [77] behaviour by infecting dormant cells does not provide immediate growth of the phage population, it may serve as a time capsule for a virulent phage to survive a harsh environment for a phage particle.

Outlook

We have presented a few aspects of phage-bacteria interactions that make the coexistence of many species more sustainable (Figure 1). The 'Eliminate the winner' due to possible interaction network structure opens for slow growers to remain in the ecosystem. A dense bacterial colony provides 'shielding for bacteria deep inside the colony by cells on the surface, absorbing most of the phages attacking from outside. The phage proliferation dependence on host physiology may reduce the impact of phage attack when infected dormant cells do not produce progeny ('Phage loss'). At the same time, if a phage can resume proliferation when an infected dormant cell resuscitates, infecting a dormant cell may work as a 'Time capsule' for the phage where the cell and phage stay dormant together and preserved through a crisis that is hard for a phage to survive alone.

These modulations are not specific to certain molecular mechanisms and therefore expected to be effective in phage-bacteria ecosystems in general. In addition, players in these systems exhibit many other strategies that makes the system even more sustainable. We have briefly mentioned the lysis-lysogeny choice in temperate phage [72–75]; such temperate phage may themselves carry genes that prevent invasion of other phage types [78] or genes that allow using other phage genomes to produce offspring (pirate phages [79–81]). Many phage defence mechanisms and anti-phage defence mechanisms obviously contribute to sustaining the phage-bacteria coexistence and diversity arising from coevolution [7,8,11,16]. The fascinating diversity of molecular mechanisms challenges the theoretical microbial ecology to provide a unified picture to help us navigate different systems' individuality.

Declaration of competing interest

The authors declare that they have no known competing financial interests or personal relationships that could have appeared to influence the work reported in this paper.

Data availability

Data will be made available on request.

Acknowledgement

This work was supported by Novo Nordisk Foundation (NNF21OC0068775).

References

Papers of particular interest, published within the period of review, have been highlighted as:

* of special interest
** of outstanding interest

1. Thingstad TF: **Elements of a theory for the mechanisms controlling abundance, diversity, and biogeochemical role of lytic bacterial viruses in aquatic systems**. *Limnol Oceanogr* 2000, **45**:1320–1328.

2. Thingstad T, Våge S, Storesund JE, Sandaa R-A, Giske J: **A theoretical analysis of how strain-specific viruses can control microbial species diversity**. In *Proceedings of the National Academy of Sciences*, **111**; 2014:7813–7818.

3. Haerter JO, Mitarai N, Sneppen K: **Phage and bacteria support mutual diversity in a narrowing staircase of coexistence**. *ISME J* 2014, **8**:2317–2326.

4. ** Marantos A, Mitarai N, Sneppen K: **From kill the winner to eliminate the winner in open phage-bacteria systems**. *PLoS Comput Biol* 2022, **18**, e1010400.
Model analysis on "eliminate the winner".

5. Dixit PD, Pang TY, Studier FW, Maslov S: **Recombinant transfer in the basic genome of escherichia coli**. In *Proceedings of the National Academy of Sciences*, **112**; 2015:9070–9075.

6. Koonin EV, Dolja VV: **A virocentric perspective on the evolution of life**. *Current opinion in virology* 2013, **3**:546–557.

7. Eriksen RS, Malhotra N, Seshasayee ASN, Sneppen K, Krishna S: **Emergence of networks of shared restriction-modification systems in phage–bacteria ecosystems**. *J Biosci* 2022, **47**:38.

8. ** Tesson F, Bernheim A: **Synergy and regulation of antiphage systems: toward the existence of a bacterial immune system?** *Curr Opin Microbiol* 2023, **71**, 102238.
Timely review on phage defence systems.

9. Jinek M, Chylinski K, Fonfara I, Hauer M, Doudna JA, Charpentier E: **A programmable dual-rna–guided dna endonuclease in adaptive bacterial immunity**. *Science* 2012, **337**:816–821.

10. Ishino Y, Krupovic M, Forterre P: **History of crispr-cas from encounter with a mysterious repeated sequence to genome editing technology**. *J Bacteriol* 2018, **200**, e00580. 17.

11. Rostøl JT, Marraffini L: **(ph) ighting phages: how bacteria resist their parasites**. *Cell Host Microbe* 2019, **25**:184–194.

12. Scholl D, Adhya S, Merril C: **Escherichia coli k1's capsule is a barrier to bacteriophage t7**. *Appl Environ Microbiol* 2005, **71**: 4872–4874.

13. Song S, Wood TK: **A primary physiological role of toxin/antitoxin systems is phage inhibition**. *Front Microbiol* 2020, **11**: 1895.

14. Chaudhry W, Lee E, Worthy A, Weiss Z, Grabowicz M, Vega N, Levin B: **Mucoidy, a general mechanism for maintaining lytic phage in populations of bacteria**. *FEMS (Fed Eur Microbiol Soc) Microbiol Ecol* 2020, **96**. fiaa162.

15. Laughlin TG, Deep A, Prichard AM, Seitz C, Gu Y, Enustun E, Suslov S, Khanna K, Birkholz EA, Armbruster E, *et al.*: **Architecture and self-assembly of the jumbo bacteriophage nuclear shell**. *Nature* 2022, **608**:429–435.

16. Millman A, Melamed S, Leavitt A, Doron S, Bernheim A, Hör J, Garb J, Bechon N, Brandis A, Lopatina A, *et al.*: **An expanded arsenal of immune systems that protect bacteria from phages**. *Cell Host Microbe* 2022, **30**:1556–1569.

17. Whitman WB, Coleman DC, Wiebe WJ: **Prokaryotes: the unseen majority**. In *Proceedings of the National Academy of Sciences*, **95**; 1998:6578–6583.

18. Breitbart M, Rohwer F: **Here a virus, there a virus, everywhere the same virus?** *Trends Microbiol* 2005, **13**:278–284.

19. Gause G: *The struggle for existence*. Baltimore, Maryland: Williams & Wilkins; 2008.

20. Hardin G: **The competitive exclusion principle: an idea that took a century to be born has implications in ecology, economics, and genetics**. *Science* 1960, **131**:1292–1297.

21. Seth EC, Taga ME: **Nutrient cross-feeding in the microbial world**. *Front Microbiol* 2014, **5**:350.

22. Goldford JE, Lu N, Bajić D, Estrela S, Tikhonov M, Sanchez-Gorostiaga A, Segrè D, Mehta P, Sanchez A: **Emergent simplicity in microbial community assembly**. *Science* 2018, **361**:469–474.

23. Goyal A, Maslov S: **Diversity, stability, and reproducibility in stochastically assembled microbial ecosystems**. *Phys Rev Lett* 2018, **120**, 158102.

24. Wang Z, Goyal A, Dubinkina V, George AB, Wang T, Fridman Y, Maslov S: **Complementary resource preferences spontaneously emerge in diauxic microbial communities**. *Nat Commun* 2021, **12**:1–12.

25. Tilman D: **Competition and biodiversity in spatially structured habitats**. *Ecology* 1994, **75**:2–16.

26. Yanni D, Márquez-Zacarías P, Yunker PJ, Ratcliff WC: **Drivers of spatial structure in social microbial communities**. *Curr Biol* 2019, **29**:R545–R550.

27. Weitz JS, Poisot T, Meyer JR, Flores CO, Valverde S, Sullivan MB, Hochberg ME: **Phage–bacteria infection networks**. *Trends Microbiol* 2013, **21**:82–91.

28. Jover LF, Flores CO, Cortez MH, Weitz JS: **Multiple regimes of robust patterns between network structure and biodiversity**. *Sci Rep* 2015, **5**:1–12.

29. Xue C, Goldenfeld N: **Coevolution maintains diversity in the stochastic "kill the winner" model**. *Phys Rev Lett* 2017, **119**, 268101.

30. C.A.: **Conditions for the existence of bacteriophage**. *Evolution* 1961, **15**:153–165.

31. Haerter JO, Mitarai N, Sneppen K: **Theory of invasion extinction dynamics in minimal food webs**. *Phys Rev* 2018, **97**, 022404.

32. Holt RD: **Predation, apparent competition, and the structure of prey communities**. *Theor Popul Biol* 1977, **12**:197–229.

33. Lenski RE, Levin BR: **Constraints on the coevolution of bacteria and virulent phage: a model, some experiments, and predictions for natural communities**. *Am Nat* 1985, **125**: 585–602.

34. Beckett SJ, Williams HT: **Coevolutionary diversification creates nested-modular structure in phage–bacteria interaction networks**. *Interface focus* 2013, **3**, 20130033.

35. * Piel D, Bruto M, Labreuche Y, Blanquart F, Goudenège D, Barcia-Cruz R, Chenivesse S, Le Panse S, James A, Dubert J, *et al.*: **Phage–host coevolution in natural populations**. *Nature Microbiology* 2022, **7**:1075–1086.
Comprehensive study of phage-host coevolution in a wild population.

36. Morgan AD, Gandon S, Buckling A: **The effect of migration on local adaptation in a coevolving host–parasite system**. *Nature* 2005, **437**:253–256.

37. Moebus K, Nattkemper H: **Bacteriophage sensitivity patterns among bacteria isolated from marine waters**. *Helgol Meeresunters* 1981, **34**:375–385.

38. ** Kauffman KM, Chang WK, Brown JM, Hussain FA, Yang J, Polz MF, Kelly L: **Resolving the structure of phage–bacteria interactions in the context of natural diversity**. *Nat Commun* 2022, **13**:1–20.

Comprehensive study of lytic interactions in a marine microbial ecosystem.

39. May RM: **Will a large complex system be stable?** *Nature* 1972, **238**:413–414.

40. Mathiesen J, Mitarai N, Sneppen K, Trusina A: **Ecosystems with mutually exclusive interactions self-organize to a state of high diversity**. *Phys Rev Lett* 2011, **107**, 188101.

41. Mitarai N, Brown S, Sneppen K: **Population dynamics of phage and bacteria in spatially structured habitats using phage λ and escherichia coli**. *J Bacteriol* 2016, **198**:1783–1793.

42. Eriksen RS, Svenningsen SL, Sneppen K, Mitarai N: **A growing microcolony can survive and support persistent propagation of virulent phages**. In *Proceedings of the National Academy of Sciences*, **115**; 2018:337–342.

43. Heilmann S, Sneppen K, Krishna S: **Coexistence of phage and bacteria on the boundary of self-organized refuges**. In *Proceedings of the National Academy of Sciences*, **109**; 2012: 12828–12833.

44. Bull JJ, Christensen KA, Scott C, Jack BR, Crandall CJ, Krone SM: **Phage-bacterial dynamics with spatial structure: self organization around phage sinks can promote increased cell densities**. *Antibiotics* 2018, **7**:8.

45. Taylor BP, Penington CJ, Weitz JS: **Emergence of increased frequency and severity of multiple infections by viruses due to spatial clustering of hosts**. *Phys Biol* 2017, **13**, 066014.

46. Hansen MF, Svenningsen SL, Røder HL, Middelboe M, Burmølle M: **Big impact of the tiny: bacteriophage–bacteria interactions in biofilms**. *Trends Microbiol* 2019, **27**:739–752.

47. Vidakovic L, Singh PK, Hartmann R, Nadell CD, Drescher K: **Dynamic biofilm architecture confers individual and collective mechanisms of viral protection**. *Nature microbiology* 2018, **3**:26–31.

48. Bond MC, Vidakovic L, Singh PK, Drescher K, Nadell CD: **Matrix-trapped viruses can prevent invasion of bacterial biofilms by colonizing cells**. *Elife* 2021, **10**, e65355.

49. * Winans JB, Wucher BR, Nadell CD: **Multispecies biofilm architecture determines bacterial exposure to phages**. *PLoS Biol* 2022, **20**, e3001913.
Experimental study on how multi-species biofilm architecture can alter the phage-bacteria interaction.

50. Simmons EL, Drescher K, Nadell CD, Bucci V: **Phage mobility is a core determinant of phage–bacteria coexistence in biofilms**. *ISME J* 2018, **12**:531–543.

51. Abedon ST: **Spatial vulnerability: bacterial arrangements, microcolonies, and biofilms as responses to low rather than high phage densities**. *Viruses* 2012, **4**:663–687.

52. Eriksen RS, Mitarai N, Sneppen K: **On phage adsorption to bacterial chains**. *Biophys J* 2020, **119**:1896–1904.

53. * Eriksen RS, Mitarai N, Sneppen K: **Sustainability of spatially distributed bacteria-phage systems**. *Sci Rep* 2020, **10**:1–12.
Hybrid model to simulate shielding of phage attack effectively in population dynamics

54. Ricciuti CP: **Host-virus interactions in escherichia coli: effect of stationary phase on viral release from ms2-infected bacteria**. *J Virol* 1972, **10**:162–165.

55. Haywood A: **Lysis of rna phage-infected cells depends upon culture conditions**. *J Gen Virol* 1974, **22**:431–435.

56. Hadas H, Einav M, Fishov I, Zaritsky A: **Bacteriophage t4 development depends on the physiology of its host escherichia coli**. *Microbiology* 1997, **143**:179–185.

57. Middelboe M: **Bacterial growth rate and marine virus–host dynamics**. *Microb Ecol* 2000, **40**:114–124.

58. You L, Suthers PF, Yin J: **Effects of escherichia coli physiology on growth of phage t7 in vivo and in silico**. *J Bacteriol* 2002, **184**:1888–1894.

59. Abedon ST, Yin J: **Bacteriophage plaques: theory and analysis**. In *Bacteriophages*. Springer; 2009:161–174.

60. Weitz JS, Dushoff J: **Alternative stable states in host–phage dynamics**. *Theor Ecol* 2008, **1**:13–19.

61. Yin J, McCaskill J: **Replication of viruses in a growing plaque: a reaction-diffusion model**. *Biophys J* 1992, **61**:1540–1549.

62. * Brown S, Mitarai N, Sneppen K: **Protection of bacteriophage-sensitive escherichia coli by lysogens**. In *Proceedings of the National Academy of Sciences*, **119**; 2022, e2106005119.
Experimental evidence that wild type λ-phage adsorbs better to metabolically active cells than inactive cells.

63. Oddershede L, Kisbye J, Grego S, Brown S, Berg-Sørensen K: **The motion of a single protein, the λ-receptor, in the bacterial outer membrane**. *Biophys J* 2002, **83**:3152–3161.

64. Winther T, Xu L, Berg-Sørensen K, Brown S, Oddershede L: **Effect of energy metabolism on protein motility in the bacterial outer membrane**. *Biophys J* 2002, **97**:1305–1312.

65. Schwartz M: **Reversible interaction between coliphage λ and its receptor protein**. *J Mol Biol* 1975, **99**:185–201, https://doi.org/10.1016/S0022-2836(75)80167-7.

66. Lennon JT, Jones SE: **Microbial seed banks: the ecological and evolutionary implications of dormancy**. *Nat Rev Microbiol* 2011, **9**:119–130.

67. ** Kolter R, Balaban N, Julou T: **Bacteria grow swiftly and live thriftily**. *Curr Biol* 2022, **32**:R599. R605.
Review on the role of dormancy in bacterial physiology and evolution.

68. Errington J: **Regulation of endospore formation in bacillus subtilis**. *Nat Rev Microbiol* 2003, **1**:117–126.

69. Sonenshein AL: **Bacteriophages: how bacterial spores capture and protect phage dna**. *Curr Biol* 2006, **16**:R14–R16.

70. Schwartz D, Lehmkuhl B, Lennon J: **Phage-encoded sigma factors alter bacterial dormancy**. *mSphere* 2022, **7**, e00297. 22.

71. Pearl S, Gabay C, Kishony R, Oppenheim A, Balaban NQ: **Nongenetic individuality in the host–phage interaction**. *PLoS Biol* 2008, **6**, e120.

72. Stewart FM, Levin BR: **The population biology of bacterial viruses: why be temperate**. *Theor Popul Biol* 1984, **26**:93–117.

73. Maslov S, Sneppen K: **Well-temperate phage: optimal bet-hedging against local environmental collapses**. *Sci Rep* 2015, **5**:1–11.

74. Gandon S: **Why be temperate: lessons from bacteriophage λ**. *Trends Microbiol* 2016, **24**:356–365.

75. * Correa AM, Howard-Varona C, Coy SR, Buchan A, Sullivan MB, Weitz JS: **Revisiting the rules of life for viruses of microorganisms**. *Nat Rev Microbiol* 2021, **19**:501–513.
Review focused on the eco-evolutional perspective of various life cycles of viruses.

76. Howard-Varona C, Hargreaves KR, Abedon ST, Sullivan MB: **Lysogeny in nature: mechanisms, impact and ecology of temperate phages**. *ISME J* 2017, **11**:1511–1520.

77. Łoś M, Wegrzyn G: **Pseudolysogeny**. *Advances in virus research* 2012, **82**:339–349.

78. Zheng Z, Bao M, Wu F, Van Horn C, Chen J, Deng X: **A type 3 prophage of 'candidatus liberibacter asiaticus' carrying a restriction-modification system**. *Phytopathology* 2018, **108**: 454–461.

79. Lindqvist BH, Dehò G, Calendar R: **Mechanisms of genome propagation and helper exploitation by satellite phage p4**. *Microbiol Rev* 1993, **57**:683–702.

80. Christie GE, Dokland T: **Pirates of the caudovirales**. *Virology* 2012, **434**:210–221.

81. Mitarai N: **How pirate phage interferes with helper phage: comparison of the two distinct strategies**. *J Theor Biol* 2020, **486**, 110096.

3 The role of dormancy in phage-bacteria dynamics

3.1 Introduction

Microorganisms are arguably the most abundant and diverse organisms on Earth [1]. The previous chapter was dedicated to the mechanisms under which microbiological ecosystems can sustain their diversity in the upper layers of the oceans under severe pressure imposed by viruses and limited resources. However, from a global perspective, these conditions are far from extreme. Microorganisms can colonize almost every conceivable habitat, ranging from high-temperature hot springs [25, 22] to hyperarid, irradiated deserts [24] and the cold, high-pressure deep-sea sediment [23]. Most of these environments are characterized by their fluctuating and unpredictable nature, often leading to prolonged periods where conditions are not only suboptimal for growth and reproduction, but also for basic cellular maintenance [121, 26, 122, 123, 124, 125, 126]. Given the frequency with which microorganisms are encountered in these challenging habitats, it has been argued that energy limitation constitutes a pervasive constraint on microbial growth [127, 128, 129].

3.1.1 Microbial dormancy, seed-banks and host-paracite interactions

To adapt to energy limitations and fluctuating environmental conditions, many microorganisms enter dormancy, a reversible state of reduced metabolic activity [130, 131]. By entering a dormant state, cells can temporarily reduce their energetic requirements by halting growth and cutting down maintenance costs until environmental conditions improve [132, 133, 131]. However, opting for dormancy comes with its trade-offs. Dormant cells forgo reproductive opportunities and allocate valuable internal resources to the maintenance of resting structures and ongoing energy needs [134, 135, 136]. To minimize these costs, dormant cells must invest in the costly development and maintenance of specialized mechanisms that enable them to recognize and react to signals indicative of favorable conditions. Therefore, dormancy can be seen as an adaptive bet-hedging strategy where the cells sacrifice short-term reproductive success for long-term benefits under fluctuating and often challenging environmental conditions [130].

This adaptation is often crucial for survival as it has evolved multiple times independently across a phylogenetically diverse range of microorganisms [137]. From the human gut to the immense depths of the world's oceans, dormancy is consistently observed [138, 131]. For instance, over 80% of the microbial biomass in soils remains metabolically inactive [139, 131, 140]. Dormancy also plays a pivotal role in human diseases like anthrax, cholera, and tuberculosis [141] and in explaining how pathogenic persister cells can withstand high antibiotic concentrations [142, 143, 144, 145, 146]. In light of its implications, there is a growing interest in the scientific community to study and decode the intricacies of dormancy.

Key insights from the studies so far have revealed that microorganisms can transition be-

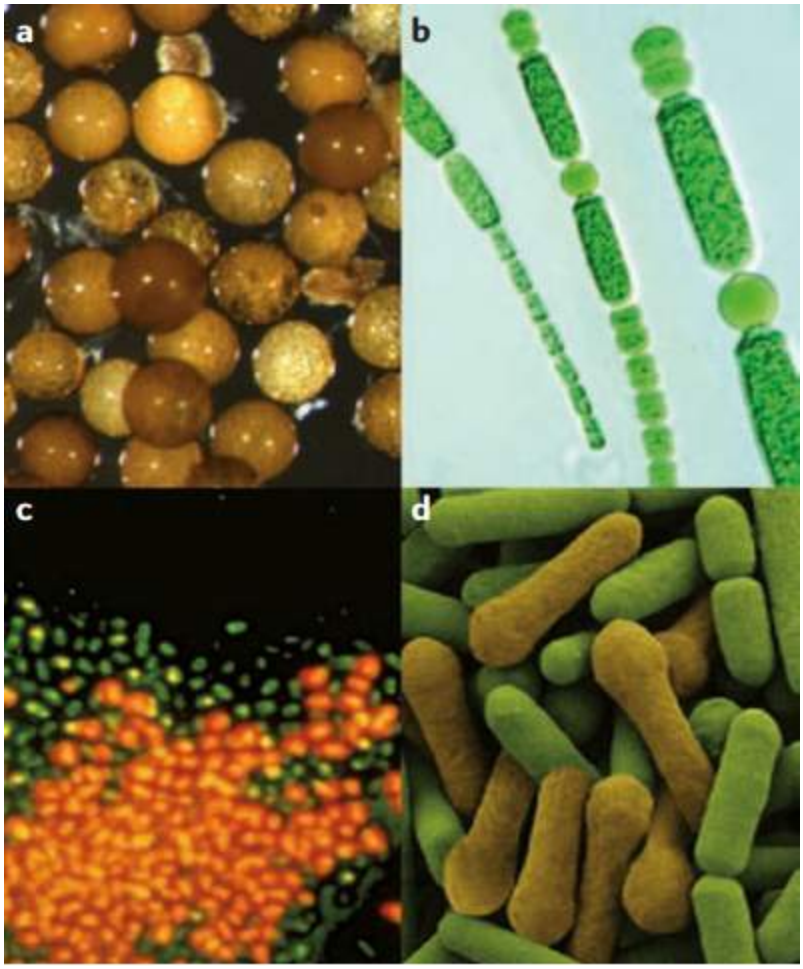

Figure 16: **Microorganisms in a dormant state.** Dormancy is a widespread bet-hedging strategy against adverse conditions in the microbial world. This figure shows examples of dormancy in **a** *arbuscular mycorrhizal fungus*, **b** *cyanobacteria*, **c** *Klebsiella pneumoniae* and *Pseudomonas aeruginosa*, and **d** *Viridibacillus arvi*. It should be noted that not all forms of dormancy are associated with a distinctive and externally observable structure. (Adapted from [131]. Credits to A. Brennwald (picture a), Y. Tsukii (picture b), and Dennis Kunkel (picture d)).

tween active and dormant phases relatively rapidly [147, 148, 149]. Although such transitions can sometimes be stochastic [150], they are often modulated by environmental factors like temperature [132], pH levels [151], hydration conditions [152], and resource availability [153]. The accumulation of dormant cells gives rise to a ”seed bank”, a reservoir of dormant individuals that encapsulates genetic and phenotypic diversity until the environmental conditions become favorable enough to allow for potential resuscitation [131, 154]. This happens via the storage effect, which suggests that environmental fluctuations lead to variations in population growth, resulting in the emergence of long-lived organisms [131]. Interestingly, the durability of dormant entities is highly variable. While some dormant microorganisms are susceptible to environmental stresses, succumbing within days [155], others can endure extended periods that reach hundreds of thousands or even millions of years! Remarkably, dormant cells have been revived from ancient materials, such as amber and halite crystals, that are hundreds of millions of years old [156]. Hence, the longevity of dormant

cells can dramatically surpass the average life span of actively reproducing ones [157, 158].

The extended life span of dormant cells plays a crucial role in biodiversity maintenance [159] and in community stability, robustness, and recovery [160, 161]. Furthermore, studies on trophic interactions reveal predators' preference for active over dormant prey [162] and reduced susceptibility of inactive hosts to parasitic infections [163]. From an evolutionary perspective, seed banks can reduce the frequency of mutations and weaken the effects of random drift and natural selection [164]. These discoveries, complemented by recent studies [107, 165, 166, 167, 168, 169], support Lenski's "physiological refuge" concept [170, 171] and suggest that the role of dormancy in host-parasite eco-evolutionary dynamics has been overlooked.

3.1.2 Sporulation in *Bacillus subtilis*: A model for the study of dormancy

A number of species enter dormancy by producing a specialized structure. This makes the dormant state easier to identify and study. One of the most well-studied forms of dormancy is the production of endospores in *Bacillus subtilis*.

Part of the Firmicutes phylum, *Bacillus subtilis*, is typically found in plants as an epiphyte and within the rhizosphere [19]. Its fast growth, easy cultivation, and ability to switch from classical binary fission to asymmetrical division during spore formation captured the scientific community's attention. This led to extensive studies that made *Bacillus subtilis* the best-studied model organism of the Gram-positive lineage [1]. Today, *Bacillus subtilis* has important environmental applications in plant protection and growth promotion and industrial applications in the production of fine chemicals, probiotics, vitamins (e.g., riboflavin) and in the food industry (e.g., Natto) [19].

During the process of endospore formation, or "sporulation", an asymmetrical division occurs (see Figure 17), producing a smaller prespore and a larger mother cell, each with distinct transcription patterns [172]. Originating over 2.3 billion years ago, sporulation is not a feature exclusive to *B. Subtilis* [173]. It is an ancient evolutionary trait, with studies suggesting that the last bacterial common ancestor (LBCA) had endospore-forming capabilities [174]. These spores are widespread and ubiquitous, with a staggering 10^{29} endospores estimated in marine sediments alone [126].

Remarkably resilient, dormant endospores can withstand extreme conditions, from intense heat and radiation to the vacuum of space for extended periods before germinating and returning to vegetative growth [175, 176]. Their biological inertness allows some bacteria to persist for millennia [177]. Impressively, even after such prolonged dormancy, a slight change in resource availability can reactivate these spores within minutes [16]. Despite the presence of stochastic switching between active and inactive states [150], this complex and energetically demanding process that involves the upregulation of more than 500 genes [178] is believed to be tightly regulated by environmental cues and initiated by starvation [179]

The starvation-triggered switch to sporulation marks the first significant phase in this process

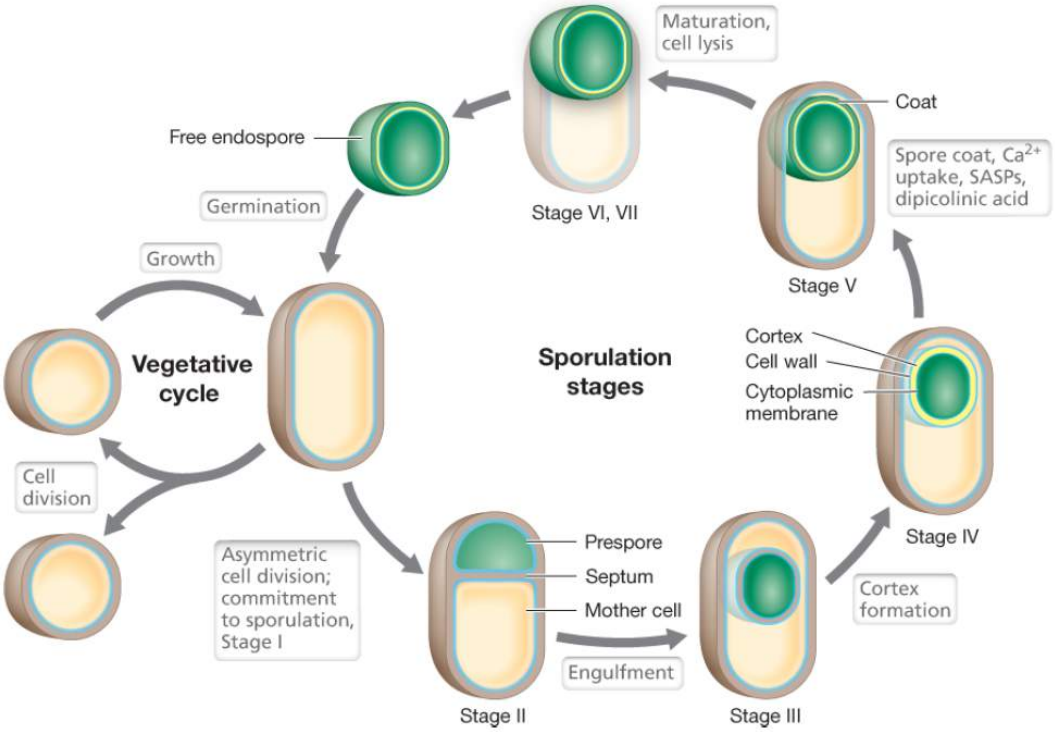

Figure 17: **Sporulation process in *Bacillus Subtilis*.** This illustration shows the key stages of *B. Subtilis* sporulation process and their reversible connection with the vegetative state of the cell. (Adapted from [1])

(see Figure 17). The second one is when the spore is formed. Not only do these mature spores safeguard the host's DNA against extreme temperatures, UV radiation, and chemicals [180, 18, 16], but they also shield the host from bacteriophages. Viral protection is achieved through an outer layer that either lacks completely or has significantly fewer phage receptor binding domains [181]. As a result, phage adsorption to spores can be dramatically decreased, or even completely halted, in comparison to growing cells [181]. However, if phages penetrate cells prior to the spore's maturation, the resulting spore may carry both cellular and viral genomes, posing latent risks to the hosts over extended periods.

Taking everything into account, it is evident that sporulation can have an important impact on parasite-host interactions, not only at an individual level but also on a population level. A serial transfer coevolutionary experiment has demonstrated that sporulation can transiently stabilize the oscillatory population dynamics prompted by phages [181]. Additionally, there is evidence suggesting that phages can obtain transcription factors and influence sporulation within the host, though the effects on infection dynamics remain elusive [182]. These studies have limitations, primarily because they focus on infection dynamics in well-mixed liquid media. In contrast, phage infections of *B. Subtilis* bacteria predominantly occur in soils and on surfaces. These environments offer an inherently spatial context and present distinct selection criteria when compared to viral infections in liquid cultures. This chapter aims to explore the effects of dormancy on phage-bacteria

interactions at the community level in such spatial settings, and delve deeper into potential factors triggering sporulation.

3.2 Experimental methods and results

3.2.1 Sporulation limits viral plaques

To investigate the influence of dormancy on the infection dynamics between *Bacillus subtilis* and its bacteriophages in a spatial context, our collaborator Dr. Andreea Măgălie designed and conducted plaque assays under the supervision of Dr. Daniel Schwartz and Prof. Jay Lennon (see Măgălie et al. Manuscript). Plaque assays are standard and fundamental laboratory methods where a dilution of virus is placed on a petri dish containing a lawn of susceptible cells [1]. As the viruses diffuse, infect, and lyse the cells, clear zones, known as plaques, form. Each circular plaque originates from a single virus particle and represents a localized area where the cells have been destroyed due to the presence of that virus. Plaque assays are utilized to visualize and quantify virus-host interactions, determine phage titers and cell-virus life history traits, and purify clonal viral populations [183, 184, 185]. Importantly, plaque assays also enable us to explore bacterial antiviral strategies and their impact on limiting plaque propagation [186].

Our assays involve two $\Delta 6$ *Bacillus subtilis* strains (see Măgălie et al. Manuscript). The first is a wild type (WT) that can undergo sporulation, while the second is a $SPOIIE$ mutant characterized by a $SPOII$ mutation at locus E. This mutation halts sporulation during the asymmetrical division stage II (see Stage II at Figure 17). For ease of reference, we denote the WT as S^+, and the $SPOIIE$ as S^- (see Măgălie et al. Manuscript). After being streaked from glycerol stocks, the bacterial cultures were let to grow overnight at 37°C in the widely used for sporulation medium DSM (Difco Sporulation Media) [187, 175, 188]. Post overnight growth, cells were inoculated from a singular colony and incubated for approximately 5 hours until they reached OD $\approx$ 0.5. Subsequently, the bacterial strains were exposed to the wild-type lytic bacteriophage SPO1, while the wild-type lytic bacteriophage SPP1 was also used for comparison (see Supplementary Information in Măgălie et al. Manuscript). Following the 'tube free agar-overlay' protocol [189], a mixture of cell culture, viral solution, and soft agar was applied to petri dishes. Consequently, the plates were incubated overnight at 37°C. The growth dynamics of SPO1 plaques were recorded in a time-lapse over 15 hours. Plaque sizes were analyzed using image techniques detailed in Măgălie et al. Manuscript.

Starting at the 3-hour mark, both S^+ and S^- plaques grow, maintaining a similar rate for about 2 hours. However, while the S^+ plaques plateau just after 5 hours, the S^- plaques continue growing until reaching a plateau at 13 hours, making them roughly three times larger than the S^+ plaques. This early termination of growth in sporulating as opposed to non-sporulating hosts points to microscopic mechanisms, implying that sporulation curtails the phages' lysing ability, leading to smaller plaques.

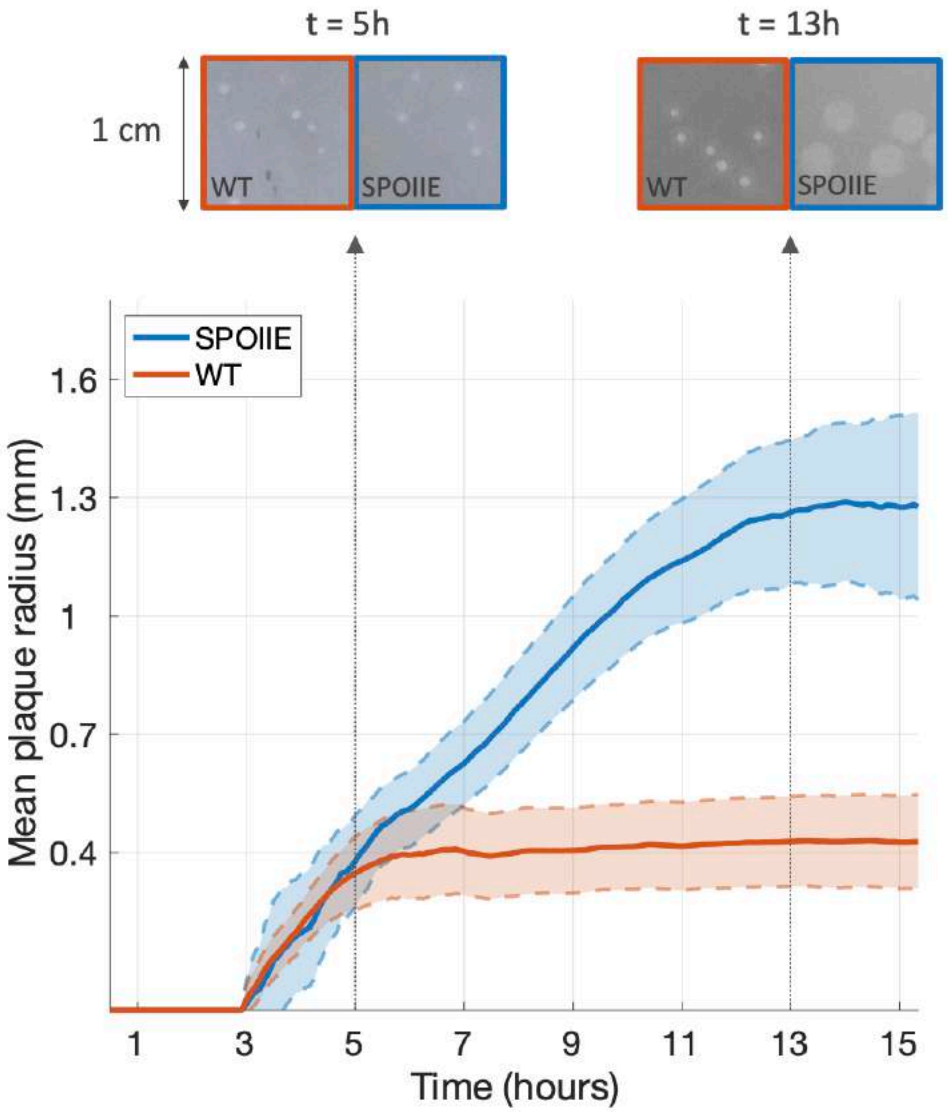

Figure 18: **Plaque growth time lapse for WT (S^+) and SPOIIE (S^-) hosts**. A plaque assay was conducted at 37°C, capturing images every 5 minutes across a span of 15 hours. Image analysis methods (as detailed in the Măgălie et al. Manuscript) allowed for plaque size determination. The solid line represents the mean size across all plaques, while the shaded area indicates the standard deviation. On the top part of the figure we show 1cm x 1cm pictures of the plaques side by side for WT (S^+) and SPOIIE (S^-) hosts at t = 5 hrs and t = 13 hrs respectively. (Adapted from the preprint of Măgălie et al. The intermediate images of individual plaque trajectories can be found in the Supplementary Information).

3.2.2 Sporulation is enhanced around the plaques' edges

To study the microscopic impact of sporulation on the dynamics of the plaques, our experimental collaborators developed an inverted plaque assay (details in Măgălie et al.). For the inverted plaque assay, the bacterial cultures were grown to re-store exponential growth. Alongside, a viral dilution was prepared in Eppendorf tubes. Once the bacterial culture reached an OD of around 0.5, a sample was centrifuged and then mixed with a portion of the viral solution. A small amount of this blend was then placed on a glass-bottom petri dish tailored for microscopic imaging (see

Figure 20).

Simultaneously, agar pads were crafted by solidifying DSM media with agarose in a larger petri dish, as per the method from [190]. Using sterile methods, these pads were cut into nine squares (Figure 19A-D). Each square was positioned over a sample droplet on the glass dish. A single glass-bottom petri dish can accommodate up to four such setups. Once arranged, the petri dish was sealed and placed in a 37°C incubator for 8-12 hours, after which it was ready for imaging (Figure 19E).

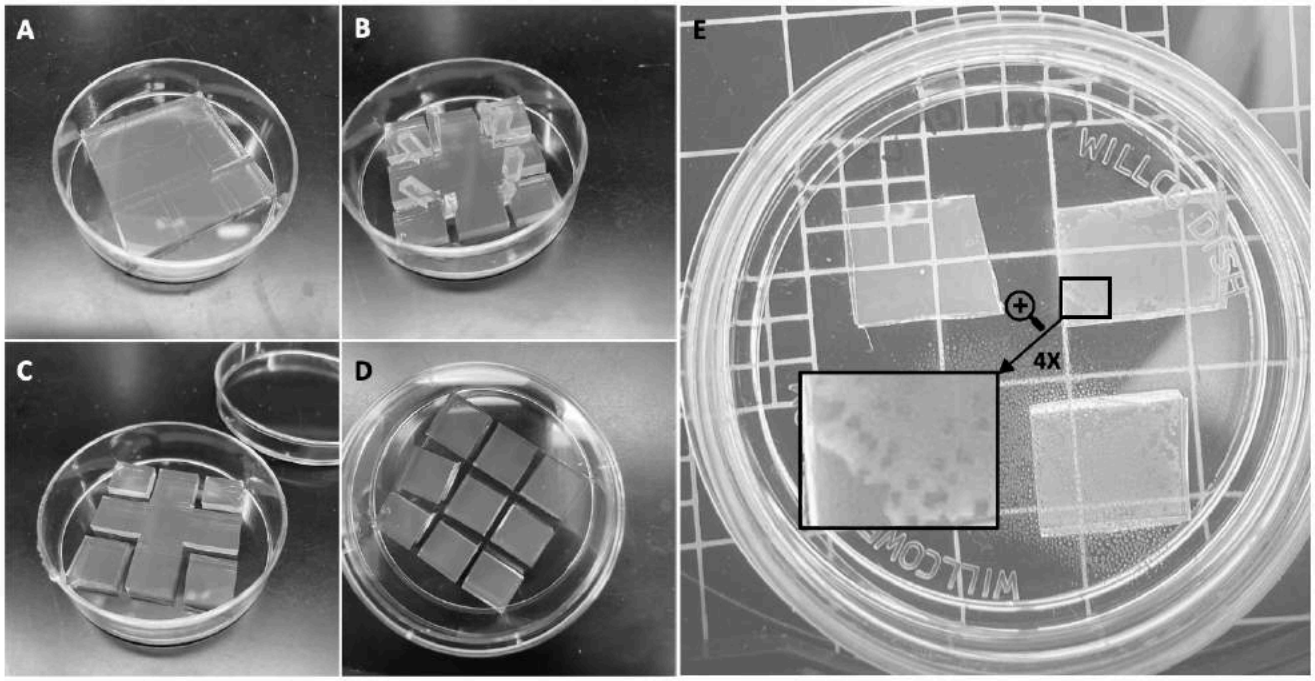

Figure 19: **Inverted plaque assay protocol.** Panels **A** to **D** chronologically illustrate the preparation of the agar pad for the inverted plaque assay. The agar is sliced with a sterile scalpel, ensuring the square pads remain in place while the excess agar is carefully removed. Panel **E** showcases a top-down perspective of the assay, with a fourfold magnification emphasizing the distinctive darker plaques of phage SPO1 on the S^+ host in DSM media. (Adapted from the preprint of Măgălie et al.).

A re-assessment of the plaque sizes for S^+ vs S^- hosts corroborated the results of the first assay by showing that S^+ plaques are roughly 3 times smaller than that of the S^- host (see Supplementary Information in Măgălie et al. Manuscript). Additionally, the inverted plaque assay allowed for microscopic analysis of the region containing the plaque. Crucially to our work, it allowed for a quantification of the sporulation levels. In Figure 21A, we can see the viral plaque as it appears in a bright-field image of the inverted plaque assay. If the same plaque is captured with a fluorescent channel sensitive to Green Fluorescent Protein (GFP) emitted by the genetically modified spores, then the patterns of sporulation become apparent (see an example of the idea in Figure 20). In Figure 21B, sporulation is notably absent inside the plaque and in regions distant from it. However, intriguingly, there is a pronounced enhancement of sporulation at the plaque's periphery. This observation was quantitatively supported by measuring the GFP intensity distribution with distance and proved consistent across various experiments and stages of

plaque growth (see Figure 19). The process for evaluating average GFP intensity after adjusting for background fluorescence is elaborated on in Măgălie et al.

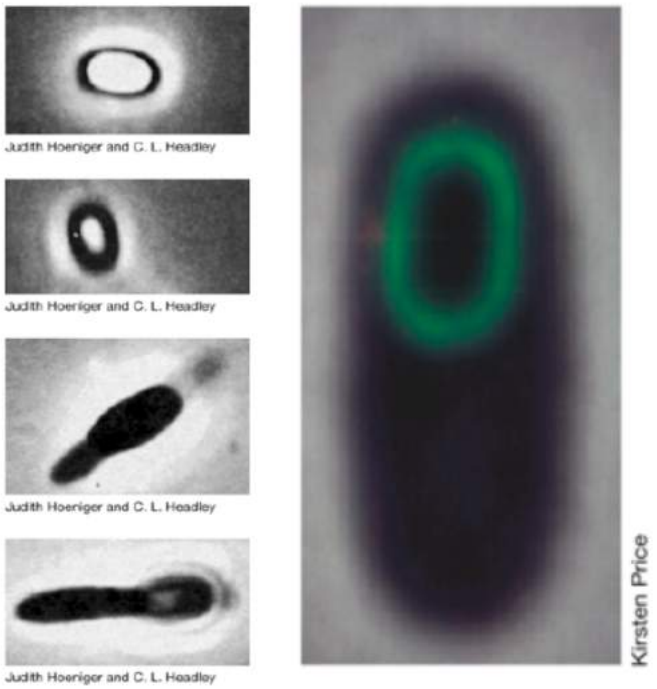

Figure 20: **Examples of sporulation imaging.** The amalgamation of advanced microscopy, sophisticated genetic methods, and the distinct, detectable characteristics of spores has facilitated dynamic observations and studies of the sporulation process. The photomicrographs in the left column of this figure depict the transformation of a *Bacillus Subtilis* spore into a vegetative cell. Conversely, the right column showcases a fluorescent photomicrograph representing the reverse process where a cell initiates sporulation. (Adapted from [1]. Credits go to Judith Hoeringer and C.L. Headley for the left column and Kristen Price for the right column).

While the absence of sporulation in the plaque's inner regions is anticipated due to the clearing of hosts by viruses, the enhanced sporulation at the periphery and its link to the reduced plaque sizes for S^+ urgently requires a theoretical explanation.

3.3 Theoretical methods and results

3.3.1 Modeling with resource-only induced dormancy can reproduce the plaque growth dynamics, but not the spore enhancement around the plaques

As mentioned in the introduction, it is widely accepted in the scientific community that sporulation in *Bacillus subtilis* is triggered by starvation when resource levels are low [191, 192, 131]. Therefore, we developed a PDE model where dormancy is solely a function of available resources to delve deeper into the factors influencing plaque growth. We formulate the mathematical model using a Lotka-Volterra-like system of equations, where viruses V diffuse across a bacterial lawn containing either sporulating (S^+) or non-sporulating (S^-) susceptible bacteria S, that grow on explicit resources R. Susceptible bacteria can turn into infected cells I when viruses adsorb to them

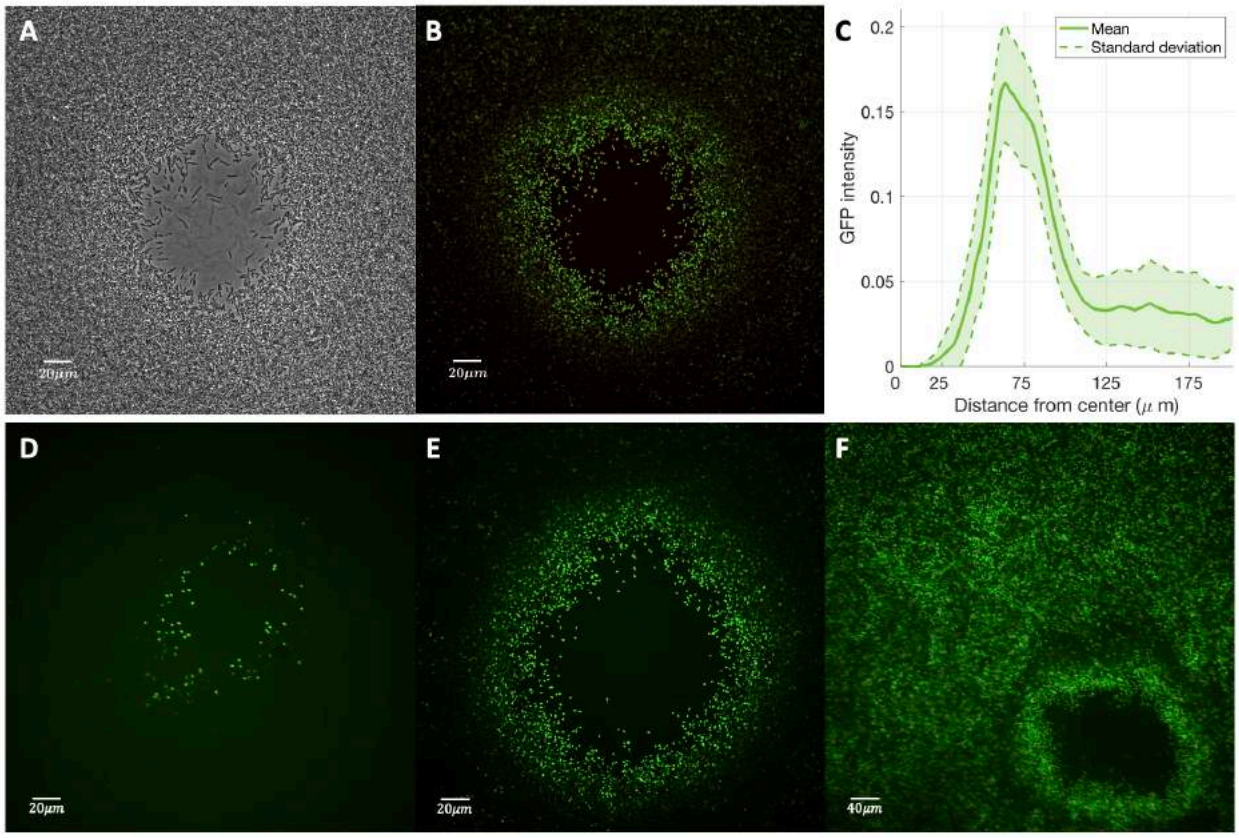

Figure 21: **Sporulation is enhanced at the plaque periphery. A and B** Bright-field (panel A) and fluorescent (panel B) images from the inverted plaque assay, both captured at 40x magnification. The assay was conducted using DSM media and the SPO1 phage. The GFP image underwent processing to intensify contrast and diminish background noise. (more details on image analysis can be found in Măgălie et al. Manuscript) **C** GFP intensity as a function of the distance from the plaque's center. This is a radial analysis of the image in panel B. The solid line represents the mean, and the shaded area is the standard deviation. **D-F** Fluorescent images from the inverted plaque assay showing the evolution of sporulation distribution. The timeframes correspond to approximately 7 hours, 8 hours and 12 hours for **D**, **E** and **F** respectively. (Adapted from the preprint of Măgălie et al.).

until they are lysed. The Susceptible bacteria can also transition into dormant cells D, which are resistant to phage adsorption.

More specifically, dormancy is initiated at a low rate when resources are high (accounting for stochastic dormancy [193, 131]) and at a much higher rate when resources are depleted. We refer to this model as Model R (see Figure 23) and present the associated two-dimensional system of partial differential equations below:

$$
\begin{aligned}
\frac{\partial \tilde{R}}{\partial t} &= -\underbrace{g(\tilde{R})S}_{\text{cell growth}} + \underbrace{D_R \nabla^2 \tilde{R}}_{\text{resource diffusion}} \\
\frac{\partial S}{\partial t} &= \underbrace{g(\tilde{R})S}_{\text{cell growth}} - \underbrace{\phi S V}_{\text{viral infection}} - \underbrace{f(\tilde{R})S}_{\text{dormancy initiation}} \\
\frac{\partial I_1}{\partial t} &= \underbrace{\phi S V}_{\text{viral infection}} - \underbrace{\eta(\tilde{R}) n_I I_1}_{\text{to next infected state}} \\
\frac{\partial I_i}{\partial t} &= \underbrace{\eta(\tilde{R}) n_I I_{i-1}}_{\text{from previous infected state}} - \underbrace{\eta(\tilde{R}) n_I I_i}_{\text{to next infected state or viral lysis}} \\
\frac{\partial V}{\partial t} &= \underbrace{\beta \eta(\tilde{R}) I_{n_I}}_{\text{viral lysis}} - \underbrace{\omega V}_{\text{viral decay}} - \underbrace{\phi(S + I_{total})V}_{\text{viral infection}} + \underbrace{D_V \nabla^2 V}_{\text{viral diffusion}} \\
\frac{\partial D}{\partial t} &= \underbrace{f(\tilde{R})S}_{\text{dormancy initiation}}
\end{aligned}
$$

$\tilde{R}(\mathbf{x}, t)$ denotes the rescaled resource density in units of cells/mL. This rescaling is defined as $[\tilde{R}] = [R/\epsilon] = \frac{\frac{\mu g}{mL}}{\frac{\mu g}{cells}} = \frac{cells}{mL}$, with ϵ signifying the conversion rate from resources to bacteria, expressed in μg/cells. Similarly, $S(\mathbf{x}, t), I(\mathbf{x}, t)$ and $D(\mathbf{x}, t)$ represent the densities of susceptible, infected, and dormant bacteria respectively, each in units of cells/mL. V designates the phage density, given in viruses/mL. Given our experimental setup, bacteria are considered immotile, non-diffusing entities that grow by metabolizing resources. In contrast, resources and viruses are assumed to diffuse. Susceptible cells can either get infected by virulent phages with an infection rate of ϕ or transition to dormancy in response to resource scarcity. When infected, these cells undergo a sequence of stages n_I of infected states I_i (cumulatively represented as $I_{total} = \sum_{i=1}^{n_I} I_i$), resulting in an effective latent period which follows an Erlang distribution. After this latent period, the infected cells can burst, releasing new free viruses with burst size β. Virus particles can bind to cells at an absorption rate ϕ and degrade at a decay rate ω. The bacterial growth rate $g(\tilde{R})$, dormancy rate $f(\tilde{R})$ and latent time $\eta(\tilde{R})$ are all resource-dependent and given by:

$$
g(\tilde{R}) = r_{max} \frac{\tilde{R}}{\tilde{K_g} + \tilde{R}} \tag{1}
$$

$$
f(\tilde{R}) = \frac{d_{max}}{1 + e^{s(\tilde{R} - \sigma)}} \tag{2}
$$

$$
\eta(\tilde{R}) = \eta_{max} \frac{g(\tilde{R})}{g(\tilde{R_0})}. \tag{3}
$$

The growth rate function follows the Monod equation were r_{max} is the maximum bacterial growth rate and $\tilde{K_g}$ the rescaled Monod constant (similarly to R, $[\tilde{K_g}] = [K_g/\epsilon] = \frac{\frac{\mu g}{mL}}{\frac{\mu g}{cells}} = \frac{cells}{mL}$). The

Parameters common to all models				
Variable	*Meaning*	*Value*	*Unit*	*Source*
R_0	Initial resource level	10^3	μg/mL	Estimate
$\tilde{R}_0$	Rescaled initial resource level	10^9	(cells)/mL	Estimate
S_0	Initial cell density	10^7	(cells)/mL	This work
V_0	Initial viral density	10^6	(viruses)/mL	This work
r_{max}	Maximum bacterial growth rate	2	hrs^{-1}	Literature
ε	Resource to bacteria conversion rate	10^{-6}	μ g/(cell)	Estimate
K_g	Monod constant	$3.2 \cdot R_0$	μ g/mL	This work
$\tilde{K}_g$	Rescaled Monod constant	$3.2 \cdot \tilde{R}_0$	(cells)/mL	This work
ϕ	Infection rate	$1.8 \cdot 10^{-8}$	mL/(hrs $\cdot$ (virus))	This work/Literature
η_{max}	Maximum latent rate	4/3	$\text{h}rs^{-1}$	Literature
d_{max}	Maximum transition to dormancy rate	1	$\text{h}rs^{-1}$	This work
β	Burst size	100	(viruses/cell)	Literature
ω	Viral decay	0.001	hrs^{-1}	Literature
D_R	Resource diffusion constant	$4 \cdot 10^5$	μm^2/hrs	Literature
D_V	Phage diffusion constant	$2 \cdot 10^3$	μm^2/hrs	Estimate/Literature
n_I	Number of infected states	10		This work
s	"Sharpness" of transition to dormancy	10^{-7}		Estimate

Table 1: Parameters common to all models (Adapted from the preprint of Măgălie et al.)

dormancy rate function is assumed to be solely dependent on resources. However, sporulation becomes significant only when the resource density approaches a fraction σ of the Monod's constant. The value of parameter s determines the 'sharpness' of the transition to dormancy. Finally, we choose a resource-dependent lysis rate proportional to the growth rate g(R) [194, 195]. This approach is rooted in the observation that plaque growth ceases when bacteria deplete nutrients. For the initial conditions ($t = 0$), we assume uniformly distributed susceptible cells and resources on a plane while the viruses are concentrated at the central point of the area of interest. Neither dormant nor infected cells are present initially. Table 1 contains each model parameter's meaning, value, and units (see Măgălie et al. for a more detailed approach).

Model R can replicate the plaque growth dynamics with great precision. This becomes clear by comparing the experimental results in Figure 18 with the theoretical predictions in Figure 22A, B. Our theoretical analysis suggests that sporulation can contain the plaque expansion by reducing the available targets for infection for the free viruses in the S^+ case compared to the S^- one. Therefore, plaque growth ceases earlier, resulting in smaller plaques in the S^+ strain. In a model with starvation-induced sporulation and uniformly distributed initial resources, dormancy is most evident in plate regions with the highest bacterial concentrations. These regions, distant from the plaque, are where phages have minimal presence and exhibit the highest resource consumption. Phages originating from the plaque's center will diffuse and expand until they encounter an area

densely populated with dormant cells, inhibiting further infection and plaque growth. This wave of dormancy that halts their expansion, though, would have to travel from outwards to inwards. This inhibitory dormancy wave moves from the outer regions inward. Therefore, a model relying solely on resource exhaustion as a trigger for dormancy cannot replicate the observed sporulation enhancement circle at the plaque's periphery. This is corroborated by comparing the distribution of the GFP intensity in Figure 21 with the modeling results on the distribution of dormant cells in Figure 24A, B.

The evident gap in our understanding underscores the need to introduce a yet-to-be-identified component capable of directing the dormancy trigger signal wave from the plaque's center outwards. Given that viruses are the only entities moving outward from the plaque's center, they emerge as a compelling choice, pointing to an avenue for model refinements and exploration.

3.3.2 Phage-triggered sporulation can enhance dormant cells at the edge of the plaque

We explore the possibility of virally induced dormancy by introducing it as an additional sporulation trigger alongside the traditional starvation-induced one. In the new Model V, when a cell encounters a viral particle, it can enter dormancy with probability $p \in (0, 1)$ or get infected with probability $1 - p$. Identical plaque growth dynamics are observed across multiple (p, σ) combinations, with the (p = 0, $\sigma = 0.282\ \tilde{K_g}$) combination corresponding to Model R. To incorporate a time delay in spore formation, we present a possible series of consecutive states n_E as part of transitioning to dormancy. Therefore, this process follows an Erlang distribution. For $n_E = 0$, the transition to dormancy is instantaneous, whereas $n_E > 0$ introduces a time delay. We select the net transition rate between the E-states to be λn_E, where $\lambda = \frac{4}{3} hrs^{-1}$, to ensure the mean transition rate remains constant with variations in the number of states. During these initial stages of dormancy, cells are still vulnerable to phage infections, unlike the mature spores. Except for these differences, Models R and V share the same variables with values set on Table 1. Model V is described by the following set of equations. Elements in black are derived from Model R, whereas the terms in red are introduced in Model V.

$$\frac{\partial \tilde{R}}{\partial t} = -\underbrace{g(\tilde{R})(S + E_{total})}_{\text{cell growth}} + \underbrace{D_R \nabla^2 \tilde{R}}_{\text{resource diffusion}}$$

$$\frac{\partial S}{\partial t} = \underbrace{g(\tilde{R})S}_{\text{cell growth}} - \underbrace{f(\tilde{R})S}_{\text{dormancy initiation}} - \underbrace{(1-p)\phi SV}_{\text{viral infection}} - \underbrace{p\phi SV}_{\text{dormancy initiation}}$$

$$\frac{\partial I_1}{\partial t} = \underbrace{(1-p)\phi(S + E_{total})V}_{\text{viral infection}} - \underbrace{\eta(\tilde{R})n_I I_1}_{\text{to next infected state}}$$

$$\frac{\partial I_i}{\partial t} = \underbrace{\eta(\tilde{R})n_I I_{i-1}}_{\text{from previous infected state}} - \underbrace{\eta(\tilde{R})n_I I_i}_{\text{to next infected state or viral lysis}}$$

$$\frac{\partial V}{\partial t} = \underbrace{\beta\eta(\tilde{R})n_I I_{n_I}}_{\text{viral lysis}} - \underbrace{\phi(S + I_{total} + E_{total})V}_{\text{viral infection}} - \underbrace{\omega V}_{\text{viral decay}} + \underbrace{D_V \nabla^2 V}_{\text{viral diffusion}}$$

$$\frac{\partial E_1}{\partial t} = \underbrace{f(\tilde{R})S}_{\text{dormancy initiation}} + \underbrace{p\phi SV}_{\text{dormancy initiation}} - \underbrace{\lambda n_E E_1}_{\text{dormancy process}} - \underbrace{(1-p)\phi E_1 V}_{\text{infection of exposed transitioning cells}}$$

$$\frac{\partial E_i}{\partial t} = \underbrace{\lambda n_E E_{i-1}}_{\text{from previous transitioning state}} - \underbrace{\lambda n_E E_i}_{\text{to next transitioning state or to dormancy}} - \underbrace{(1-p)\phi E_i V}_{\text{infection of exposed transitioning cells}}$$

$$\frac{\partial D}{\partial t} = \begin{cases} \underbrace{f(\tilde{R})S}_{\text{dormancy initiation}} + \underbrace{p\phi SV}_{\text{dormancy initiation}} & , n_E = 0 \\ \underbrace{\lambda n_E E_{n_E}}_{\text{transition to dormancy}} & , n_E > 0 \end{cases}$$

where $E_{total} = \sum_{i=1}^{n_E} E_i$.

In Model V, the diffusing viruses trigger dormancy by contact at the expanding plaque's forefront, where most of the bacteria have not yet been lysed. Phage-induced dormancy decreases towards the center, as most of the cells there are lysed. Additionally, if resources remain above σ, dormancy also decreases further away from the plaque's front, where phages are absent and cannot trigger dormancy. Consequently, the model can reproduce the experimentally observed peak in sporulation around the plaque's edges semi-quantitatively, as evident in the comparison between experimental and modeling results in Figure 21 and Figure 24C, D respectively at t = 5 hrs.

Consistent with our experimental data, the peak in sporulation is transient, appearing at t $\approx$ 3 hrs and lasting until t $\approx$ 7 hrs (see Figure 24C, D). Given a 4-5 hour gap between dormancy transition and GFP expression, this simulated onset at t $\approx$ 3 hrs matches well with our empirical data, where the peak is noted at t $\approx$ 8 hrs (see Figure 21). As resources get exhausted, nutrient scarcity triggers dormancy, making this model eventually converge to the same steady-state spore density as Model R. Given that the presence of viruses immediately produces some spores, this

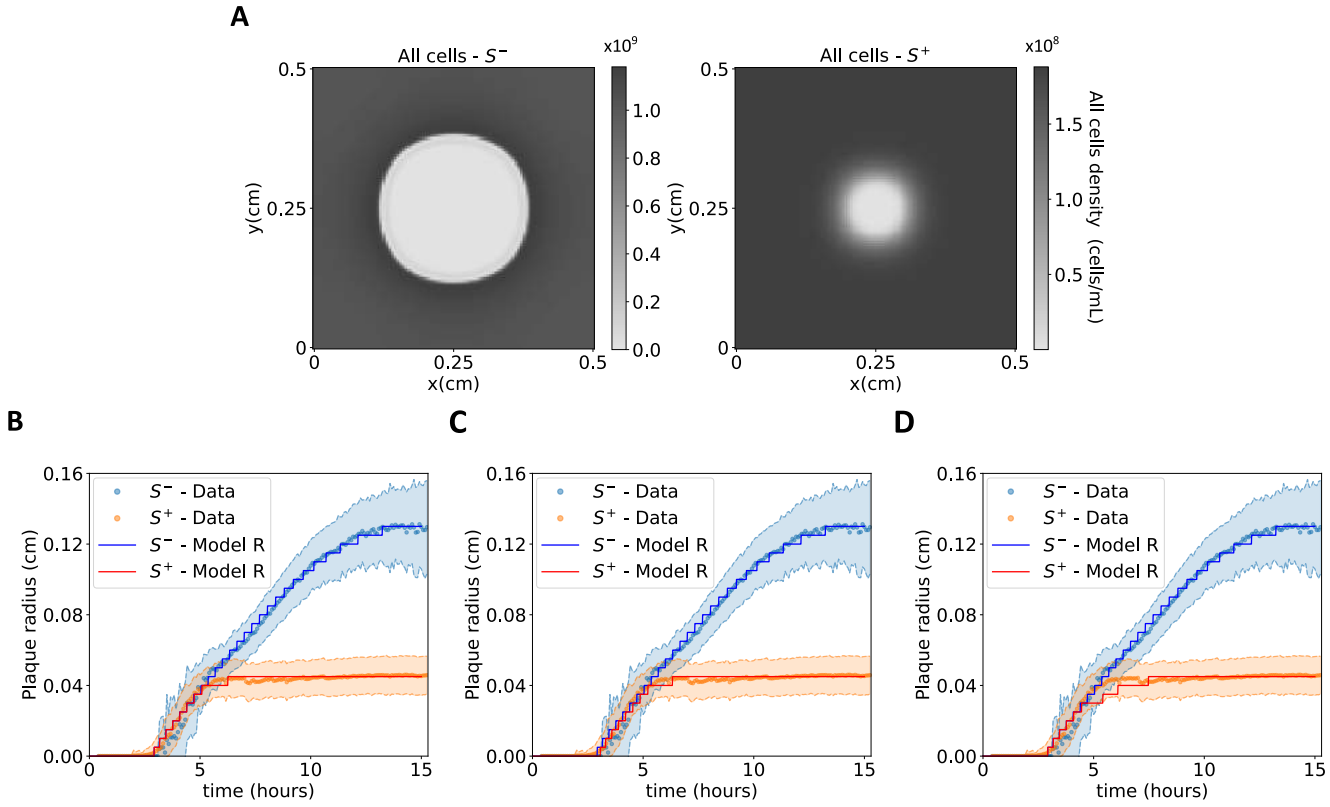

Figure 22: **Impact of sporulation on plaque size for Models R, V, and M. A** A representative image of the spatial simulation of bacterial densities for Model R. The snapshot is captured at t = 15 hrs, which corresponds to the endpoint of both experiments and simulation as shown in **B**. **B-D** Overlay of experimental data and simulation results shows the time evolution of the mean plaque radius for the S^- and S^+ strains in Models R, V, and M, respectively. The panels demonstrate that all of our models can replicate the plaque growth dynamics. We define a plaque in the simulations as any region where the cell density is below 10% of its peak value at that moment. The results are robust to threshold changes, ascribed to the sharp change in density at the plaque boundaries. Panels C and D present simulations of Model V and Model M, respectively, for $n_E = 10$, but the results are reproducible across different values of n_E (see Măgălie et al. for more details). (Adapted from Măgălie et al.).

model produces dormant cells from early in the plaque's development, with spores within the plaque building up right away from its center (see Figure 24C, D). In contrast, experimental observations typically show a spore-free central region of the plaque, as depicted in Figure 21.

The results in Figure 24C, D are based on the assumption that the transition from Susceptible to Dormant cell is instantaneous. However, transitioning to the spore state is a process that takes time, during which sporulating cells remain vulnerable to lysis by phages [1]. By introducing a delay in the dormancy process via a series of multiple intermittent states n_E, the dormancy peak around the plaque vanishes, as depicted in Figure 24E, F. This is because the bacteria that transition to dormancy are in a phage-dense environment. Therefore, the time window is too short for them to build up their defenses, making them vulnerable to infections and lysis by other phages. By introducing a time delay in the transition to sporulation, Model V becomes equivalent to Model R, as the diminishing resources emerge as the sole significant catalyst for dormancy. Nevertheless, Model V consistently captures the plaque growth dynamics, irrespective of the time delay, as evidenced in Figure 22C.

The fragility of the sporulation ring arises from the implications of assuming sporulation initiation through direct contact with viruses. An alternative hypothesis suggests that sporulation could be induced indirectly by a molecular component released upon infection and/or cell lysis. If this molecule is smaller than the viruses, its faster diffusion could preemptively trigger sporulation in cells, serving as a timely alert for the approaching viruses. We refer to this model as 'Model M'. This model integrates new parameters, namely the rate at which molecules are adsorbed by susceptible bacteria, $\mu = 5 \cdot 10^{-11}$mL/(hrs $\cdot$ (cells)), the number of molecules released upon lysis $m = 10^4$ and the molecule diffusion constant $D_M = 4 \cdot 10^5 \mu$m^2/hrs. Furthermore, $\sigma = 0.2\tilde{K}_g$ and molecular concentrations are expressed in cells/mL - representing the equivalent density of cell to spore transitions molecules can trigger (similar to the expression of resource density in terms of equivalent cell density). Model M is described by the following system of equations. The black elements come from Model R, the red terms were introduced in Model V, and the blue ones are unique to Model M. For the connection between the three models, see also the schematics in Figure 23.

$$\frac{\partial \tilde{R}}{\partial t} = -\underbrace{g(\tilde{R})(S + E_{total})}_{\text{cell growth}} + \underbrace{D_R \nabla^2 \tilde{R}}_{\text{resource diffusion}}$$

$$\frac{\partial S}{\partial t} = \underbrace{g(\tilde{R})S}_{\text{cell growth}} - \underbrace{\phi S V}_{\text{viral infection}} - \underbrace{f(\tilde{R})S}_{\text{dormancy initiation}} - \underbrace{\mu M S}_{\text{dormancy initiation}}$$

$$\frac{\partial M}{\partial t} = \underbrace{m\eta(\tilde{R})I_{n_I}}_{\text{molecule from lysate}} - \underbrace{\mu M S}_{\text{dormancy initiation}} + \underbrace{D_M \nabla^2 M}_{\text{molecule diffusion}}$$

$$\frac{\partial I_1}{\partial t} = \underbrace{\phi(S + E_{total})V}_{\text{viral infection}} - \underbrace{\eta(\tilde{R})n_I I_1}_{\text{to next infected state}}$$

$$\frac{\partial I_i}{\partial t} = \underbrace{\eta(\tilde{R})n_I I_{i-1}}_{\text{from previous infected state}} - \underbrace{\eta(\tilde{R})n_I I_i}_{\text{to next infected state or viral lysis}}$$

$$\frac{\partial V}{\partial t} = \underbrace{\beta\eta(\tilde{R})I_{n_I}}_{\text{viral lysis}} - \underbrace{\phi(S + I_{total} + E_{total})V}_{\text{viral infection}} - \underbrace{\omega V}_{\text{viral decay}} + \underbrace{D_V \nabla^2 V}_{\text{viral diffusion}}$$

$$\frac{\partial E_1}{\partial t} = \underbrace{f(\tilde{R})S}_{\text{dormancy initiation}} + \underbrace{\mu M S}_{\text{dormancy initiation}} - \underbrace{\lambda n_E E_1}_{\text{dormancy initiation}} - \underbrace{\phi E_1 V}_{\text{infection of exposed transitioning cells}}$$

$$\frac{\partial E_i}{\partial t} = \underbrace{\lambda n_E E_{i-1}}_{\text{from previous transitioning state}} - \underbrace{\lambda n_E E_i}_{\text{to next transitioning state or to dormancy}} - \underbrace{\phi E_i V}_{\text{infection of exposed transitioning cells}}$$

$$\frac{\partial D}{\partial t} = \underbrace{\lambda n_E E_{n_E}}_{\text{transition to dormancy}}$$

In line with the experimental observations, Model M can replicate both the reduced plaque

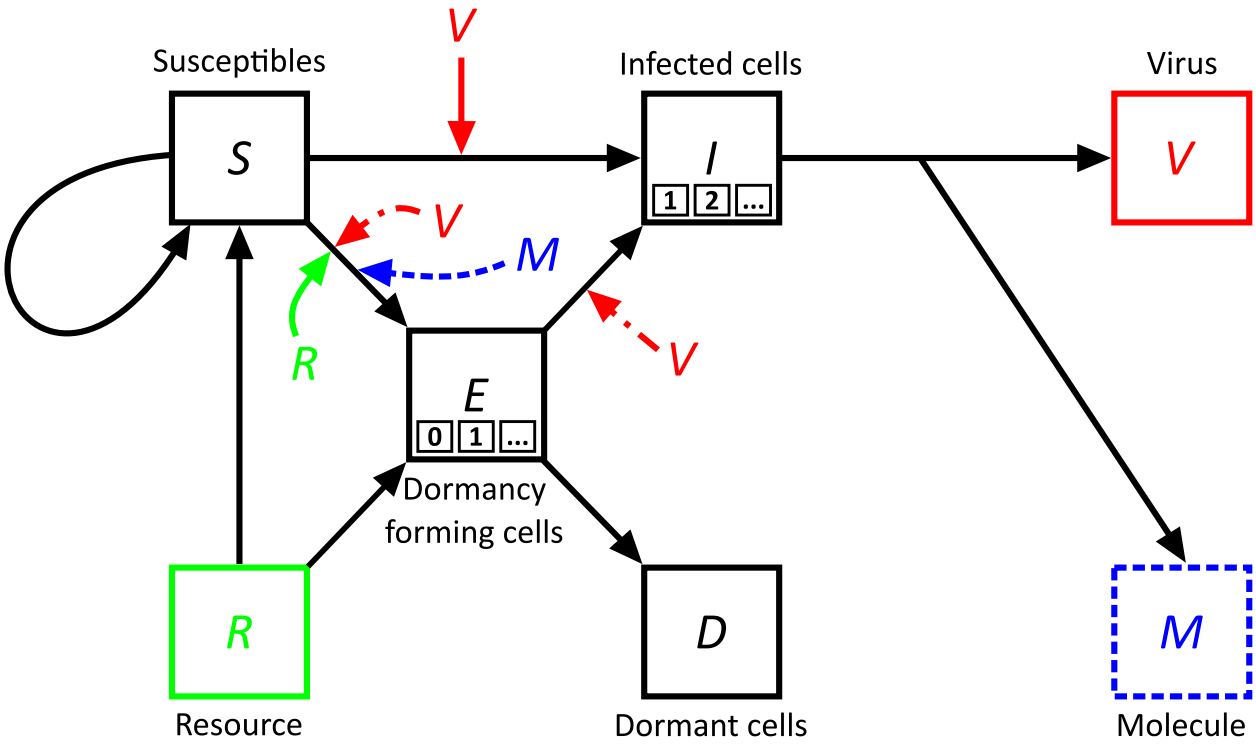

Figure 23: **Schematic representation of Models R, V, and M.** Each shape corresponds to distinct elements in the system. Specifically, squares represent explicit limited resources (R), susceptible bacteria (S), infected bacteria (I), dormant bacteria (D), bacteria transitioning to dormancy upon virus encounter (E), free viruses (V), and signalling molecules (M). The smaller boxes contained in the E and I sections indicate the potential count of E and I states, symbolized by n_E and n_I, respectively. The time cells spend in a specific state is dictated by the number of the states. For the E states, n_E can be set equal to zero, corresponding to a direct transition from the Susceptible state to the Dormant state. The arrows represent interactions, and the direction they point to signifies causality. The central elements of Model R, Model V, and Model M are highlighted in green, red, and blue, respectively. These are the Resource for Model R, where we assume resource-only dependent dormancy, the Virus for Model V, where dormancy can be triggered by viral contact aside from starvation and the Molecule for Model M, where we assume a small molecule in the lysate as an additional initiator for dormancy. Common elements across all models are marked with solid lines, while model-specific components are outlined with dashed lines, each in its respective color.

size in S^+ and the growth dynamics as shown in Figure 22D. But in contrast to the other models, Model M can also reproduce the transient sporulation peak at the plaque's periphery even when accounting for a time delay in the transition to dormancy. An example for t = 5 hrs is shown in Figure 24 G-J, but the observed phenomenon persists for roughly the same time period represented by the $n_E = 0$ Model V. This happens because the small molecule diffuses faster and reaches the susceptible cells before the phages do. While phages will reach a number of these cells before they can fully develop their defenses, there exists a distance where the signalling molecules arrive early enough to allow cells adequate time to transition to dormancy before the viruses approach. At that distance, we will have the formation of the ring of sporulation that will block the phage expansion, resulting in a smaller plaque. Given an absorbable molecule, as in our model, its quantity would diminish while traveling outward. In the absence of new phage targets for lysis and molecule production, this leads to a localized and prolonged enhancement of sporulation around the plaques. This phenomenon persists until the outer region resources fall below σ. Unlike Model V, this model also accurately replicates a central region within the plaque that's devoid of both

spores and cells (see Figure 24H, J) as observed experimentally (see Figure 21).

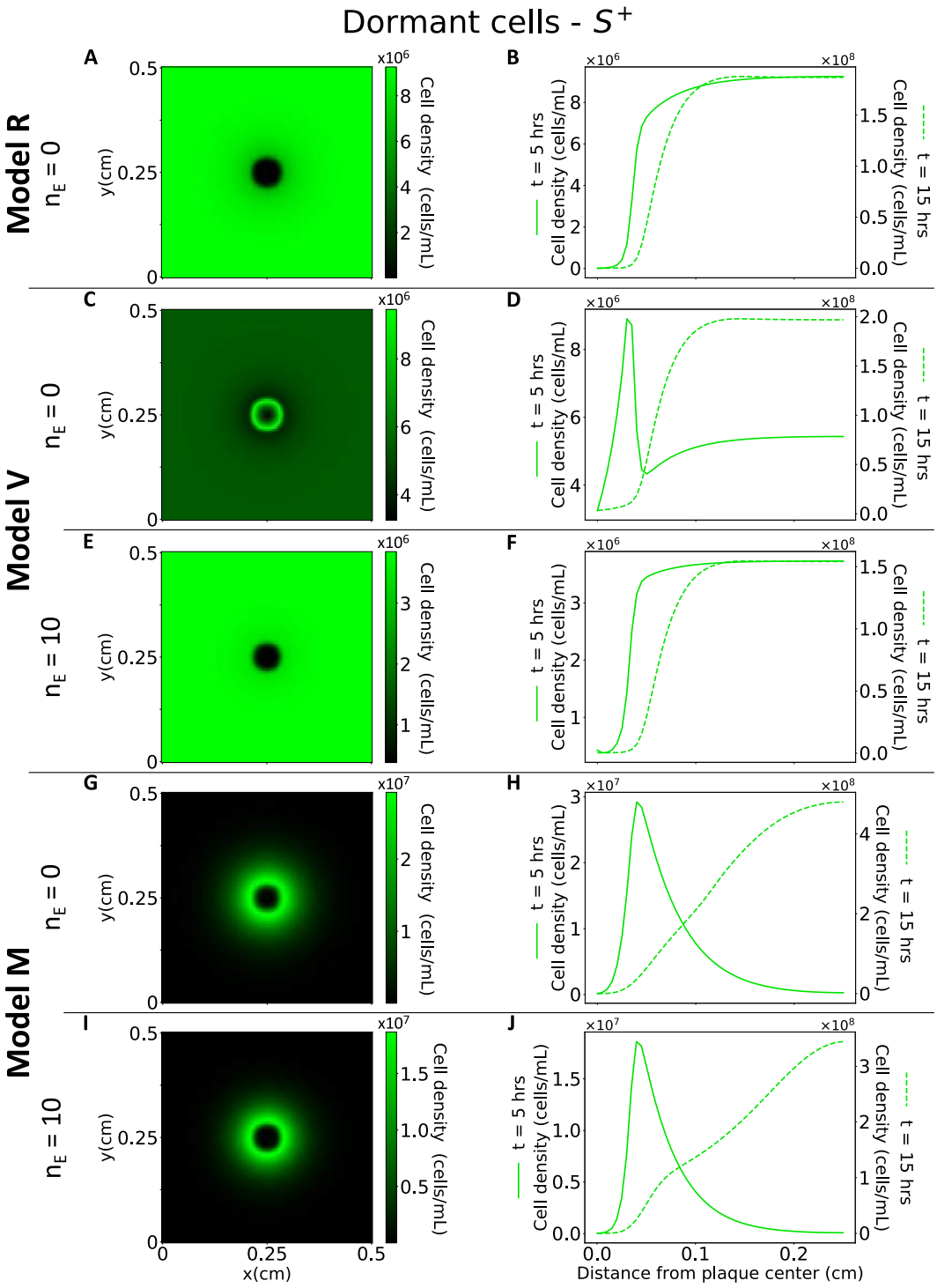

Figure 24: **Simulated plaque growth and distribution of dormant cells for the S^+ host at t = 5 hrs after phage addition.** The layout of the simulation results follows that of Figure 21B,C. Rows categorize results by model type: Models R, V, and M. The left column panels A, C, E, G, and I depict dormant cell densities' 2-D spatial distribution at t = 5 hrs. This is the central time point within the t 3 - 7 hrs window when our simulations show a transient spike in sporulation around the plaque. The right column panels B, D, F, H, and J present the radial profile of dormant cells' distribution. Displayed on the primary y-axis, the solid line shows the radial distribution of dormant cells at t = 5 hrs, offering a one-dimensional perspective corresponding to the left panel in its row. The dashed line on the secondary y-axis traces the evolution of these results at t = 15 hrs.

3.4 Conclusion

While most experimental studies are conducted under optimal conditions for bacterial growth, in nature, bacteria often encounter challenging environmental conditions [131, 196]. Our study focuses on sporulation in *Bacillus subtilis*, a widely studied dormancy process in a model organism for Gram-positive bacteria. We show that sporulation in *Bacillus subtilis* is not solely a function of resource availability but can also be induced by viral presence, with profound implications for phage-bacterial community dynamics. This complements earlier research highlighting that dormancy in Listeria [197] and Archaea [167] can be virus-induced. However, while previous works suggest direct viral contact as a trigger, our results lean towards an indirect mechanism mediated by a small molecule released upon cell lysis, akin to the recent discovery by [186] regarding phage tolerance in *Bacillus subtilis*. Identifying this molecule and understanding the exact sporulation triggering mechanisms remains an exciting frontier for subsequent investigations.

3.5 Manuscript: Phage infection fronts trigger early sporulation and collective defense in *Bacillus subtilis* populations

Authors: Andreea Măgălie[1,2], **Anastasios Marantos**[3], Jacopo Marchi[1], Daniel Schwartz[4], Jay Lennon[4], Joshua Weitz[5,6,7]

Affiliations: [1] School of Biological Sciences, Georgia Institute of Technology, Atlanta, GA, USA
[2]Interdisciplinary Graduate Program in Quantitative Biosciences, Georgia Institute of Technology, Atlanta, GA, USA
[3]**Center for Models of Life, Niels Bohr Institute, University of Copenhagen, Copenhagen, Denmark**
[4]School of Biological Sciences, Georgia Institute of Technology, Atlanta, GA, USA
[5]Department of Biology, University of Maryland, College Park, MD USA
[6]Department of Physics, University of Maryland, College Park, MD USA
[7] Institut de Biologie, École Normale Supérieure, Paris, France

My contribution: I have contributed to the modeling/theoretical part. Under the supervision of Dr. Jacopo Marchi and Prof. Joshua Weitz, I made the models and the associated computational work, processed data, produced the theoretical figures, and contributed to the writing and editing of the work. I have also contributed conceptually with the introduction of the idea of the molecule and how the introduction of the time delay to dormancy can help us differentiate between the dormancy trigger by direct contact and the trigger by a signaling molecule. I also showed that the a model based on resources cannot create an enhancement of sporulation around the plaques. My contribution to the experimental part was limited to suggestions and discussions with the experimental part of the team.

Supervision: I worked under the supervision of Dr. Jacopo Marchi and Prof. Joshua Weitz, with important input from Dr. Andreea Măgălie.

Publication status: Awaiting submission.

Phage infection fronts trigger early sporulation and collective defense in *Bacillus subtilis* populations

Andreea Măgălie,[1,2] Anastasios Marantos,[3] Jacopo Marchi,[1]
Daniel A. Schwartz,[4] Jay T. Lennon,[4] and Joshua S. Weitz[5,6,7,*]

[1]*School of Biological Sciences, Georgia Institute of Technology, Atlanta, GA, USA*
[2]*Interdisciplinary Graduate Program in Quantitative Biosciences, Georgia Institute of Technology, Atlanta, GA, USA*
[3]*Center for Models of Life, Niels Bohr Institute, University of Copenhagen, Copenhagen, Denmark.*
[4]*Department of Biology, Indiana University, Bloomington, IN, USA*
[5]*Department of Biology, University of Maryland, College Park, MD USA*
[6]*Department of Physics, University of Maryland, College Park, MD USA*
[7]*Institut de Biologie, École Normale Supérieure, Paris, France*

I. ABSTRACT

Dormancy is a common life history trait that allows individuals to enter a reversible state of reduced metabolic activity . Among microorganisms, an archetypal example of dormancy involves the generation of endospores by *Bacillus* and its relatives. While endospores confer tolerance to environmental stressors like energy limitation and other abiotic conditions, they can also provide protect cells against virus infection . Here, we explore the effects of sporulation on viral infection dynamics by examining the spatiotemporal spread of phage on *B. subtilis* populations in a spatially structured environment. By comparing phage front dynamics in a sporulating bacterial strain to a non-sporulating one, we show that sporulation decreases in plaque size by 2.x fold. This reduction arises due to an early termination of the front rather than due to a change in front speed. Via a microscopic plaque assay protocol we observe that spores are enhanced around the edges of the plaque. We then develop and evaluate mathematical models of phage, bacteria, and spore dynamics to explore the effect of sporulation on phage-bacteria interactions and on plaque formation. Our results suggest that sporulation is responsive to viral-induced lysis - likely via the release of small molecules that diffuse before the arrival of virions - opening new avenues to explore the entangled fates of phage and their bacterial hosts. End on coevolution? We will also have opportunity/need to develop a Significance section if targetting PNAS

II. INTRODUCTION

Dormancy is a survival strategy found across different types of organisms, including bacteria. Through dormancy, bacteria enter a reversible low-metabolic state, allowing them to survive for long periods of time without dividing [1–3]. An extensively studied type of dormancy in bacteria is sporulation in *Bacillus subtilis*. During sporulation, *B. subtilis* goes through asymmetric cell division, followed by a lengthy developmental stage to create an extremely resilient spore. Spores have been shown to be resistant to extreme temperatures, UV radiation and chemicals and can thus survive for decades under stressful laboratory conditions and even longer in natural environments (e.g., in some cases, at least tens of thousands of years) [4–6]. At an ecological scale, spores also increase genetic and phenotypic diversity in a population, thus increasing biodiversity [7, 8]. Sporulation can thus provide multiple types of adaptive benefits to the host both at an individual and population level.

Another putative benefit of sporulation is to protect the host against phage infections. Bacterial viruses, commonly referred to as bacteriophages or phages, are a significant driver of bacterial mortality. Bacteria have evolved intracellular and extracellular mechanisms to prevent phage infection and/or inhibit the viral replication cycle [9–12]. Sporulation provides an extreme example: the protective outer layer is distinct from that of the actively growing cell and can be depleted or devoid of phage receptor binding domains. As a result, phage adsorption to spores can be reduced significantly and potentially stopped entirely [13]. Given its protective benefits, dormancy initiation may be linked to the presence of viruses. In one recent example, dormancy in *Listeria ivanovii* cells was shown to be triggered in response to viral infection in the population [14, 15]. Several studies have identified transcription factors found in phage genomes that have the potential to change sporulation patterns in the host [16–20]. These works have led to the hypothesis - not yet supported by direct evidence - that phages could modulate or even control sporulation decisions in the host, however, to our knowledge, no work has provided any evidence supporting this claim.

Typeset by REVTEX
*Electronic address: jsweitz@umd.edu - Former affiliation: School of Biological Sciences, Georgia Institute of Technology, Atlanta, GA, USA

Sporulation can also change the phage infection dynamics at a population level. In a serial transfer coevolutionary experiment, sporulation has shown to stabilize oscillatory population dynamics induced by phages [13]. This effect however was quickly overshadowed by evolution of other mechanisms of resistance in the host. In this work, the infection dynamics was carried out in a well mixed environment in liquid media. On the other hand, phage infection of bacteria in an explicit spatial context mimics conditions found in soils and on surfaces and also provides distinct selection criteria compared to viral infection in liquid cultures [21–24].

Plaque assays are a standard technique in which bacteria and viruses grow in a spatially structured environment and can be used to determine phage titers and infection dynamics kinetics. In a plaque assay, bacteria and phages are grown on a petri dish such that phages infect and diffuse to generate a plaque, i.e., a circular clearing in the bacterial lawn. As such, this experimental approach has been used to determine phage infectivity and study bacterial antiviral strategies [25, 26]. In parallel to experimental work, mathematical and numerical methods can also be used to model plaque development [27, 28]. Classic models express the plaque growth rate based on viral infection parameters such as viral diffusion, latent time or burst size [29, 30]. Other works use this framework to model bacteria-phage interactions in spatial setting [31, 32]. Using mathematical models alongside experimental data of plaque assays can provide a means to study the effects of sporulation in a spatially complex environment.

In this study we use plaque assays to understand how dormancy changes the infection dynamics between *B. subtilis* and bacteriophages. We use a sporulating (WT) and non sporulating (SPOIIE) host to compare and contrast how the plaques grow over time. We also develop an inverted plaque assay to observe the plaques at a microscopic level and quantify sporulation with respect to the plaque. Using mathematical models, we address the interplay between sporulation and phage infection dynamics. Our results give insights on how sporulation can limit the spread of phages in a bacteria population, reducing the plaque size, and suggest that viruses can trigger sporulation, leading to collective defense of *B. subtilis* populations.

III. METHODS

A. Experimental setup

1. Bacterial strains and growth conditions

We use two $\Delta 6$ *Bacillus subtilis* strains: a wild type (WT) which can sporulate, and a SPOIIE mutant which has a SPOII mutation at locus E. This mutation stops the cell from sporulating at the asymmetrical division stage II which is early in the sporulation process [33]. We note that the $\Delta 6$ *Bacillus* strain, a derivative of the 168 laboratory strain, has a reduced genome without prophages and is immotile [34].

Daniel section on strains and genetic analysis of the transformation.

Bacterial cultures were grown in difco sporulation media (DSM). DSM is considered a rich media and has been widely used to obtain high sporulation rates [35, 36]. The cells are streaked from glycerol stock and grow at 37C overnight. After overnight growth, cells are inoculated from a singular colony and grown at 37C and 220 rpm for $\approx$ 5 hours until they reach OD ≈ 0.5.

2. Phage strains and plaque assay

We use three wild type bacteriophages of *Bacillus subtilis*: SPO1, SP10 and SPP1. These are lytic bacteriophages and have been obtained from **viral strains origin, anything else to mention?**.

The plaque assay protocol is adapted from the 'tube free agar-overlay' protocol [37]. In brief, 100 μl of cell culture at OD 0.5, 100μl of viral solution and 2.5 ml of 0.3% agar soft overlay at 55C are spotted directly on the petri dish. Immediately after the overlay is poured, the plates are swirled so that the bacteria and viruses are evenly distributed. After the overlay sets at room temperature for 10 minutes, the plates are moved to a 37C incubator to grow overnight.

To acquire a time-lapse of the plaque assays, the plates are placed on top of a white LED screen in a 37C room. Top-down images are captured every 5 minutes for 15 hours. The imaging protocol is the same for end-point images in that plates are set on top of a white LED screen and a top-down image is acquired. The end-point images are taken once the plaques reach a stable state, after 15 hours at 37C.

3. Inverted plaque assay

To prepare an inverted plaque assay, the bacterial cultures are grown to reach exponential phase as described in section III A 1. In the meantime a viral dilution is prepared in 1.7 ml eppendorf tubes to reach a concentration of $\approx 4 \cdot 10^4 pfu/ml$. This is done in order to obtain about 2000 viruses in $50\mu l$ of solution and between 20-30 in the final dilution. During this time, agar pads are also prepared by pouring 6 ml of DSM media with a 2% agarose concentration on a 60 x 15 mm petri dish (based on protocol 3.3 from [38]). Using sterile techniques, the agar is cut with a scalpel in 9 squares of size 1cm x 1 cm (Fig. S1 panels A-D).

Once the bacterial cultures reach OD ≈ 0.5, 1ml of culture is centrifuged at 15000 rpm for 5 minutes. 900 μl of supernatant is removed before tubes are mixed in a vortex and spinned down. The remaining $100\mu l$ of concentrated culture is mixed with $50\mu l$ of viral solution. Immediately afterwards, $2\mu l$ of the bacteria-virus mixture are spotted on a 50 mm glass-bottom petri dish (prod no 14027-20 Ted Pella). These smaller plates have a 50 mm glass bottom and are ideal for microscopy imaging. A 1 cm x 1cm agar pad is placed on top of each droplet and each glass-bottom petri dish can fit four experiments. The petri dish is covered and set it in a 37C incubator for 8-12 hours after which it can be imaged (Fig. S1 panel E).

B. Image analysis

1. Time-lapse and final point image analysis

A binarization method that separates a plaque from the bacterial lawn is used to obtain the final size of plaques of the traditional plaque assay. To analyze the plaque sizes over time, we obtain the plaques and their centers for the last frame. The centers are defined as the centroid or center of mass of a connected component and once the centers of the plaques are identified, a rectangular search window is defined for each plaque and used to determine the plaque size in the previous frames. This method is used because of the difficulty to identify plaques when the contrast between the plaques and lawn is not as high as it is in the last frame. A more in depth description of this inward moving plaque identification algorithm with intermediate images is shown in SI sections VII A 1 and VII A 2.

2. GFP image analysis

To compute the average GFP intensity relative to the center of the plaque, the background fluorescence is first subtracted. The corrected image is then blurred and the center of the plaque is defined based on the row and column GFP levels. Finally, the distance between each pixel and the center is calculated to obtain panel B in Fig. 3. A more in depth description is given in SI section VII A 3.

C. Mathematical models and simulations

1. Mathematical modeling

We express the mathematical model as a Lotka-Volterra model, where viruses V infect susceptible bacteria S, which grow on explicit resources R. Susceptible bacteria can become infected cells I when viruses adsorb to them until they are lysed. Susceptible cells can also transition to dormant cells D, immune to phage adsorption. To account for different modes of dormancy initiation, we build 3 different compartmental models: Model R, Model V and Model M explained below and sketched in Fig. 4. For the initial conditions, we consider susceptible cells and resources are uniformly distributed on a plane at time $t = 0$ and viruses are concentrated at the central point of the area of interest. There are no dormant or infected cells at the beginning.

Model R - Resource-only dependent dormancy

In Model R dormancy is initiated at a low rate when resources are high (accounting for stochastic dormancy [8, 39] and at a much higher rate when resources are depleted. This is in line with the fact that starvation-triggered dormancy is the most widely accepted mechanism to describe dormancy initiation in Bacilus Subtillis [8, 33, 40]. We write the associated system of differential equations below as a two dimensional Lotka-Volterra-type model, with

explicit resources and dormancy that depends solely on the amount of resources:

$$
\begin{aligned}
\frac{\partial \tilde{R}}{\partial t} &= -\underbrace{g(\tilde{R})S}_{\text{cell growth}} + \underbrace{D_R\nabla^2\tilde{R}}_{\text{resource diffusion}} \\
\frac{\partial S}{\partial t} &= \underbrace{g(\tilde{R})S}_{\text{cell growth}} - \underbrace{\phi SV}_{\text{viral infection}} - \underbrace{f(\tilde{R})S}_{\text{dormancy initiation}} \\
\frac{\partial I_1}{\partial t} &= \underbrace{\phi SV}_{\text{viral infection}} - \underbrace{\eta(\tilde{R})n_I I_1}_{\text{to next infected state}} \\
\frac{\partial I_i}{\partial t} &= \underbrace{\eta(\tilde{R})n_I I_{i-1}}_{\text{from previous infected state}} - \underbrace{\eta(\tilde{R})n_I I_i}_{\text{to next infected state or viral lysis}} \\
\frac{\partial V}{\partial t} &= \underbrace{\beta\eta(\tilde{R})I_{n_I}}_{\text{viral lysis}} - \underbrace{\omega V}_{\text{viral decay}} - \underbrace{\phi(S+I_{total})V}_{\text{viral infection}} + \underbrace{D_V\nabla^2 V}_{\text{viral diffusion}} \\
\frac{\partial D}{\partial t} &= \underbrace{f(\tilde{R})S.}_{\text{dormancy initiation}}
\end{aligned}
\tag{1}
$$

where $\tilde{R}(\mathbf{x},t)$ is the rescaled density of resources, expressed in units of cells/mL. The rescaling is performed as $[\tilde{R}] = [R/\epsilon] = \frac{\frac{\mu g}{mL}}{\frac{\mu g}{cells}} = \frac{cells}{mL}$, where ϵ denotes the rate of resource to bacteria conversion measured in μg/cells (see Table I and Parameter estimations for details). Similarly, $S(\mathbf{x},t), I(\mathbf{x},t)$ and $D(\mathbf{x},t)$ are the densities of susceptible, infected, and dormant bacteria, respectively, each in units of cells/mL. V designates the density of phages in viruses/mL. Given our experimental setup, we assume immotile and non-diffusing bacteria that grow by consuming resources. In contrast, resources and viruses are assumed to diffuse. The susceptible cells can either get infected by virulent phage with infection rate ϕ or become dormant if the density of the resources is low. Once infected, the cells go through a series of sequential stages n_I of infected states I_i (the sum of which is given by $I_{total} = \sum_{i=1}^{n_I} I_i$), resulting in an effective latent time delay which follows an Erlang distribution. After the latency period, the infected cells can burst yielding new free viruses with burst size β. Virus particles can adsorb to cells at a rate ϕ and decay with rate ω. The bacterial growth rate $g(\tilde{R})$, dormancy rate $f(\tilde{R})$ and latent time $\eta(\tilde{R})$ are dependent on the available resources and are given by:

$$g(\tilde{R}) = r_{max}\frac{\tilde{R}}{\tilde{K_g} + \tilde{R}} \tag{2}$$

$$f(\tilde{R}) = \frac{d_{max}}{1 + e^{s(\tilde{R}-\sigma)}} \tag{3}$$

$$\eta(\tilde{R}) = \eta_{max}\frac{g(\tilde{R})}{g(\tilde{R_0})}. \tag{4}$$

The growth rate function follows the Monod equation were r_{max} is the maximum bacterial growth rate and $\tilde{K_g}$ the rescaled Monod constant (similarly to R, $[\tilde{K_g}] = [K_g/\epsilon] = \frac{\frac{\mu g}{mL}}{\frac{\mu g}{cells}} = \frac{cells}{mL}$). The dormancy rate function is assumed to be solely dependent on resources but with sporulation starting effectively only when the resource density is close to a fraction σ of the Monod's constant (for Model R $\sigma \approx 0.282\tilde{K_g}$. As a reminder, when the resources are equal to the Monod's constant the growth rate is equal to the half of the growth rate). The 'sharpness' of the transition to dormancy is determined by the value of parameter s. Finally, we choose a resource dependent lysis rate that is proportional to the growth rate g(R) [41, 42]. This choice is justified by the fact that the plaques stop growing as bacteria have exhausted the available nutrients. The meaning, value and units of the model parameters are contained in the following table. Full details of parameter estimation are in Section VII B 2.

Parameters common to all models				
Variable	*Meaning*	*Value*	*Unit*	*Source*
R_0	Initial resource level	10^3	μg/mL	Estimate
$\tilde{R}_0$	Rescaled initial resource level	10^9	(cells)/mL	Estimate
S_0	Initial cell density	10^7	(cells)/mL	This work
V_0	Initial viral density	10^6	(viruses)/mL	This work
r_{max}	Maximum bacterial growth rate	2	hrs^{-1}	Literature
ε	Resource to bacteria conversion rate	10^{-6}	μ g/(cell)	Estimate
K_g	Monod constant	$3.2 \cdot R_0$	μ g/mL	This work
$\tilde{K}_g$	Rescaled Monod constant	$3.2 \cdot \tilde{R}_0$	(cells)/mL	This work
ϕ	Infection rate	$1.8 \cdot 10^{-8}$	mL/(hrs $\cdot$ (virus))	This work/Literature
η_{max}	Maximum latent rate	4/3	hrs^{-1}	Literature
d_{max}	Maximum transition to dormancy rate	1	hrs^{-1}	This work
β	Burst size	100	(viruses/cell)	Literature
ω	Viral decay	0.001	hrs^{-1}	Literature
D_R	Resource diffusion constant	$4 \cdot 10^5$	μm^2/hrs	Literature
D_V	Phage diffusion constant	$2 \cdot 10^3$	μm^2/hrs	Estimate/Literature
n_I	Number of infected states	10		This work
s	"Sharpness" of transition to dormancy	10^{-7}		Estimate

TABLE I: Parameters common to all models

Model V - Direct interaction with viruses as an additional trigger of dormancy

We expand on resource dependent dormancy and consider a scenario in which viruses can also trigger sporulation. Specifically, in Model V, in addition to the conventional starvation-induced dormancy, a cell may enter a dormant state with a probability $p \in (0, 1)$ or become infected with a probability $1-p$ upon encountering a viral particle. This yields a family of (p, σ) combinations that exhibit identical plaque growth dynamics, with the $(p = 0, \sigma = 0.282\tilde{K_g})$ case corresponding to Model R. In order to account for a time delay for spore formation we introduce a potential series of multiple sequential stages n_E to become dormant. Hence, the dormancy initiation time follows an Erlang distribution. The transition to dormancy is immediate for $n_E = 0$, while a delay is introduced for $n_E > 0$ ($E_{total} = \sum_{i=1}^{n_E} E_i$). The net transition rate between the E-states is λn_E, where $\lambda = \frac{4}{3} hrs^{-1}$, so that the mean transition rate remains constant with varying number of states. Cells in the dormancy initiation phase can become infected by phage, whereas spores cannot be infected. All the rest of the variable values are the same between models R and V (as shown in Fig. 4 and in the table of common variables for the two models). The following system of equations expands Model R (see equations set (1) for comparison) with the red terms that are introduced in Model V.

$$
\begin{aligned}
\frac{\partial \tilde{R}}{\partial t} &= -\underbrace{g(\tilde{R})(S+E_{total})}_{\text{cell growth}} + \underbrace{D_R\nabla^2\tilde{R}}_{\text{resource diffusion}} \\
\frac{\partial S}{\partial t} &= \underbrace{g(\tilde{R})S}_{\text{cell growth}} - \underbrace{f(\tilde{R})S}_{\text{dormancy initiation}} - \underbrace{(1-p)\phi SV}_{\text{viral infection}} - \underbrace{p\phi SV}_{\text{dormancy initiation}} \\
\frac{\partial I_1}{\partial t} &= \underbrace{(1-p)\phi(S+E_{total})V}_{\text{viral infection}} - \underbrace{\eta(\tilde{R})n_I I_1}_{\text{to next infected state}} \\
\frac{\partial I_i}{\partial t} &= \underbrace{\eta(\tilde{R})n_I I_{i-1}}_{\text{from previous infected state}} - \underbrace{\eta(\tilde{R})n_I I_i}_{\text{to next infected state or viral lysis}} \\
\frac{\partial V}{\partial t} &= \underbrace{\beta\eta(\tilde{R})n_I I_{n_I}}_{\text{viral lysis}} - \underbrace{\phi(S+I_{total}+E_{total})V}_{\text{viral infection}} - \underbrace{\omega V}_{\text{viral decay}} + \underbrace{D_V\nabla^2 V}_{\text{viral diffusion}} \\
\frac{\partial E_1}{\partial t} &= \underbrace{f(\tilde{R})S}_{\text{dormancy initiation}} + \underbrace{p\phi SV}_{\text{dormancy initiation}} - \underbrace{\lambda n_E E_1}_{\text{dormancy process}} - \underbrace{(1-p)\phi E_1 V}_{\text{infection of exposed transitioning cells}} \\
\frac{\partial E_i}{\partial t} &= \underbrace{\lambda n_E E_{i-1}}_{\text{from previous transitioning state}} - \underbrace{\lambda n_E E_i}_{\text{to next transitioning state or to dormancy}} - \underbrace{(1-p)\phi E_i V}_{\text{infection of exposed transitioning cells}} \\
\frac{\partial D}{\partial t} &= \begin{cases} \underbrace{f(\tilde{R})S}_{\text{dormancy initiation}} + \underbrace{p\phi SV}_{\text{dormancy initiation}} & , n_E = 0 \\ \underbrace{\lambda n_E E_{n_E}}_{\text{transition to dormancy}} & , n_E > 0. \end{cases}
\end{aligned}
\tag{5}
$$

Model M - A messenger molecule in the lysate triggers dormancy

Model M represent a scenario where sporulation is triggered by a small molecule that is released to the environment upon cell lysis. The new parameters include the rate at which messenger molecules are adsorbed by susceptible bacteria, $\mu = 5 \cdot 10^{-11}$mL/(hrs $\cdot$ (cells)), the number of messenger molecules released upon lysis $m = 10^4$ and the molecule diffusion constant $D_M = 4 \cdot 10^5 \mu$m^2/hrs. It should be noted that $\sigma = 0.2\tilde{K_g}$ and molecular concentrations are represented in cells/mL - representing the equivalent density of cell to spore transitions molecules can trigger (analogous to the representation of resource concentrations in terms of equivalent cell densities).

The following system of equations expands Model R and Model V (see equations sets (1) and (5) for comparison with the black and red elements in Model M respectively) with the blue terms that are introduced in Model M.

$$
\begin{aligned}
\frac{\partial \tilde{R}}{\partial t} &= \underbrace{-g(\tilde{R})(S+E_{total})}_{\text{cell growth}} + \underbrace{D_R\nabla^2\tilde{R}}_{\text{resource diffusion}} \\
\frac{\partial S}{\partial t} &= \underbrace{g(\tilde{R})S}_{\text{cell growth}} - \underbrace{\phi SV}_{\text{viral infection}} - \underbrace{f(\tilde{R})S}_{\text{dormancy initiation}} - \underbrace{\mu MS}_{\text{dormancy initiation}} \\
\frac{\partial M}{\partial t} &= \underbrace{m\eta(\tilde{R})I_{n_I}}_{\text{molecule from lysate}} - \underbrace{\mu MS}_{\text{dormancy initiation}} + \underbrace{D_M\nabla^2 M}_{\text{molecule diffusion}} \\
\frac{\partial I_1}{\partial t} &= \underbrace{\phi(S+E_{total})V}_{\text{viral infection}} - \underbrace{\eta(\tilde{R})n_I I_1}_{\text{to next infected state}} \\
\frac{\partial I_i}{\partial t} &= \underbrace{\eta(\tilde{R})n_I I_{i-1}}_{\text{from previous infected state}} - \underbrace{\eta(\tilde{R})n_I I_i}_{\text{to next infected state or viral lysis}} \\
\frac{\partial V}{\partial t} &= \underbrace{\beta\eta(\tilde{R})I_{n_I}}_{\text{viral lysis}} - \underbrace{\phi(S+I_{total}+E_{total})V}_{\text{viral infection}} - \underbrace{\omega V}_{\text{viral decay}} + \underbrace{D_V\nabla^2 V}_{\text{viral diffusion}} \\
\frac{\partial E_1}{\partial t} &= \underbrace{f(\tilde{R})S}_{\text{dormancy initiation}} + \underbrace{\mu MS}_{\text{dormancy initiation}} - \underbrace{\lambda n_E E_1}_{\text{dormancy initiation}} - \underbrace{\phi E_1 V}_{\text{infection of exposed transitioning cells}} \\
\frac{\partial E_i}{\partial t} &= \underbrace{\lambda n_E E_{i-1}}_{\text{from previous transitioning state}} - \underbrace{\lambda n_E E_i}_{\text{to next transitioning state or to dormancy}} - \underbrace{\phi E_i V}_{\text{infection of exposed transitioning cells}} \\
\frac{\partial D}{\partial t} &= \underbrace{\lambda n_E E_{n_E}}_{\text{transition to dormancy}}.
\end{aligned}
\tag{6}
$$

D. Data and code availability

All simulations were carried out in Python (Jupyter notebooks) and image analysis was carried out in MATLAB v 2020a. Scripts and data are available on Github at https://github.com/WeitzGroup/Plaque_early_sporulation.

IV. RESULTS

A. SPOIIE plaques are larger than WT plaques

We perform standard plaque assays of phage SPO1 with SPOIIE and WT hosts, as described in section III A 2. After 15 hours at 37C, the plaques stop growing in all conditions examined. The measured SPOIIE plaques are larger than WT plaques (Fig. 1 A). On average, the radius of SPOIIE plaques is ~ 2.2 fold greater than the radius of WT plaques and a two-sample t-test confirms that the two data sets have unequal means with a p-value $p < 10^{-3}$ (SPOIIE plaques are $1.43mm \pm 0.33mm$ and WT plaques are $0.64mm \pm 0.2mm$). We assessed the robustness of this finding by comparing plaque sizes on sporulating vs. non-sporulating hosts using bacteriophage SPP1. A 3.5 fold plaque radius reduction was observed for bacteriophage SPP1 as the two-sample t-test confirmed unequal means with a p-value smaller than 10^{-3} (SPOIIE are $1.22mm \pm 0.15mm$ and WT plaques are $0.35mm \pm 0.12mm$ as shown in Fig. S2). These results indicate that sporulation limits the spread of phage infections in *B. subtilis* populations.

B. SPOIIE and WT plaques have similar growth rates, but WT plaques stop growing early

To quantify plaque growth dynamics, we record a time-lapse of the SPO1 plaques. We extract the plaque sizes at every 5 minutes over 15 hours (see methods section III B and SI section VII A 2 for in depth details) and show growth curves for the SPOIIE plaques and WT plaques in Fig. 2. Both SPOIIE and WT plaques start growing at the 3 hour mark and continue to grow in unison for 2 hours. However, the WT plaques reach a plateau shortly after 5 hours, whereas the SPOIIE plaques continue to grow until reaching plateau at 13 hours (see WT and SPOIIE plate sections

in Figure 2). This leads to a SPOIIE mean plaque size of $1.28 \pm 0.24mm$ and WT mean plaque size of $0.43 \pm 0.12mm$. We note that even though the experiments in Figures 1 and 2 have the same setup, the final WT plaque sizes are smaller in the time-lapse experiment compared to the endpoint one. This could be due to small differences in initial conditions or due to different experimental conditions, e.g. different incubators and imaging equipment are needed for a time-lapse compared to an endpoint experiment.

We distinguish three phases of plaque development: a lag phase in which plaques are not visible, an enlargement phase in which the plaque appears to be growing at a constant rate and a final phase in which phages stop replicating [27]. We fit a linear function to the enlargement phase for each SPOIIE and WT trajectory to obtain 46 growth rates for SPOIIE plaques and 100 growth rates for WT plaques. The SPOIIE mean growth rate is $117 \pm 26\mu m/hr$ and the mean WT growth rate is $136 \pm 69\mu m/hr$. We conclude that the two bacterial strains have similar growth rates even though the final mean plaque size is almost 3 times larger for SPOIIE compared to WT. The early cessation of plaque growth for sporulating vs. non-sporulating hosts suggests that although phage propagate at a similar rate on either host, there is an additional microscopic mechanisms limiting the ability of phage to lyse hosts.

C. Sporulation is enhanced around plaques edges

We developed an inverted plaque assay to study the impact of sporulation on the microscopic dynamics of plaques (see section III A 3). Before doing so, we first repeated our analysis of plaque size in SPOIIE vs WT hosts as measured using an inverted plaque assay. Consistent with the findings of a traditional plaque assay, we found that WT inverted plaques are smaller than SPOIIE by a factor of 2.8 and reported p-value smaller than 10^{-3} (Fig. S3).

In addition to quantifying plaque size, we can use the inverted plaque assay to analyze viral plaques at a microscopic scale and quantify sporulation levels at the center and edge of a plaque (Fig. 3). The bright-field image of a plaque is shown in panel A and we see that it resembles a traditional viral plaque with a clearing in the middle surrounded by a bacterial lawn. Using the GFP channel in panel B, we notice that there are no spores at the center and spores are enhanced around the edge of the plaque compared to the bacterial lawn closer to the edge of the image. We note that this effect is transient and was captured 8 hours after the experiment was set up. Indeed, after a prolonged time period of $\approx 16h$, a different experiment shows that the bacterial lawn reaches sporulation levels similar to those found around the plaque edge (Fig. 3 F). This suggests that sporulation is triggered early in cells that are close to viral-induced lysis.

The distribution of spores can be quantified by measuring the GFP intensity as a function of the distance to the center of the plaque (Fig. 3 C). Consistent with there being no spores inside the plaque, the lowest GFP level is obtained when the distance to plaque center is less than $\approx 25\mu m$. GFP expression is increased between $\approx 15 - 100\mu m$ before decreasing to background far from plaque centers. We note that the enhancement of sporulation around the plaque edge in Fig. 3B is not an isolated event and we can observe this effect in repeated experiments and at different stages of the plaque formation process in Fig. S6D-F.

D. Modeling with resource-only induced dormancy can reproduce the plaque growth dynamics, but not the spore enhancement around the plaques

To better understand what factors affect plaque growth, we developed and analyzed a PDE model (see section III C 1) of phages spreading across a bacterial lawn including either sporulating (S^+) or non-sporulating (S^-) bacteria. Our objective is to compare simulated plaque spreading dynamics at both macroscopic and microscopic scales with observations, in light of alternative hypotheses for sporulation initiation. We first test the scenario where dormancy is only resource-dependent (Model R), mimicking starvation-induced sporulation at low resource concentration, which is the most widely accepted dormancy initiation mechanism in *B. Subtilis* [8, 33, 40].

The initiation of dormancy via resource depletion effectively reproduces the observed reduction in plaque size in our experiments, as evidenced by a comparison between Fig. 1 (experimental results) and Fig. 5A (simulation results). The underlying reason for this is that viruses in the S^+ model have fewer available cells to infect compared to those in the S^- model. Furthermore, Model R precisely replicates the dynamics of plaque growth, accurately capturing the early cessation of expansion observed in plaques associated with the S^+ strain, as corroborated by Fig. 5B. In a model with starvation-induced sporulation, dormancy typically starts from the exterior part of the plate where bacteria growth is not controlled by phages. Therefore outside the plaque resources are abruptly depleted sooner, triggering dormancy in a large fraction of cells uniformly distributed out of the reach of phage activity (i.e., outside the plaque). Phages originating from the plaque's center will eventually reach a region with dormant cells in high density, which will prevent further infection spread leading to smaller plaques for the S^+ strain.

Importantly, Model R cannot replicate the key, dynamical phenomenon of the enhancement of sporulation around the plaques, as indicated in Fig.6 A,B. This is due to the fact that in the absence of viruses (far out of the plaque) resources will be consumed equally triggering a uniformly distributed background of dormant cells. With increasing proximity to the plaque there will be less bacteria due to lysis, therefore more resources and lower dormant cell densities. At the edge of the plaque there is a precipitous decrease in bacteria density as all cells are killed, corresponding to a sharp decrease in dormant cells (see Fig. 6 A,B). Therefore, in this model the only signal triggering dormancy, lack of resources, travels from outside the plate towards the phage-occupied center. In the absence of a dormancy signal coming from the center there cannot be a peak in spore density at the edge of the plaque. Thus, while the model offers valuable insights into the dynamics of plaque growth and bacterial dormancy, it falls short in reproducing the experimentally observed localized peak in dormant cell density at the plaque's edge. This limitation highlights the need for incorporating a missing element in the modeling of dormancy triggers, one that can relay information from the plaque's center to its periphery. Given that viruses (and viral lysate products) are the only entities present at the center, they are prime candidates for this role, presenting an avenue for further investigation and model refinement.

E. Phage-triggered sporulation can enhance dormant cells at the edge of the plaque

First, we study a model where bacteria dormancy is triggered both by resource depletion and by contact with phages (see Model V in Methods). In our simulations, when a cell encounters a viral particle, it can enter a dormant state with probability p or get infected with probability $1 - p$. Model V can also reproduce the plaque growth dynamics (see Fig. 5C and Fig. S8). In this model, viruses diffusing just outside the plaque trigger dormancy while most of the bacteria have not yet been lysed, whereas the spore density decreases towards the center as there are not enough cells inside the plaque. Further away from the plaque, there is less phage-induced dormancy. If resources have not dropped yet below σ, the spore density drops, reproducing the experimentally observed peak at the edge of the plaque (see Fig. 6C,D). Similarly to our experiments (Fig. 3D-F), the peak in our simulations is transient, emerging at t $\approx$ 3 hrs and persisting until t $\approx$ 7 hrs. Given that there is a 4-5 hour interval between the transition to dormancy and the expression of GFP, this simulated onset at t $\approx$ 3 hrs closely aligns with our experimental observations, which show the peak at t $\approx$ 8 hrs.

The peak is transient because, when all resources are depleted at the end, dormancy is triggered by a lack of nutrients. Consequently, Model V will relax to the same steady-state spore density profile as Model R. Therefore Model V can qualitatively reproduce the transient sporulation enhancement around the plaques as manifested in the comparison between the experimental (Fig. 3) and the modeling results (Fig. 6C,D)) at t = 5 hrs. Since the presence of viruses immediately produces some spores, Model V produces dormant cells from the early stages of the plaque formation, with spores within the plaque building up right away from its center (see Fig. 6C,D). Conversely, in the experiments, the central region of the plaque typically does not have spores (see Fig. 3).

The results in Fig. 6C,D assume direct conversion from susceptible cell (S) to dormant cell (D). Reaching the spore state, though, requires some time in which sporulating cells could still be lysed by phages (cite Daniel). When adding a delay to dormancy, through the introduction of a sequence of multiple intermittent states n_E (see Methods, Model V), Model V retains its ability to reproduce the plaque growth dynamics (see Fig. 5C and Fig. S8A) but it fails to reproduce the peak in dormancy around the plaque (see Fig. 6E,F and Fig. S9). The inability to capture the peak in dormancy is a consequence of the fact that the bacteria that initiated the slow dormancy transition due to direct contact with phages are in a phage-dense environment. Therefore, the cells will not have enough time to build their defenses before they get infected and lysed by other phages. With the introduction of time delay for transition to sporulation, Model V becomes effectively equivalent to Model R since the reduction in the amount of resources is the only consequential driver of dormancy.

An alternative hypothesis is that sporulation is induced indirectly through some molecular cue rather than by direct contact. We propose a model (Model M) in which dormancy is triggered by the adsorption of a small molecule released from cells during infection and/or released into the environment upon lysis. Model M can reproduce the observed reduction of the plaque size in systems with sporulating cell strains and the plaque growth dynamics, as shown in Fig. 5D and Fig. S8B. Notably, Model M also successfully replicates the transient peak of sporulation around the plaques for the same time-period as Model V with $n_E = 0$, even with a delayed transition to dormancy (see Fig. 6G-J). Central to this observation is the assumption that the signaling molecule diffuses faster than viruses (compatible with it being much smaller). At a certain distance from the center, cells encountering the molecule complete spores at densities high enough to stop phage infections before phage diffuse that far. Towards the center, lysis kills cells that are transitioning to spores, reducing their density. Farther out than the peak, where the molecule did not get to high densities yet and cells did not have time to complete the sporulation process, spore density decreases again. Model M can also reproduce a central region of the plaque, empty of spores and cells (see Fig. 6G-J) as observed experimentally (see Fig. 3).

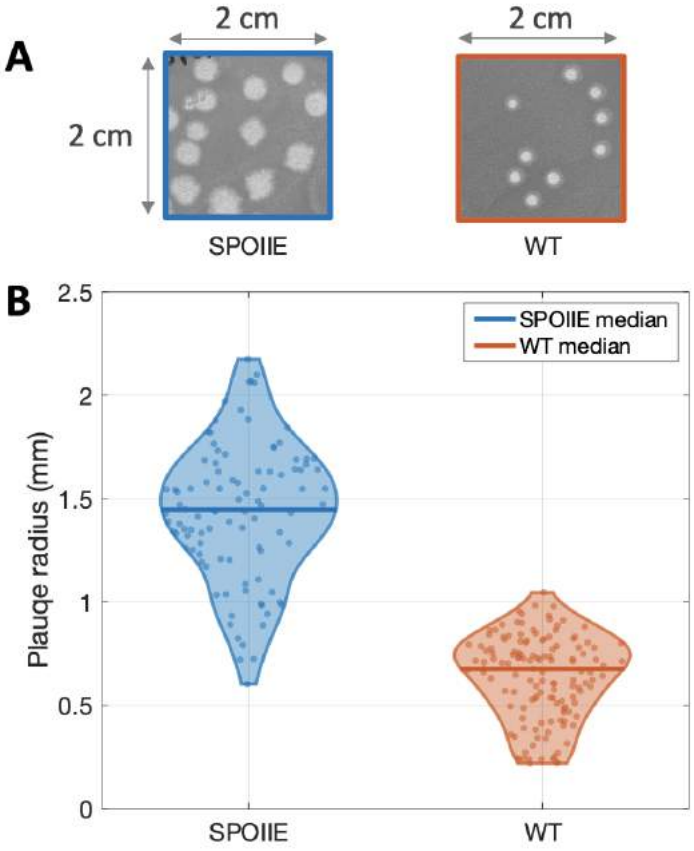

FIG. 1: **Plaque sizes of phage SPO1 with SPOIIE and WT host**. **A** Square cropped sections of size 2cm x 2cm from SPOIIE (left) and WT (right) plaque assays are shown. Both plaque assays were carried as described in section III A 2. SPOIIE and WT plaque assays where prepared in parallel and have the same initial and growth conditions. **B** Final plaque size of the two plaque assays shown in panel A. The images were analyzed using binarization and watershed algorithm (see SI section VII A 1). The plaque sizes (98 plaques for SPOIIE and 137 for WT) were plotted using a violin plot and individual points are shown as a scatter plot. The median SPOIIE and WT plaque sizes are shown through the horizontal bold lines. SPOIIE plaques have a radius of $1.43 \pm 0.33mm$ and WT plaques have a radius of $0.64 \pm 0.2mm$. A two sample t-test was performed to reject the hypothesis that the two distributions have equal means with a p-value less than 10^-3.

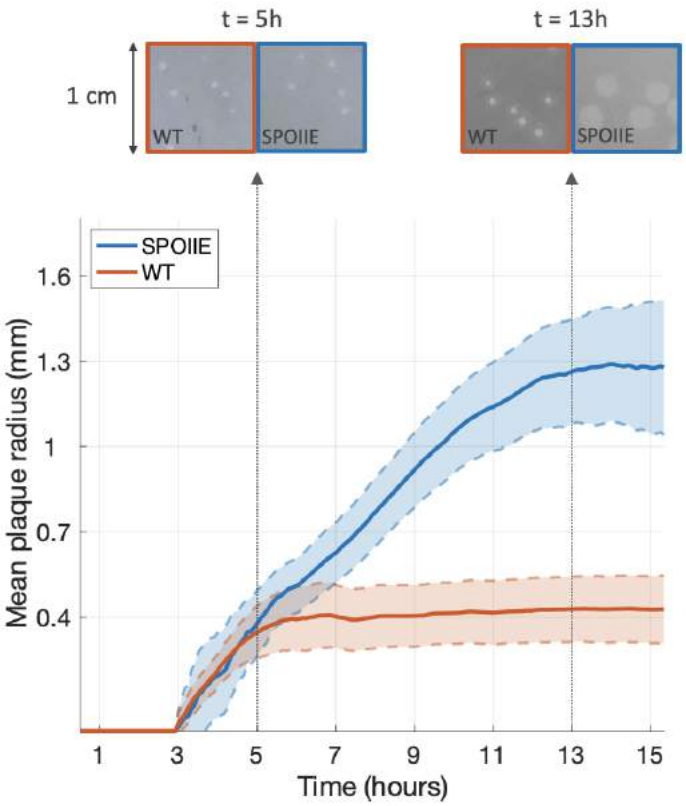

FIG. 2: **Time lapse of plaque growth for SPOIIE and WT host**. A traditional plaque assay was performed at 37C and images were captured every 5 minutes over a period of 15 hours. The plaque sizes were estimated for each time point (46 plaques for SPOIIE and 100 plaques for WT) using image analysis techniques described in brief in section III B and in detail in SI section VII A 2. Cropped sections from the time-lapse are shown at 5 and 13 hours for parts of the WT and SPOIIE plates. The mean over all plaques is shown in the solid line and the standard deviation is shown in the shaded area. Intermediate images of the independent plaque trajectories are shown in figure S5.

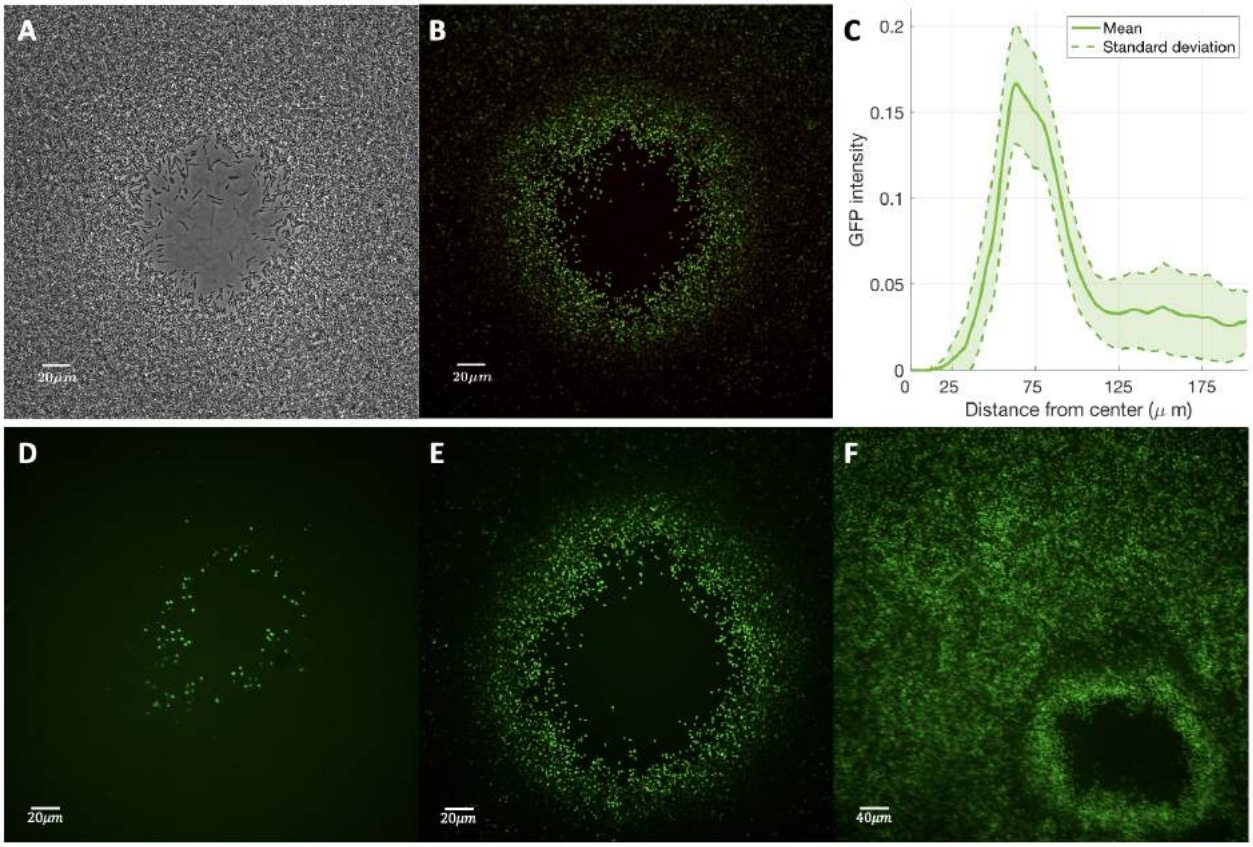

FIG. 3: **Sporulation is enhanced around plaque edges.** Bright-field image of inverted plaque assay is shown in panel A and fluorescent images are shown in panels B, D, E and F. Images A, B, D and E were taken at 40x magnification and image F at 20x magnification. The inverted plaque assay was carried out with phage SPO1. The GFP image was adjusted to remove background fluorescence and enhance contrast (see section VII A 3). **C** GFP analysis of image in panel B. The GFP image is blurred and the green component in every pixel is computed based on the distance to the center of the plaque (see SI section VII A 3). Distance to the center of the plaque is shown on the x-axis in μm and GFP intensity in the blurred image is shown on the y axis. The solid line represents the mean and the shaded area is the standard deviation. **D, E and F** show inverted plaque assays at different time points from earliest in panel D to latest in panel F. The image in panel D was taken within the first 8 hours when only cells in the vicinity of the plaque were sporulating. The image in panel F was taken after 12 hours when most of the cells have become spores.

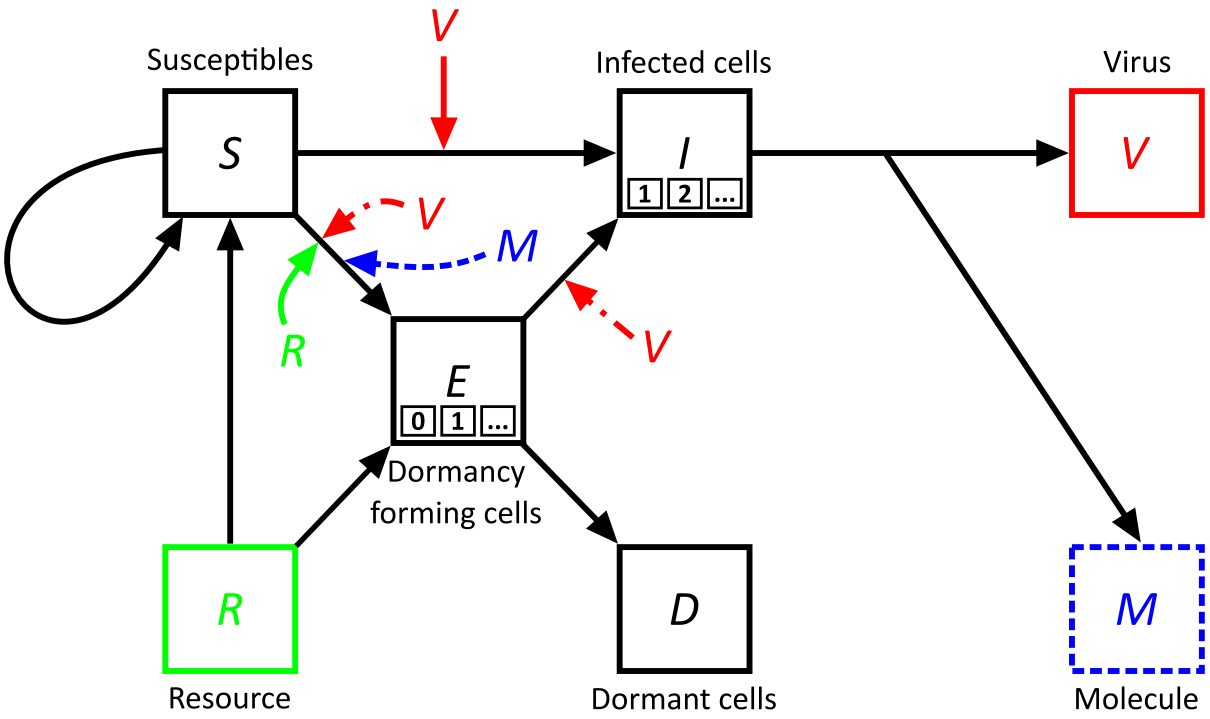

FIG. 4: **Schematic comparison of Models R, V, and M.** Each shape represents a specific element in the system. Squares correspond to explicit limited resources (R), susceptible bacteria (S), infected bacteria (I), dormant bacteria (D), bacteria transitioning to dormancy while exposed to viruses (E), free viruses (V) and signaling molecules (M). In the E and I boxes, the smaller boxes signify the potential number of E and I states, denoted as n_E and n_I respectively. The number of states defines the duration that cells spend in that state (see Methods-Mathematical Modeling III C 1). For the E states, n_E can be set equal to zero, which corresponds to a direct transition from the Susceptible state to the Dormant state. The arrows indicate interactions, with their direction showing causal effects. The central elements of Model R, Model V, and Model M are highlighted in green, red, and blue respectively. These are, the Resource for Model R, where we assume resource-only dependent dormancy, the Virus for Model V, where dormancy can be triggered by viral contact aside from starvation and the Molecule for Model M, where we assume a messenger molecule in the lysate as an additional initiator for dormancy. Elements with solid lines are shared across all models, whereas elements with dashed lines are unique to specific models and correspond to the model of the same color.

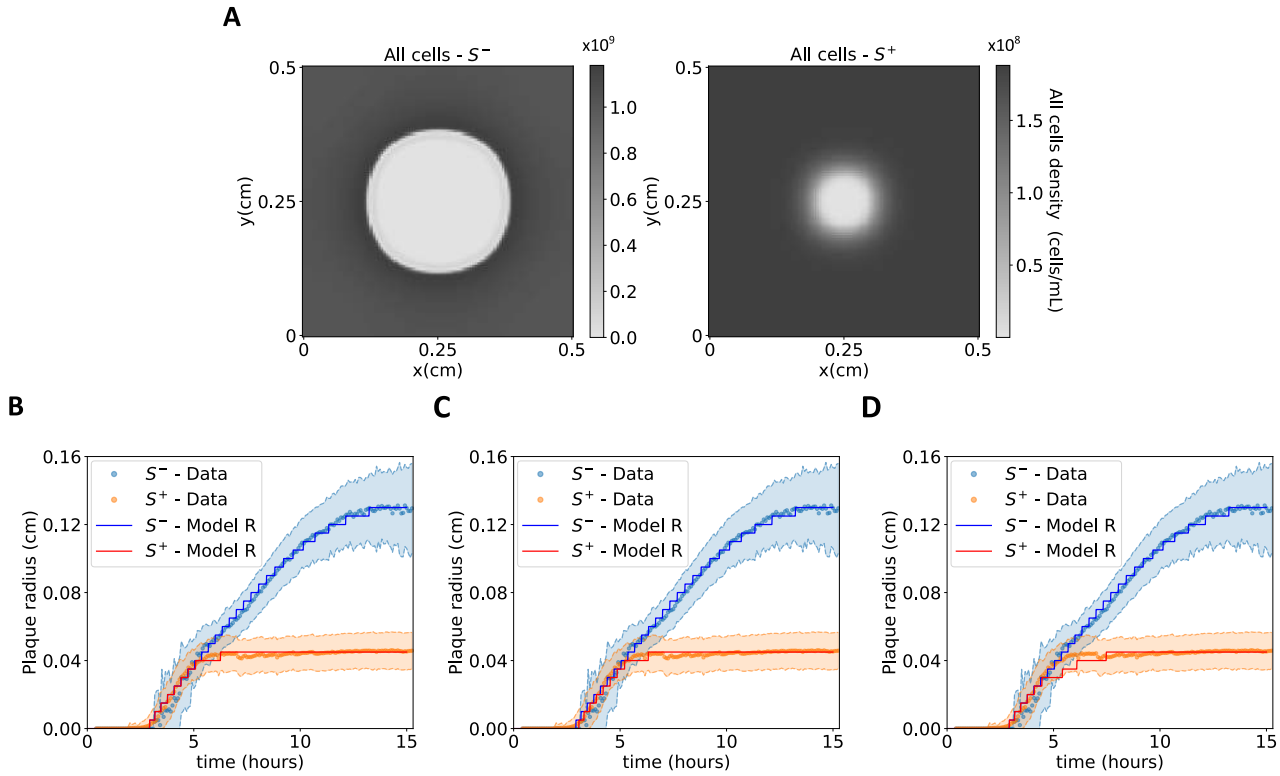

FIG. 5: **Impact of sporulation on plaque size for Models R, V, and M. A** A snapshot from the spatial simulation of bacterial densities in Model R, taken at 15 hours, corresponding to the terminal point of the time-series shown in **B**. The simulation uses the parameters from Table I and is a representative instance of the plaques' spatial simulation. **B-D** Overlay of experimental data and computational simulations shows the time evolution of the mean plaque radius for the S^- and S^+ strains in Models R, V, and M, respectively. In the simulations, a plaque is defined as the area where cell density is less than 10% of the maximum density at that time point. The results exhibit robustness to variations in that threshold, attributed to the abrupt density changes at plaque boundaries. In panels C and D, simulations for Model V and Model M respectively are performed with $n_E = 10$. Results are replicable across different values of n_E (see Fig. S8 for the $n_E = 0$ case).

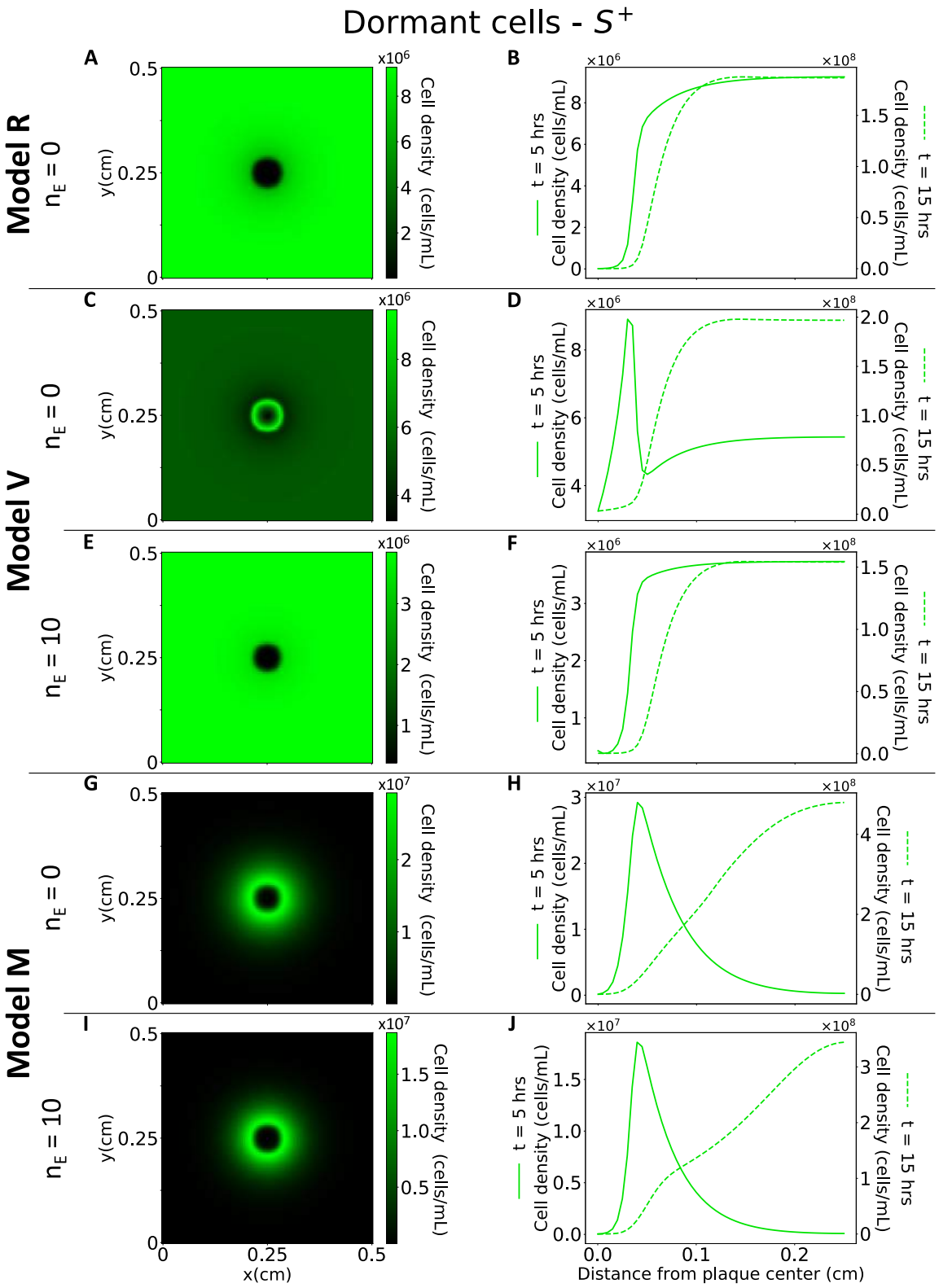

FIG. 6: **Simulated plaque growth and distribution of dormant cells for the S^+ host at t = 5 hrs after phage addition.** The arrangement of the simulation results aligns with that presented in Fig. 3B,C. Rows are organized by model type as results for Models R, V and M. The left column (panels A, C, E, G, I) depict dormant cell densities' 2-D spatial distribution. The results correspond to t = 5 hrs, which is centered in the time frame of t ≈ 3 - 7 hrs during which the transient peak in sporulation around the plaque emerges in our simulations. The right column (panels B, D, F, H, J) show the distance profile of dormant cells distribution starting from the center of the plaque. The solid line (primary y-axis) corresponds to results at time = 5 hrs and is effectively a 1-D slice of the left panel at the same row, showing the radial distribution of dormant cells starting from the center of the plaque and moving outwards. The dashed line, plotted on the secondary y-axis, represents the progression of the solid line at 15 hours.

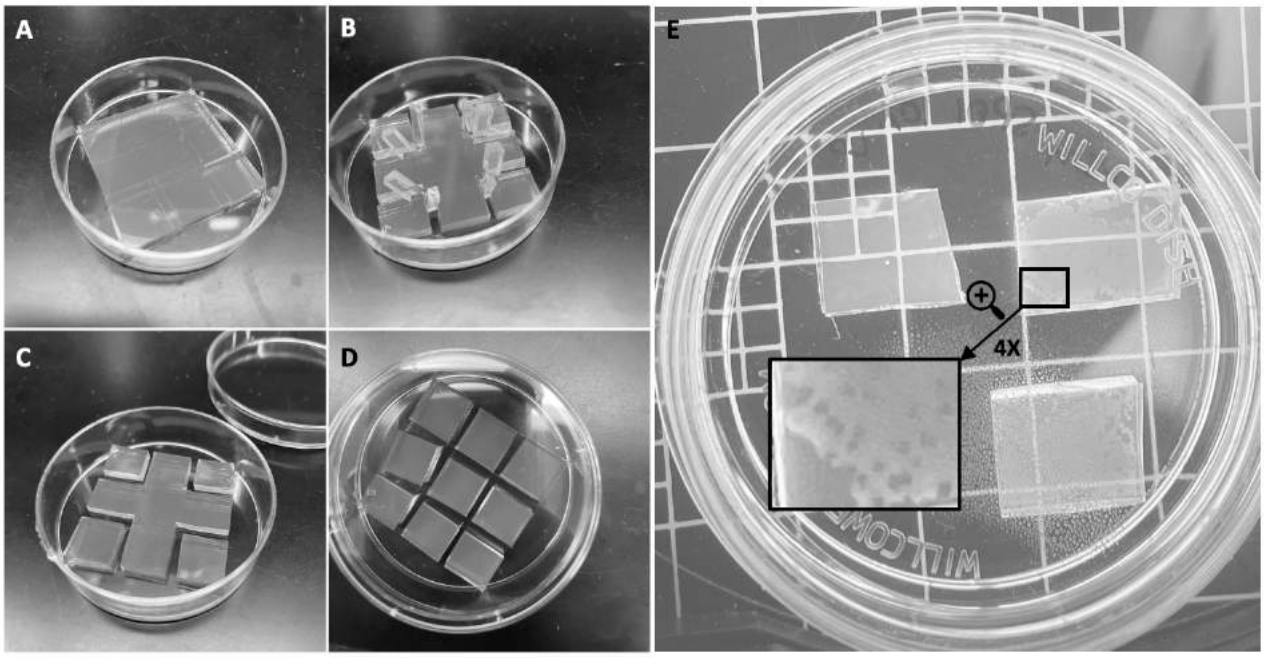

Fig. S1: **Inverted plaque assay protocol.** Panels **A** through **D** show the preparation of the agar pad for the inverted plaque assay in chronological order. The agar layer is cut with a sterile scalpel and the excess agar is removed without moving the square pads. **E** A top-down image of an inverted plaque assay is shown. The area enlarged 4 times shows the plaques (darker circular areas) of phage SPO1 on WT host and DSM media.

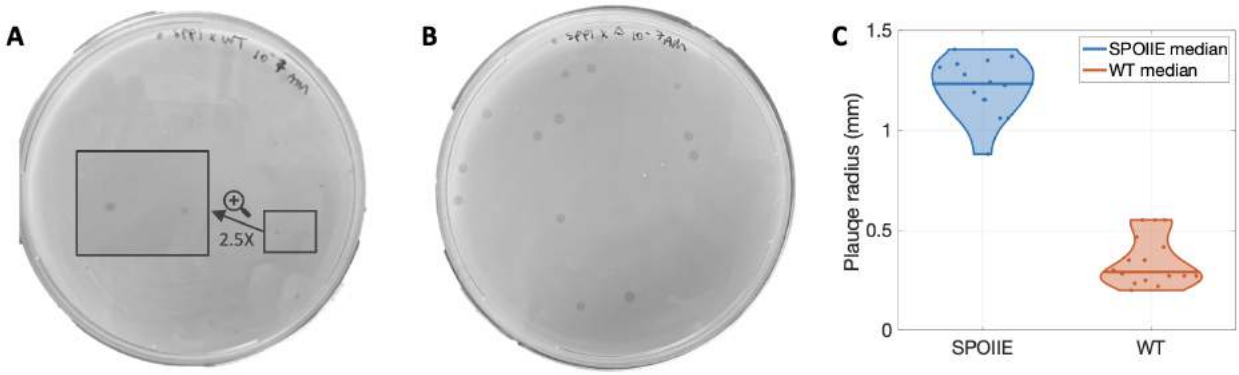

Fig. S2: **Plaque sizes of phage SPP1 with WT and SPOIIE host. A and B** Two entire plaque assays are shown on DSM media. WT host is shown in panel A and SPOIIE host in panel B. A small area in panel A is enlarged and shown at 2.5x magnification so that the plaques become visible. **C** Final plaque size of the two plaque assays shown in panels A and B. The images were analyzed by hand using FIJI. The plaque sizes (14 data points for SPOIIE and 16 for WT) were plotted using a violin plot and individual points are shown as a scatter plot. The median SPOIIE and WT plaque sizes are shown through the horizontal bold lines. SPOIIE plaques have an average radius of $\approx 1.22mm$ and standard deviation of $0.15mm$ and WT plaques have an average radius of $0.35mm$ and standard deviation of $0.12mm$. A two sample t-test was performed to reject the hypothesis that the two distributions have equal means with a p-value less than 1e-16.

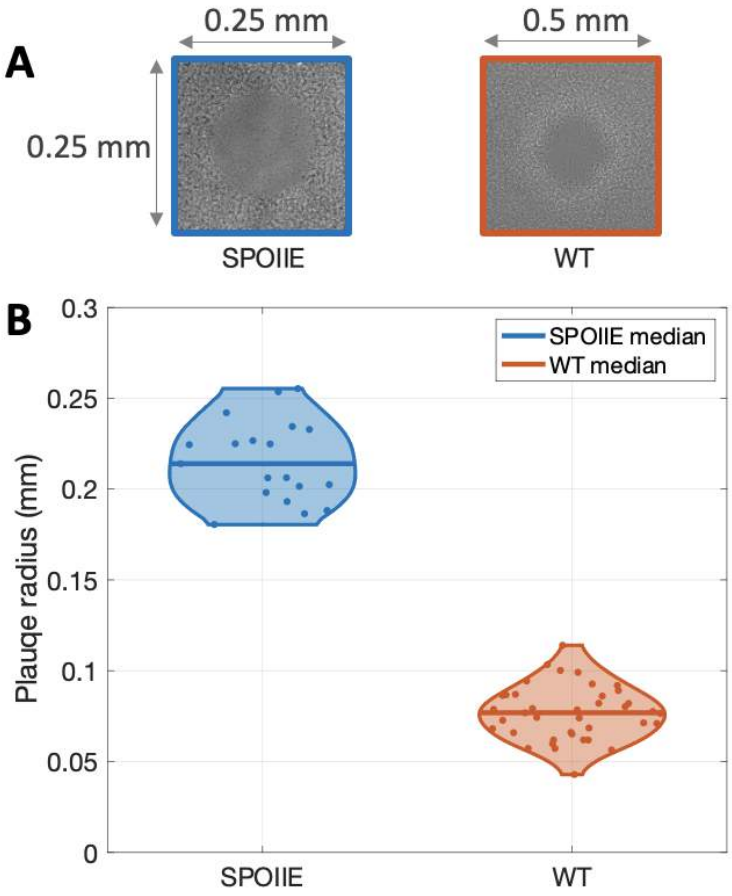

Fig. S3: **Inverted plaque sizes of phage SPO1 with SPOIIE and WT host. A** Two inverted plaques are shown, both obtained from an inverted microscope (SPOIIE host on the left is taken at 20x magnification and WT host on the right is taken at 40x magnification). **B** Multiple plaques are measured and the final size distribution is shown for WT and SPOIIE host (19 data points for SPOIIE and 39 for WT). The images were analyzed by hand using Fiji. The median SPOIIE and WT plaque sizes are shown through the horizontal bold lines. WT inverted plaques have an average radius of 77 microns and 15 microns standard deviation and SPOIIE inverted plaques have an average radius of 216 microns and 22 standard deviation. A two sample t-test was performed to reject the hypothesis that the two distributions have equal means with a p-value less than 1e-34.

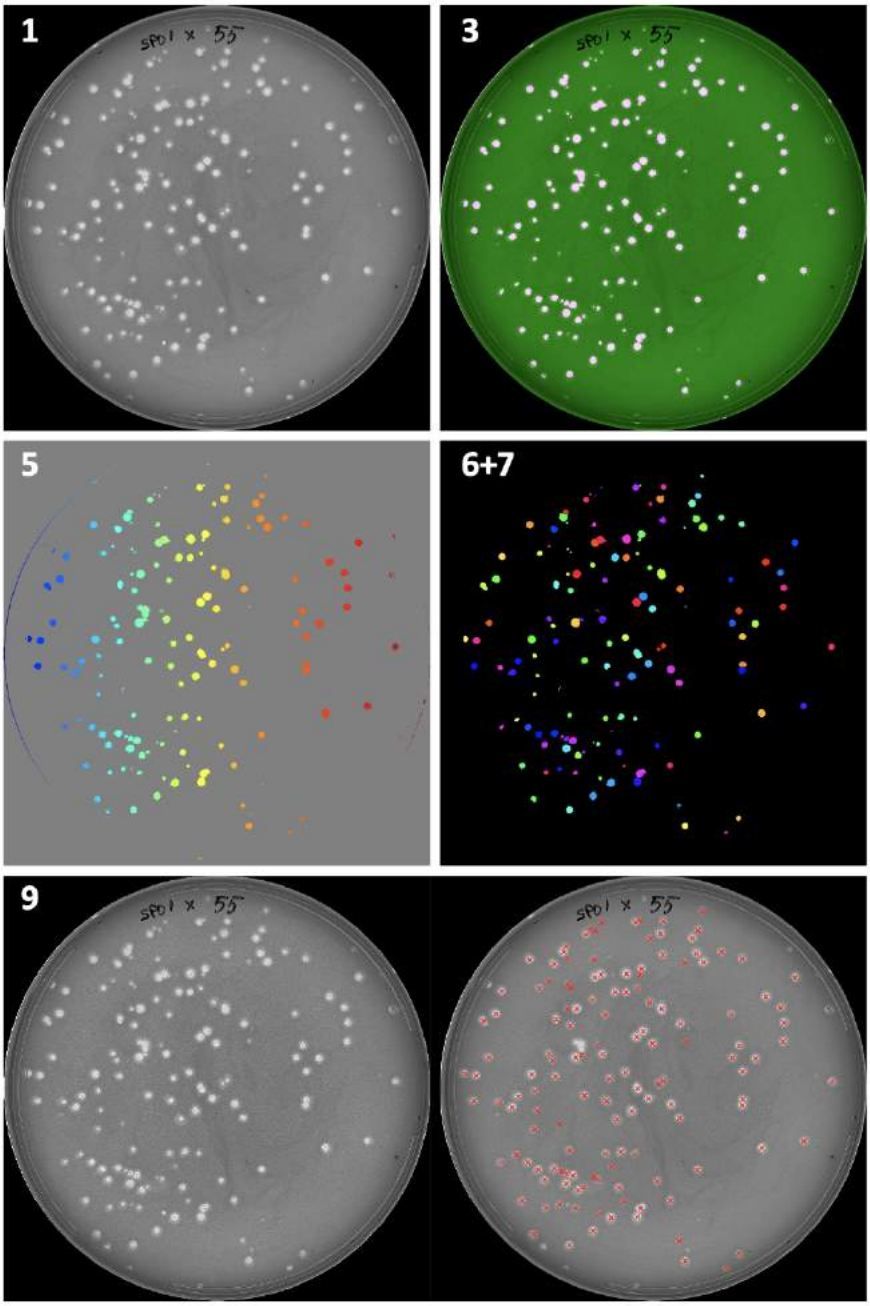

Fig. S4: **Intermediate steps for the final point image analysis algorithm.** Intermediate images for the steps outlined in section VII A 1 are shown. The steps can be described as 1 - original image, 3 - mask from threshold binarization, 5 - watershed algorithm, 6+7-exclusion of false positives, 9-comparison of original image to final plaque centers.

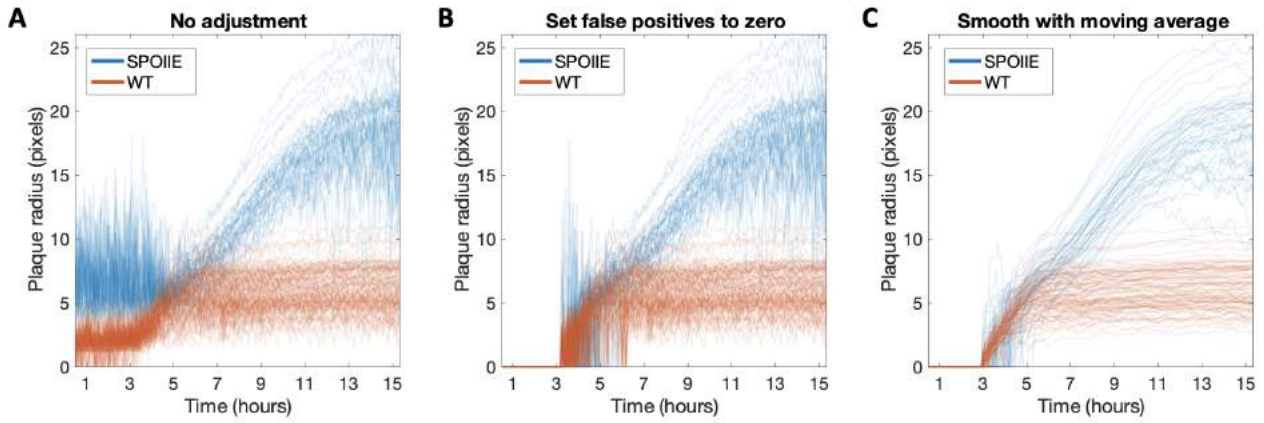

Fig. S5: **Individual plaque sizes at different stages during image analysis** SPOIIE plaques are shown in blue and WT plaques are shown in orange across all panels. **A** Raw plaque sizes data are shown after the first part in step 4 in section VII A 2. The plaque size is determined based on a re-scaling and threshold algorithm, hence many early points are false positives in that a plaque is detected when there is none in reality. **B** Plaque sizes at the end of step 4, after setting false positive plaques to zero. All data in the first 33 frames is assumed to be zero. The false positives in the frames 34-70 are determined based on the number of connected components. **C** Final individual trajectories for plaque sizes. The individual growth curves in panel B are smoothed out with a moving average of size 7. These are the trajectories used to determine the mean and standard deviation in figure 2.

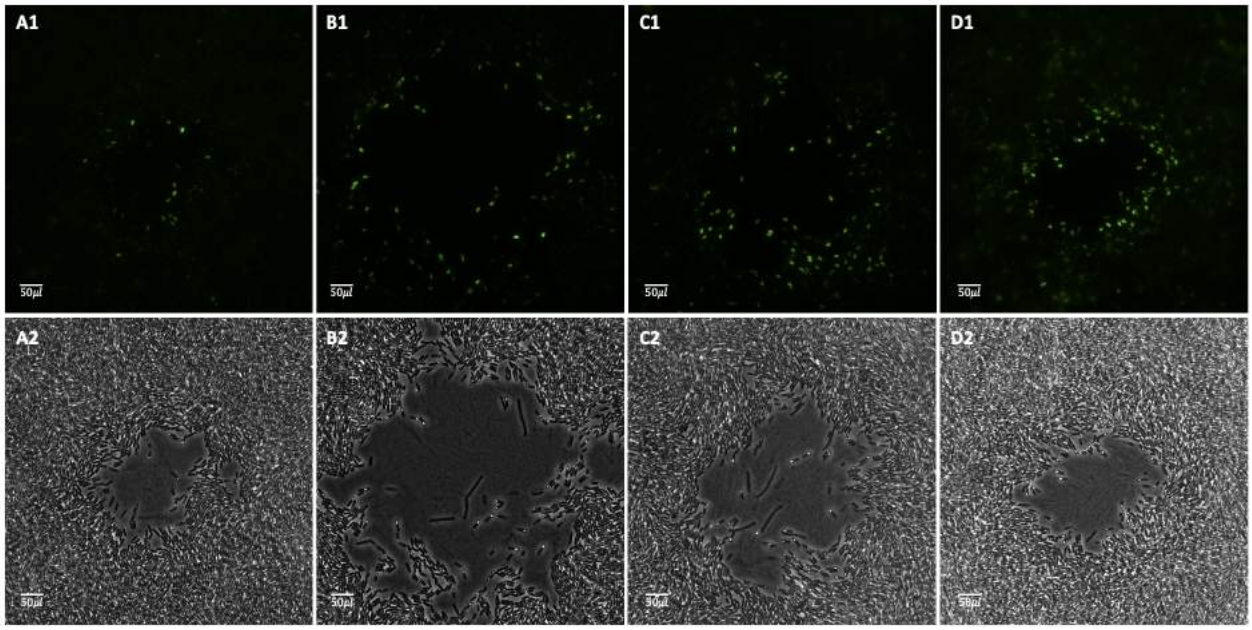

Fig. S6: **Additional images of inverted plaque assays at 100x magnification.**The top panels A1-D1 represent the raw GFP image and the bottom ones A2-D2 the raw bright-field corresponding image. All plaques are of phage SPO1 and DSM media. The scale bar in each panel represents $50\mu m$.

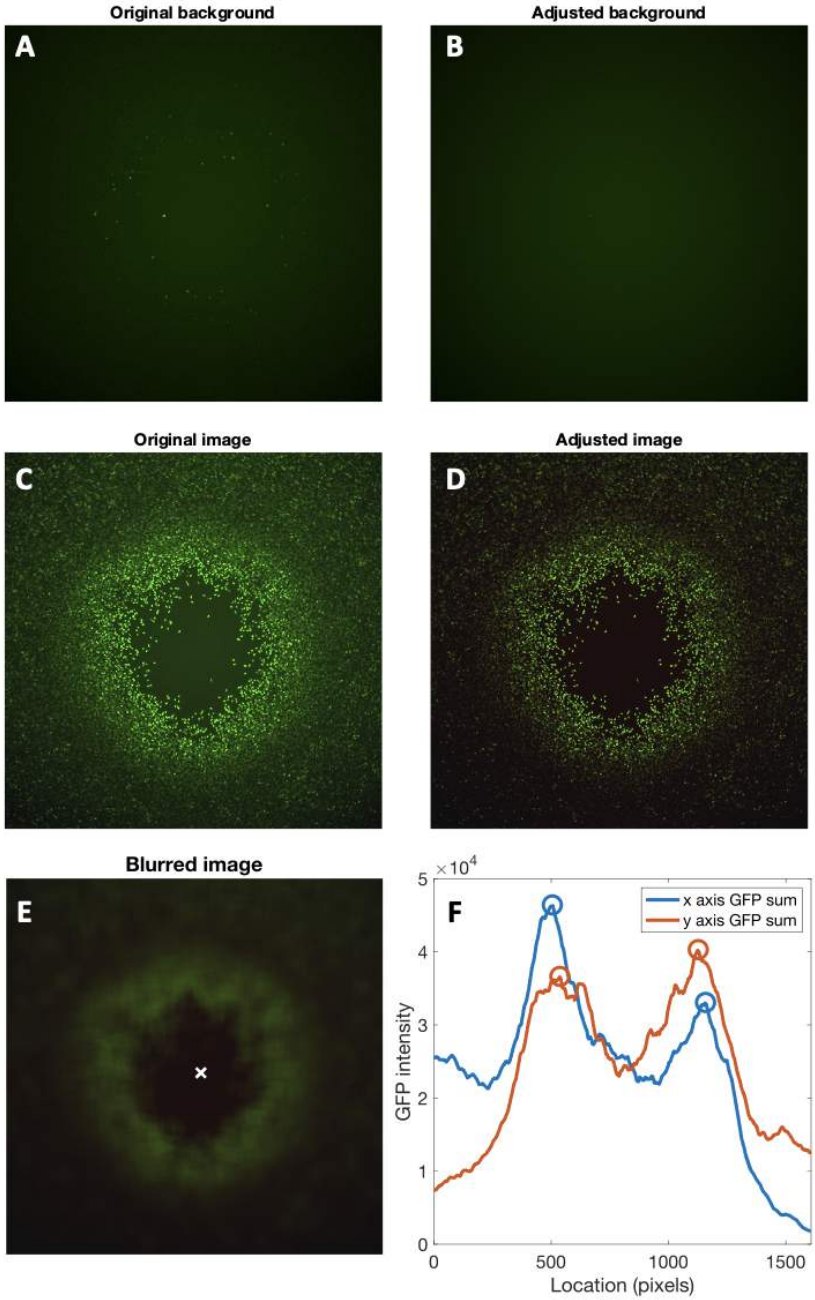

Fig. S7: **Intermediate steps for GFP image analysis A** Original image used to calculate the background fluorescence. This image, alongside images in panels B through E, has 1608x1608 pixels. **B** Adjusted background fluorescence in which the bright spots have been replaced with an average of the surrounding area. **C** Original GFP image of the inverted plaque. **D** Adjusted GFP image. This image is equivalent to subtracting panel B from C. **E** Blurred image obtained from applying an averaging filter of size 64x64 to the image in panel D. The white 'x' represents the center of the plaque as computed in panel F. **F** The two solid lines represent the sum and row column of the GFP intensity in panel E. The two peaks for each sum are circled with their respective colors. The midpoints of the blue and orange circles are 831.5 and 832 and represent the coordinates for the plaque center shown in panel E.

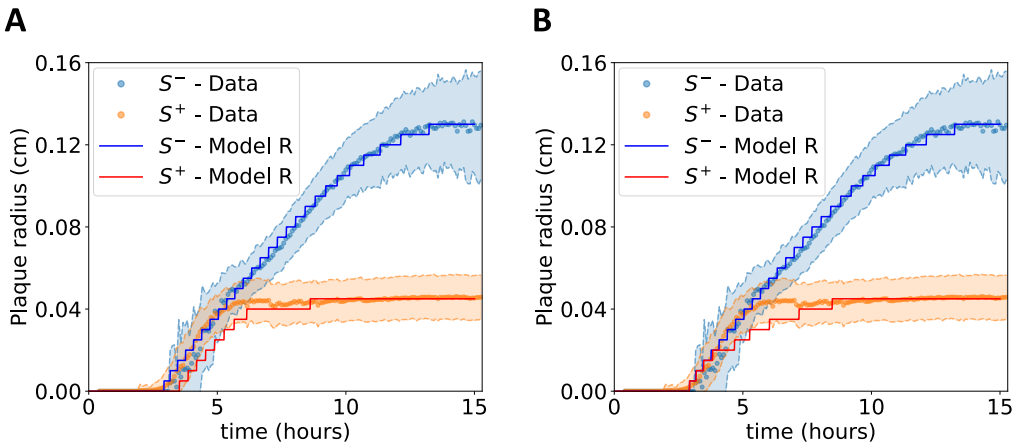

Fig. S8: **Impact of sporulation on plaque size for Models V, and M. A,B** An overlay of experimental data and computational simulations showing the time evolution of the mean plaque radius for the S^- and S^+ strains in Models V and M, respectively. The results displayed here are for $n_E = 0$, demonstrating their consistency across different values of n_E, as further supported by the data in Fig. 5C,D.

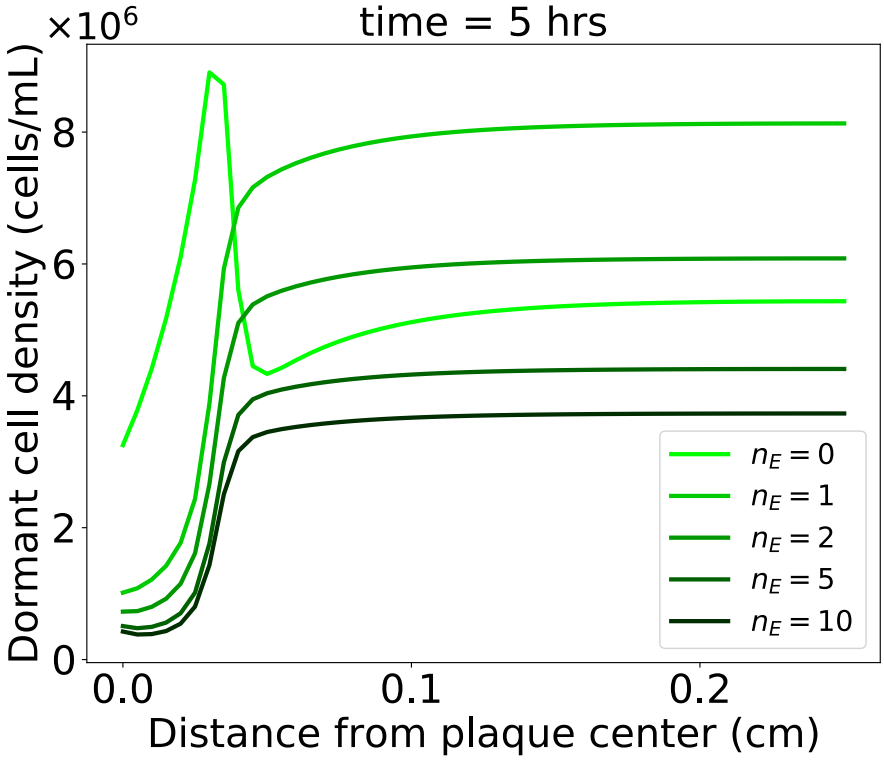

Fig. S9: **The impact of time-delayed transition to dormancy in Model V.** The figure shows how changes in n_E affect the radial profile of dormant cells' distribution for the S^+ strain at t = 5 hrs. Darker shades of green represent higher numbers of n_E states. The two extreme cases $n_E = 0$ and $n_E = 10$ correspond to the two cases of Model V presented in Fig. 6D, F.

V. DISCUSSION

In this paper we studied the propagation of phage plaque formation on *B. subtilis* strains that can (WT) and cannot sporulate (SPOIIE). Through analysis of plaque front dynamics, we found that plaques on either WT or SPOIIE population initially grow at similar speeds but that plaques on WT populations exhibit rapid decreases in front speeds, reducing plaque size by 50% or more. We developed an inverted plaque assay to image plaques at a microscopic level and found that sporulation is enhanced around the edges of the plaque well before resource depletion leads to the emergence of spores in the population as a whole. We developed a series of PDE models of phage spread in bacterial populations as a means to explore the impact of resource-, virus, or small molecular-induced initiation of dormancy. In all cases, we show that dormancy initiation can lead to reduce termination of plaque growth despite maintaining the same initial speed. However, by comparing the radial profile of spores between models, our results suggest that the early appearance of sporulation around the edge of plaque boundaries is consistent with dormancy being triggered by a small molecule released as a result of infection (and lysis). These results provide evidence that proximity to viruses can trigger sporulation in *Bacillus subtilis* which can in turn limit viral dispersion.

Sporulation is a complex and energetically costly bacterial strategy that can help cells survive through extreme environmental conditions. As demonstrated by our study, in the absence of harsh conditions, the enhancement of sporulation can serve as a protective mechanism for cell communities by limiting phage dispersion. We show that sporulation can be initiated preferentially locally, however the underlying signaling mechanism or trigger remains unidentified - and could be host-associated, viral-associated, or both. The observation that phages can induce sporulation aligns with the hypothesis that microbes evolved dormancy, in part, as a generalized defense against threats. This idea is supported by prior studies [14, 43], which reported dormancy triggered by direct contact with viruses in *Archaea* and *Listeria*, respectively. However, to the best of our knowledge, our study offers the first account of virally induced dormancy in *B. Subtilis*. Notably, a recent study [26] found that a small signaling molecule in the lysate can confer phage tolerance in *B. Subtilis*. Drawing connections with these studies can shed light on our proposed mechanism. Further work exploring the biochemical properties of plaques is needed in order to get a better understanding of the mechanism underlying spore enhancement - and its generality.

Our findings come with caveats. First, the GFP tag used to quantify spores is expressed later in the sporulation pathway. As a result, direct observation of the formation of spores is time shifted by $\approx$4 hrs after spore initiation. Improvements in quantification of the initiation of sporulation would provide additional information linking spores and plaque fronts. Indeed, we expect that the spatial localization of signals is key for reproducibility. In contrast, identifying similar phenomena in liquid cultures may be challenging. In such environments, the evolution of resistance can rapidly influence infection dynamics given the strong selective benefit for phage-resistant mutants [13]. Finally, we were able to recapitulate the plaque front dynamics and radial profile of spores with a mathematical model of virus-host feedback and small molecular-induced dormancy and not with either the resource- or virus particle-induced models. Nonetheless, the robust agreement between model and data is valid in certain parameter regimes, suggesting that life history traits will be important to characterizing the generality across other virus-microbe systems.

Our findings may have important implications on the effects of sporulation as a life-history trait on biomedical applications. By reducing viral infection in spatial settings, sporulation could significantly change the host-phage infection dynamics. Additionally, in light of viral entrapment in mature spores, phage induced sporulation could increase phage survival by providing a protective shell for phages until they are reintroduced at a later time in the population [44, 45]. On the other hand, phage induced sporulation could increase the survival of bacteria as seen by the reduction in plaque size. In closing, our findings reveal a novel mechanism by which phage infections can be self-limiting - leading to a collective defense mechanism that limits phage spatial spread even when nearby hosts remain available, albeit inaccessible.

VI. ACKNOWLEDGEMENTS

We acknowledg Zhongqing Ren, Caroline Dunn, along with the Wang and Kearns laboratories at Indiana University for assistance with microscopy and imaging. We would also like to thank Thomas Day for advice with image analysis. **Daniel, Jay - anyone else I am missing?** This work was supported by National Science Foundation (DEB - 1934554 to JTL and DS, DBI - 2022049 to JTL and DEB - 1934586 to JSW and Andreea M), US Army Research Office Grant (W911NF-14-3071-0411 and W911NF-22-1-0014 to JTL), the National Aeronautics and Space Administration (80NSSC20K0618 to JTL) and the European Research Council (Horizon 2020 research and innovation program - grant agreement No. 740704 to Anastasios M). JSW was supported, in part, by the Chaires Blaise Pascal program of the Île-de-France region.

VII. SUPPLEMENTARY INFORMATION

A. Image analysis

1. Final point analysis

We use a binarization method to extract the plaque sizes from an image of a petri dish. Specific threshold parameters vary between images, however the overall structure of the code is the same. All the analysis is done in MATLAB and a step-wise overview of the code is shown below:

1. Read image and convert to black and white
2. Apply a Gaussian filter to reduce noise
3. Apply a general threshold to obtain a mask
4. Obtain the region properties of the mask
5. Use the build-in watershed algorithm to break apart overlapping plaques
6. Select regions based on circularity and area
7. Discard any additional regions that are not plaques by hand
8. Obtain the areas and centers of the selected regions
9. Perform a final check of the final mask and overlay the centers with the original image

Note that the processed image and binarization is checked against the original image at every time step. We perform steps 3-5 such that no true plaques are being discarded. We use steps 6-7 to ensure that any false positives are not counted. Intermediate images for some of the steps are shown in Figure S4.

2. Time lapse analysis

To analyze the time lapse of plaque growth, we first analyze the last frame to identify the plaques. We then use the plaque centers and axes to track the size of the plaques in previous frames. This process can be divided into 5 steps which we describe in detail below.

Step 1. Identify plaque centers in last frame

A circular section is cropped from the original video using code adapted from MATLAB Central Answers to obtain a time lapse for each petri over time (link : https://www.mathworks.com/matlabcentral/answers/567441-how-to-crop-circle-from-an-image). We then use the same protocol as the one described in section VII A 1 to identify the centers and axes of the plaques in the last frame.

Step 2. Compute camera movement

To obtain a video of the plaques over time, we set a camera to capture a top-down image of the petri dishes every 5 minutes. We note that the camera is not perfectly still and that there is motion in the x and y direction between frames. We correct for this motion by tracking the edges of the white LED screen. The full image is cropped to contain just the corner of the LED screen. The cropped image is then binarized and 10 rows and columns are used to find the transition between the white screen and the background. The first black pixel for each row marks the transition and will be used to adjust for displacement in the x direction. Similarly, the first black pixel for each column marks the transition and will be used to adjust for displacement in the y direction. In the end we obtain 10 points marking a vertical edge and 10 points marking a horizontal edge for each frame.

Step 3. Identify search window based on centers, camera movement and axes lengths

Instead of analyzing the entire petri dish at every time step, we use the information about the plaque location and size to analyze a narrow window for each plaque. For each frame we take the mean of the 10 point marking the vertical edge and 10 points marking the horizontal edge. The mean values for the two edges are compared to the ones in the last frame to obtain the camera movement in the x and y direction with respect to the last frame. The centers of the plaques are adjusted to account for this camera movement. Thus, starting from the center of the plaques in the last frame, we have obtained the center of the plaques in all the previous frames.

Lastly, for each frame and each plaque we define a rectangular area centered at the adjusted plaque center. This rectangle has the width and length equal to the two major axes of the final plaque size. Since plaques only grow over time, it means that the plaque at the current frame is contained within the rectangle.

Step 4. Calculate plaque in each rectangle for all plaques and frames

Having defined a search area for each plaque and each frame, we still need to distinguish plaque versus lawn in each rectangle. Since the contrast between plaque and lawn is not as high in earlier time points, we cannot directly use a general threshold for this algorithm. Instead we write a short script which is used for both WT and SPOIIE time lapse. Given rectangle X, we make the following operations:

$X = \text{imadjust}(X)$ ▷ rescale of intensity values
$X_{BW} = X > 160$ ▷ threshold binarization
$X_{BW} = \text{fillholes}(X_{BW})$

The plaque sizes after this analysis are shown in Figure S5 panel A, however we note that there are plenty of false positives, i.e. areas that are not plaques but are counted as such. To fix this issue, we divide the 179 frames in 3 time intervals and adjust the false positives to zero based on the number of connected components n_{CC} in X_{BW}. A large number of connected components is an indication of a false positive. We select the n_{CC} thresholds by hand by plotting the number of connected components for each plaque over time. A brief version of the code is shown below:

if $i < 34$ **then**
    plaque size = 0 ▷ Plaques are not visible yet
end if
if $34 \leq i < 70$ **then**
    if $n_{CC} >$ threshold **then**
        plaque size = 0 ▷ Set false positive to zero
    else
        plaque size = largest connected component in X_{BW}
    end if
else
    plaque size = largest connected component in X_{BW}
end if

The plaque sizes after adjustment for false positives can be seen in Figure S5 panel B.

Step 5. Raw data and smoothing function for each plaque
We expect plaques to grow monotonically over time, however there is noise in the original video and in our image analysis algorithm. To reduce the noise and emphasize the overall trend of the plaque measurements, we take a moving average of size 7 for each plaque trajectory. These are the final plaque growth trajectories we use for the main text and they are also shown in Figure S5 panel C.

3. GFP analysis

We use a set of imagining analysis techniques to obtain the GFP intensity based on the distance to the center of the plaque shown in figure 3. The process can be described in three steps outlined below:

Step 1. Calculate background fluorescence and subtract it from original image
The original GFP image (Figure S7 panel C) has a background fluorescence level that is higher at the center of the image. To account for this, we use another GFP image with minimal fluorescent cells shown in panel A as a measure for background GFP intensity. We take out the bright spots in the original background and fill them in to obtain an adjusted background fluorescence shown in panel B. Finally, subtracting the adjusted background from the original image yields the adjusted GFP image in panel D which is used for analysis in the following steps.

Step 2. Find center of the plaque
Once we have the adjusted GFP image, we use a square averaging filter of size 64x64 to obtain a blurred image shown in Figure S7 panel E. Using the blurred image, we compute the GFP sum for each row and column and notice that there are two peaks for both the column and row sums shown in panel F. These peaks correspond to the edges of the plaque and we select the midpoint for the peaks to represent the x and y coordinate for the center of the plaque.

Step 3. Plot GFP intensity based on distance to center
Once we have found the center of the plaque, we compute the distance from each other pixel (1608^2 pixels in total) to the center. The pixels are grouped in 400 bins based on the calculated distance and a mean and standard deviation is obtained for each bin. The mean and standard deviation are the final measurements shown in figure 3 panel C.

B. Mathematical modeling and simulations methods

1. Numerical simulations

We simulate the PDEs through a finite difference method implementation on a square lattice. Each lattice sites consists of a square with $\Delta x = 50\mu$m$= \Delta y$ with 100 sites per side to represent a total length $L = 0.5$ cm. In this implementation, for each time step, the contribution to the derivatives given by the local reaction terms are computed in each site, based on the state values in that site at that given time, as when integrating ODEs. The spatial derivatives $\frac{\partial}{\partial x}, \frac{\partial}{\partial y}$ present in the diffusion terms, which couple different positions, are discretized on the square lattice. We use the following stencil matrix to discretize the laplacian operator ($\nabla^2 = \frac{\partial}{\partial x}^2 + \frac{\partial}{\partial y}^2$) in the diffusion terms:

$$\text{Kernel} = \begin{pmatrix} 0.25 & 0.5 & 0.25 \\ 0.5 & -3 & 0.5 \\ 0.25 & 0.5 & 0.25 \end{pmatrix}$$

This stencil needs to be convoluted with the state field that we are taking the laplacian of. For instance the diffusion term of resources $D_R\nabla^2 R$ at a site (x,y) can be obtained by discretising spatial derivatives to first order with respect to first- and second-neighbor sites:

$$\begin{aligned} D_R\nabla^2 R(t,x,y) &= \frac{D_R}{\Delta x^2}\begin{pmatrix} 0.25 & 0.5 & 0.25 \\ 0.5 & -3 & 0.5 \\ 0.25 & 0.5 & 0.25 \end{pmatrix} \cdot \begin{pmatrix} R(t,x-\Delta x,y+\Delta y) & R(t,x,y+\Delta y) & R(t,x+\Delta x,y+\Delta y)) \\ R(t,x-\Delta x,y) & R(t,x,y) & R(t,x+\Delta x,y) \\ R(t,x-\Delta x,y-\Delta y) & R(t,x,y-\Delta y) & R(t,x+\Delta x,y-\Delta y) \end{pmatrix} \\ &= \frac{D_R}{\Delta x^2}\Big(-3R(t,x,y) + 0.5\Big(R(t,x+\Delta x,y) + R(t,x-\Delta x,y) + R(t,x,y+\Delta y) + R(t,x,y-\Delta y)\Big) + \\ &+ 0.25\Big(R(t,x+\Delta x,y+\Delta y) + R(t,x-\Delta x,y+\Delta y) + R(t,x+\Delta x,y-\Delta y + R(t,x-\Delta x,y-\Delta y)\Big)\Big) \end{aligned}$$

Diffusion of viruses and other molecules is given by the same equation by accounting for their specific diffusion constant. Together with the site-specific reaction terms, this step completes the computation of time derivatives given all the states variables at each time point. We can then update the system for 15 hrs using time steps of 0.01 hrs, by solving an explicit Runge-Kutta method of order 5(4) (Scipy's default initial value problem solver for a system of ordinary differential equations) [46, 47].

2. Parameter estimations

- Host-growth

  A maximum growth rate of $r_{max} = 2/hrs$ corresponds to a doubling time of approximately 20 min [48]. We constrained a set of parameters to a plausible order of magnitude based on back-of-the-envelope calculations and comparisons to the elements from the literature. We set the initial amount of resources (in rescaled units) as $\tilde{R}_0 = 10^9$ cells/mL, which sets the carrying capacity for bacteria growth. Several parameters were obtained *de novo* in this work, either based on the from the experimental protocols, or inferred (qualitatively) to reproduce the experimental results. The Monod constant K_g corresponds to the resource level where the growth rate is half of its maximum value. To reproduce the experimental results we select a Monod constant that is approximately three times larger than the initial resources, with the growth rate changing almost linearly with resources. Since the maximum plaque radius is under 0.2 cm, the size of the lattice is set to $L = 0.5cm$. We estimate the initial number of cells per plate to be $100\mu l$ of culture at OD 0.5 $\approx 2 \times 10^8$ cells/mL, corresponding to $\approx 2 \times 10^7$ cells. Given a bacterial lawn height of 400 μm and plate area of $\pi \cdot 4.5^2 cm^2$, we estimate the volume of a plate where bacteria grows to be about $\pi \cdot 4.5^2 \cdot 0.04cm^3 \approx 2.5ml$. We thus obtain an estimate for $S_0 \approx 2 \times 10^7 cells/2.5ml \approx 10^7 cells/ml$.

- Viral infection

  Since in our deterministic models a plaque starts from exactly one virus (compatible with the standard definition of PFU) and the volume of one square in the lattice is $Vol = 50\mu m \cdot 50\mu m \cdot 400\mu m = 1000000\mu m^3 = 10^{-6} ml$, we get that $V_0 = 1/Vol = 10^6 ml^{-1}$. The max latent rate η_{max} and the infection constant ϕ for the Bacillus Subtilis-SPO1 pair is given by (citation Daniel), while for the burst size β [49], the viral decay ω [49] and the

resource diffusion constant D_R [31] we selected plausible values that are commonly used in similar phage-bacteria ecology studies. The values of $d_{max} = 1/hour$, n_I, n_E when > 0, and the absolute magnitude of μ and m were set to reproduce the experimental dynamics semi-quantitatively.

- Dormancy

  For the transition to dormancy we selected values for λ that would give a sporulation process that takes close to 45 minutes from a signaling event (cite Daniel). Since dormancy is the "last resort" for a bacterium under stress, we select the threshold to dormancy σ to be a small percentage of the Monod constant, at about the point where cells grow 3 to 5 times slower than normal. In order to mimic a precise signaling process that triggers sporulation at critical resource level, we set the shape parameter of the resource-triggered dormancy Hill function, s, to be two orders of magnitude smaller than the carrying capacity $\tilde{R}_0$. Finally we assume that the product between μ and m is similar to that of the infection rate ϕ and the burst size β, that is, the size of a peptide chain will correlate with both the ability of a cell to syntethize it in large numbers and with the rate at which a cell will bind to it and adsorbe it, since in a diffusion limited reaction the adsorption rate will scale linearly with the diffusion constant ([50]) which is inversely proportional to the particle size due to the Einstein-Stokes equation.

- Spatial diffusion

  To estimate the phage diffusion constant D_V we consider phages to be about two orders of magnitudes bigger than the molecular components constituting resources. Using Einstein-Stokes relation yields a value for D_V that is two orders of magnitude smaller than the resource diffusion constant. As a cross check we note that this is compatible with values proposed in literature, albeit for different phages ([51]). We selected a molecule diffusion constant D_M to be equal to the resource diffusion constant D_R since we expect the molecule to be of similar size to the resources.

---

[1] L. H. Stevenson, "A Case for Bacterial Dormancy in Aquatic Systems," *Microbial Ecology*, vol. 4, pp. 127–133, sep 1977.

[2] N. Q. Balaban, J. Merrin, R. Chait, L. Kowalik, and S. Leibler, "Bacterial persistence as a phenotypic switch," *Science*, vol. 305, no. 5690, pp. 1622–1625, 2004.

[3] E. S. Rittershaus, S. H. Baek, and C. M. Sassetti, "The normalcy of dormancy: Common themes in microbial quiescence," *Cell Host Microbe*, vol. 13, pp. 643 – 651, 2013.

[4] P. Setlow, "I will survive: DNA protection in bacterial spores," *Trends Microbiol.*, vol. 15, pp. 172–180, Apr. 2007.

[5] W. L. Nicholson, N. Munakata, G. Horneck, H. J. Melosh, and P. Setlow, "Resistance of Bacillus Endospores to Extreme Terrestrial and Extraterrestrial Environments," *Microbiology and molecular biology reviews : MMBR*, vol. 64, no. 3, pp. 548–572, 2000.

[6] S. J. Tan and TS, "Spore Formation in Baccilus Subtilis," *Bone*, vol. 23, no. 1, pp. 1–7, 2008.

[7] S. E. Jones and J. T. Lennon, "Dormancy contributes to the maintenance of microbial diversity," *Proceedings of the National Academy of Sciences of the United States of America*, 2010.

[8] J. T. Lennon and S. E. Jones, "Microbial seed banks: The ecological and evolutionary implications of dormancy," 2011.

[9] S. J. Labrie, J. E. Samson, and S. Moineau, "Bacteriophage resistance mechanisms," *Nature Reviews Microbiology*, vol. 8, no. 5, pp. 317–327, 2010.

[10] J. T. Rostøl and L. Marraffini, "(ph)ighting phages: How bacteria resist their parasites," *Cell Host & Microbe*, vol. 25, no. 2, pp. 184–194, 2019.

[11] W. P. J. Smith, B. R. Wucher, C. D. Nadell, and K. R. Foster, "Bacterial defences: mechanisms, evolution and antimicrobial resistance," *Nature Reviews Microbiology*, vol. 21, no. 8, pp. 519–534, 2023.

[12] A. Bernheim and R. Sorek, "The pan-immune system of bacteria: antiviral defence as a community resource," *Nat. Rev. Microbiol.*, vol. 18, pp. 113–119, Feb. 2020.

[13] D. A. Schwartz, W. R. Shoemaker, A. Măgălie, J. S. Weitz, and J. T. Lennon, "Bacteria-phage coevolution with a seed bank," *The ISME Journal*, 2023.

[14] A. J. Meeske, S. Nakandakari-Higa, and L. A. Marraffini, "Cas13-induced cellular dormancy prevents the rise of CRISPR-resistant bacteriophage," *Nature*, 2019.

[15] M. C. Williams, A. E. Reker, S. R. Margolis, J. Liao, M. Wiedmann, E. R. Rojas, and A. J. Meeske, "Restriction endonuclease cleavage of phage DNA enables resuscitation from Cas13-induced bacterial dormancy," *Nature Microbiology*, vol. 8, no. 3, pp. 400–409, 2023.

[16] Y. Fu, L. Liang, S. Deng, Y. Wu, Y. Yuan, and M. Gao, "Novel spore lytic enzyme from a Bacillus phage leading to spore killing," *Enzyme and Microbial Technology*, vol. 142, p. 109698, 2020.

[17] A. Dragoš, B. Priyadarshini, Z. Hasan, M. L. Strube, P. J. Kempen, G. Maróti, C. Kaspar, B. Bose, B. M. Burton, I. B. Bischofs, and Á. T. Kovács, "Pervasive prophage recombination occurs during evolution of spore-forming Bacilli," *The ISME Journal*, vol. 15, no. 5, pp. 1344–1358, 2021.

[18] D. A. Schwartz, B. K. Lehmkuhl, and J. T. Lennon, "Phage-encoded sigma factors alter bacterial dormancy," *mSphere*, vol. 7, p. e0029722, Aug. 2022.

[19] M. Butala and A. Dragoš, "Unique relationships between phages and endospore-forming hosts," *Trends Microbiol.*, vol. 31, pp. 498–510, May 2023.

[20] S. D. A, R.-R. J. A, S. Michael, F. R. M, D. R. A, W. K. C, and L. J. T, "Human-Gut Phages Harbor Sporulation Genes," *mBio*, vol. 14, pp. e00182–23, apr 2023.

[21] S. J. Schrag and J. E. Mittler, "Host-Parasite Coexistence: The Role of Spatial Refuges in Stabilizing Bacteria-Phage Interactions," *The American Naturalist*, vol. 148, pp. 348–377, sep 1996.

[22] J. J. Bull, K. A. Christensen, C. Scott, B. R. Jack, C. J. Crandall, and S. M. Krone, "Phage-bacterial dynamics with spatial structure: Self organization around phage sinks can promote increased cell densities," *Antibiotics (Basel)*, vol. 7, Jan. 2018.

[23] S. Testa, S. Berger, P. Piccardi, F. Oechslin, G. Resch, and S. Mitri, "Spatial structure affects phage efficacy in infecting dual-strain biofilms of Pseudomonas aeruginosa," *Communications Biology*, vol. 2, no. 1, p. 405, 2019.

[24] J. J. Dennehy and S. T. Abedon, *Bacteriophage Ecology*, pp. 253–294. Cham: Springer International Publishing, 2021.

[25] P. Cooper, *The Plaque Assay of Animal Viruses*, vol. 8 of *Advances in Virus Research*. Academic Press, 1962.

[26] E. Tzipilevich, O. Pollak-Fiyaksel, B. Shraiteh, and S. Ben-Yehuda, "Bacteria elicit a phage tolerance response subsequent to infection of their neighbors," *EMBO J.*, vol. 41, p. e109247, Feb. 2022.

[27] A. L. Koch, "The growth of viral plaques during the enlargement phase," *Journal of Theoretical Biology*, vol. 6, no. 3, pp. 413–431, 1964.

[28] S. T. Abedon and J. Yin, *Bacteriophage Plaques: Theory and Analysis*, pp. 161–174. Totowa, NJ: Humana Press, 2009.

[29] L. YOU and J. YIN, "Amplification and spread of viruses in a growing plaque," *Journal of Theoretical Biology*, vol. 200, no. 4, pp. 365–373, 1999.

[30] R. Gallet, S. Kannoly, and I.-N. Wang, "Effects of bacteriophage traits on plaque formation," *BMC Microbiology*, vol. 11, no. 1, p. 181, 2011.

[31] N. Mitarai, S. Brown, and K. Sneppen, "Population dynamics of phage and bacteria in spatially structured habitats using phage λ and escherichia coli," *Journal of Bacteriology*, vol. 198, no. 12, pp. 1783–1793, 2016.

[32] S. Sinha, R. K. Grewal, and S. Roy, "Chapter Three - Modeling Bacteria–Phage Interactions and Its Implications for Phage Therapy," vol. 103, pp. 103–141, Academic Press, 2018.

[33] J. G. Piggot, P.J.; Coote, "Genetic aspects of bacterial endospore formation," *Bacteriological reviews*, no. 40(4), p. 908–962, 1976.

[34] D. R. Reuß, A. Thürmer, R. Daniel, W. J. Quax, and J. Stülke, "Complete genome sequence of ¡i¿bacillus subtilis¡/i¿ subsp. ¡i¿subtilis¡/i¿ strain ∆6," *Genome Announcements*, vol. 4, no. 4, pp. 10.1128/genomea.00759–16, 2016.

[35] P. Schaeffer, J. Millet, and J. P. Aubert, "Catabolic repression of bacterial sporulation.," *Proceedings of the National Academy of Sciences*, vol. 54, no. 3, pp. 704–711, 1965.

[36] L. Li, J. Jin, H. Hu, I. F. Deveau, S. L. Foley, and H. Chen, "Optimization of sporulation and purification methods for sporicidal efficacy assessment on Bacillus spores," *Journal of Industrial Microbiology and Biotechnology*, vol. 49, p. kuac014, jul 2022.

[37] M. F. Kauffman, K.M.; Polz, "Streamlining standard bacteriophage methods for higher throughput," *MethodsX*, p. 159–172, 2018.

[38] P. Wang, X.; Montero Llopis, "Visualizing Bacillus subtilis During Vegetative Growth and Spore Formation," *In: Leake, M. (eds) Chromosome Architecture. Methods in Molecular Biology*, vol. 1431, 2016.

[39] E. Kussell and S. Leibler, "Phenotypic diversity, population growth, and information in fluctuating environments," *Science*, vol. 309, no. 5743, pp. 2075–2078, 2005.

[40] A. Aertsen and C. W. Michiels, "Stress and how bacteria cope with death and survival," *Critical Reviews in Microbiology*, vol. 30, pp. 263 – 273, 2004.

[41] J. S. Weitz and J. Dushoff, "Alternative stable states in host–phage dynamics," *Theoretical Ecology*, vol. 1, no. 1, pp. 13–19, 2008.

[42] Z. Wang and N. Goldenfeld, "Fixed points and limit cycles in the population dynamics of lysogenic viruses and their hosts," *Phys. Rev. E*, vol. 82, p. 011918, Jul 2010.

[43] H. Gulbudak and J. S. Weitz, "A touch of sleep: biophysical model of contact-mediated dormancy of archaea by viruses," *Proceedings of the Royal Society B: Biological Sciences*, vol. 283, no. 1839, p. 20161037, 2016.

[44] A. L. Sonenshein, "Bacteriophages: How bacterial spores capture and protect phage dna," *Current Biology*, vol. 16, no. 1, pp. R14–R16, 2006.

[45] N. Gabiatti, P. Yu, J. Mathieu, G. W. Lu, X. Wang, H. Zhang, H. M. Soares, and P. J. J. Alvarez, "Bacterial endospores as phage genome carriers and protective shells," *Appl. Environ. Microbiol.*, vol. 84, Sept. 2018.

[46] J. Dormand and P. Prince, "A family of embedded runge-kutta formulae," *Journal of Computational and Applied Mathematics*, vol. 6, no. 1, pp. 19–26, 1980.

[47] L. F. Shampine, "Some practical runge-kutta formulas," *Mathematics of Computation*, vol. 46, pp. 135–150, 1986.

[48] J. Errington and L. T. v. d. Aart, "Microbe profile: Bacillus subtilis: model organism for cellular development, and industrial workhorse," *Microbiology*, vol. 166, no. 5, pp. 425–427, 2020.

[49] F. De Paepe, Marianne; Taddei, "Viruses' life history: Towards a mechanistic basis of a trade-off between survival and reproduction among phages," *PLOS Biology*, vol. 4, p. null, 06 2006.

[50] H. Berg and E. Purcell, "Physics of chemoreception," *Biophysical Journal*, vol. 20, pp. 193–219, Nov. 1977. Publisher: Elsevier.

[51] J. J. Barr, R. Auro, N. Sam-Soon, S. Kassegne, G. Peters, N. Bonilla, M. Hatay, S. Mourtada, B. Bailey, M. Youle, B. Felts, A. Baljon, J. Nulton, P. Salamon, and F. Rohwer, "Subdiffusive motion of bacteriophage in mucosal surfaces increases the frequency of bacterial encounters," *Proceedings of the National Academy of Sciences*, vol. 112, no. 44, pp. 13675–13680, 2015.

4 Do bacteriophages "decide" on infection based on the host's metabolic condition?

4.1 Introduction

In the preceding chapters, we have emphasized that life under suboptimal conditions for growth is more of the rule than the exception for the microbial ecosystems in nature. These conditions can shape phage-bacteria interactions and subsequently influence ecosystem dynamics by applying strong eco-evolutionary pressure, as in chapter 2, or by profoundly affecting the physiology of host organisms, as in chapter 3.

Regarding the effect of physiological changes in host-parasite dynamics, our study focused on *Bacillus subtilis*. A significant reason for this is the distinctiveness of its dormancy, as spore formation is easily observed and has a distinctive final product [131]. However, there are many bacteria for which dormancy lacks evident indicators. Prior research underscores the prominence of dormancy across various environments, constituting from 25% of the total amount of cells in the gut to nearly 50% in marine ecosystems and over 85% in soil ecosystems (see Figure 25).

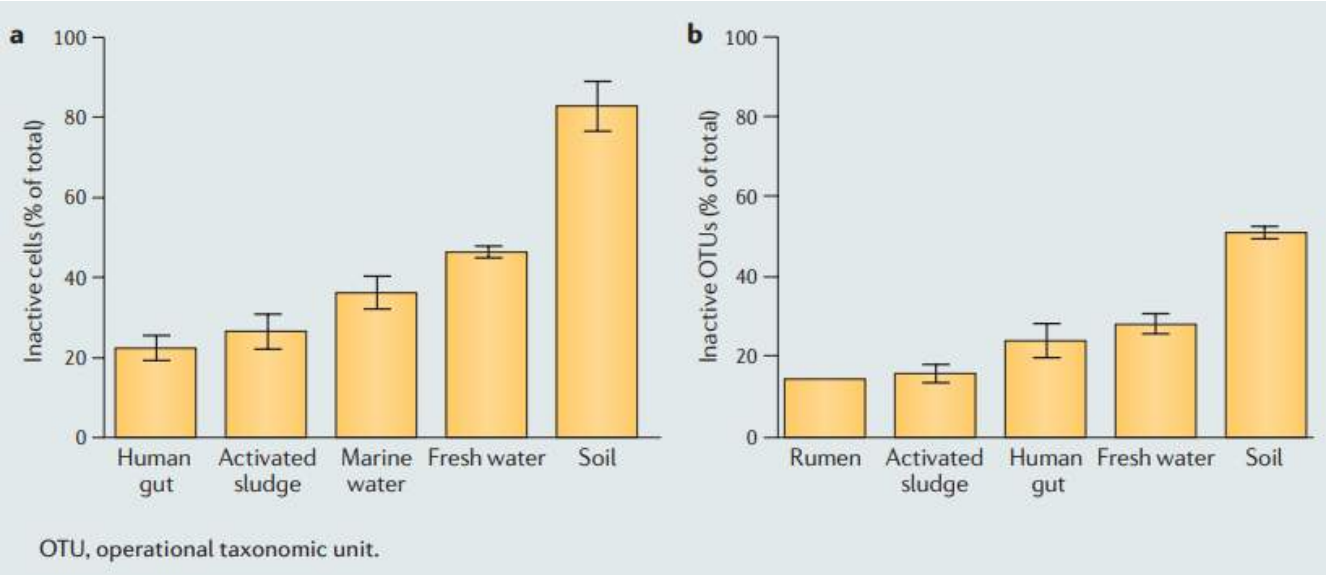

Figure 25: **Observations of dormancy across natural ecosystems.** A variety of environments have exhibited significant populations of dormant cells. The presented figure illustrates the proportion of dormant cells in different settings, as identified either through fluorescence in situ hybridization (FISH) or 5-cyano-2,3-ditolyl tetrazolium chloride (CTC) staining (panel a). Another method utilized is ribosomal RNA–ribosomal DNA terminal restriction fragment length polymorphism (TRFLP) (panel b). The provided data represents the mean along with its standard error. (Reprinted from [131])

The spores in Bacillus lack the surface receptor that phages require for infection, thereby safeguarding the host's DNA [181]. This protection extends to the community level, as we have elucidated (see our Manuscript Măgălie et al.). But what about organisms that do not exhibit such defensive structures during dormancy?

Dormancy is characterized by reduced metabolic activity. Although low cell metabolism is known to impact post-infection processes [163], its influence on the initial infection step is still not well-understood. Traditionally, infection is depicted as a lock-key mechanism, activated when the phage's tail protein binds to a specific receptor on the cell membrane [42, 1, 61]. Contrary to this traditional understanding, recent findings from the Biocomplexity group here at NBI provide intriguing insights [198]. While researching how a majority of immune *E.coli* cells can shield susceptible cells from λ bacteriophage infection by effectively removing phages from the environment in a manner similar to herd immunity, they found that their results diverge from their theoretical predictions when phages move from the exponential to the stationary phase. Surprisingly, a cross-check experiment revealed that this happens because of reduced infection of the hosts with low metabolic activity by the free viruses.

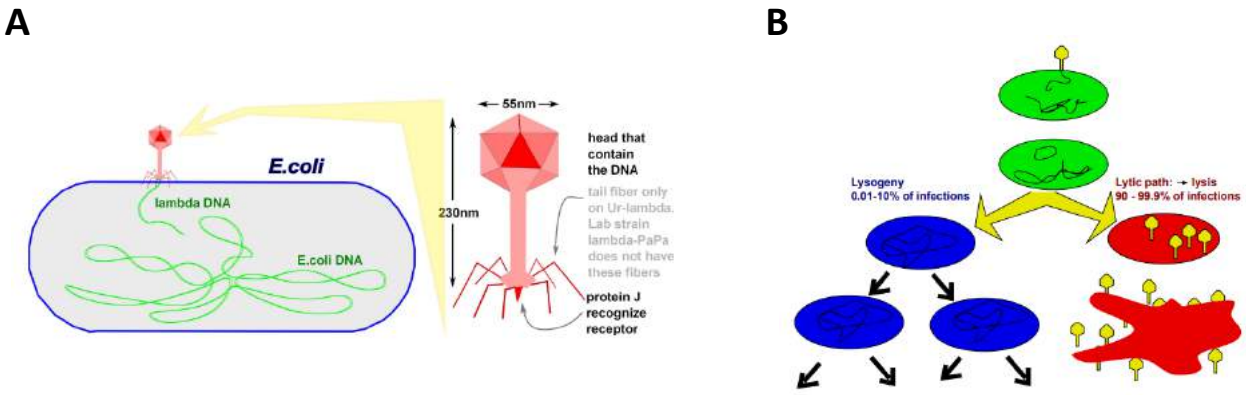

Figure 26: **Schematics of Escherichia coli and bacteriophage λ A** An illustration of bacteriophage λ during its infection of host E. coli. On the right side, basic features of phage λ anatomy are shown. **B** The post-infection decision between lysogeny and lysis for the temperate bacteriophage λ. Brown et al. demonstrated that another decision regarding infection is made before the initial step of this well-studied process. (Both images are adapted from [49])

This observation is noteworthy. Given that phages rely on diffusion for movement and necessitate a burst size of approximately 100 for survival, bypassing a less-fit cell for a potentially healthier one seems counter intuitive. Moreover, phage genomes are typically compact [46, 49]. Reserving genomic space for such processes is a significant commitment. While there are instances of phages apparently making "decisions", these are generally post-infection scenarios, such as the lysis-lysogeny "decision" [50, 51, 52, 53, 54, 55, 56, 57, 58, 59, 60, 61, 62].

Brown et al. explained this phenomenon through the lens of λ's reversible binding [199] and LamB's hyperdiffusion [200, 201]. Yet, several questions linger. Is this behavior exclusive to λ phage, or is it prevalent across bacteriophages? If widespread, is it limited to *E. coli* bacteriophages, or is it observed in other phage-bacteria systems as well? Moreover, what mechanisms underlie this behavior, and how does it influence host-parasite interactions and community dynamics? This chapter outlines our approach to these questions, though conclusive results are yet to be drawn.

4.2 Experimental method

The following protocol is adapted from the experimental methodology of the study by Brown et al. [198]. This investigation focuses on phage adsorption from cells under two contrasting metabolic states: a state of high metabolic activity due to the presence of glucose, and a state of low metabolic activity due to the presence of potassium arsenate and sodium azide.

Each bacterial culture is initiated from an independent single colony, while each phage lysate and phage lysates are correspondingly prepared from an independent plaque. Following overnight growth, the bacterial culture is diluted 20-fold with rich medium and incubated for 2 hours to restore exponential growth. Subsequently, nutrients are removed from the bacteria by centrifugation and resuspension with a nutrient-free buffer.

Thereafter, samples of washed bacteria are subjected to either favorable or unfavorable growth conditions by adding glucose or potassium arsenate and sodium azide and incubating 37 °C. Post incubation, phages are introduced and the incubation continues under identical conditions for an additional 10 minutes. The free phages are then segregated from the bacteria via centrifugation. Subsequently, a portion of the supernatant is diluted 10-fold with buffer, supplemented with potassium phosphate to inhibit toxicity from any remaining arsenate. The phage titers are assessed through subsequent dilutions in buffer, followed by spotting on a lawn of a susceptible bacterial strain. The concentration of washed bacteria is estimated by measuring the A600 optical density and by counting in a Petroff-Hausser chamber. The proportion of unbound phage is calculated by comparing the PFU/ml concentration in the supernatant derived from bacteria-containing samples to that in bacteria-free samples.

4.3 Results

The starting point of this project is to reproduce the experiment of Brown et al. [198] by replicating their results for the $\lambda cIb221$ phage, as shown in Table 2. This table displays the interaction results of the $\lambda cIb221$ phage with two bacterial strains: S3207 which is immune to λ [202] and S3222 which is essentially S3207 but with λ vir^r Mal^- modifications making it resistant to phage λ [198]. The third and fourth column of the table show the ratio of plaque forming units (PFUs) produced by the free viruses in glucose (Glu) and arsenate and azide (As/Az) relative to the phage titer in TMG. The fifth column calculates the Ratio of results from As/Az over Glu, defined as $Ratio = \frac{As/Az}{TMG} / \frac{Glu}{TMG}$.

From the results, it's evident that for S3207, where the phages are blocked by immunity within the host there's a tenfold increase in free phage particles in the As/Az environment compared to the Glu environment. This substantial effect isn't observed with the S3222 bacteria since the phages cannot enter due to its resistance. Hence, this stark difference underscores the significance of a phage's "decision" to infect a bacterium. The results suggest that phages tend to avoid infecting bacteria in poor metabolic states, which in our case is a result of poisoning with Arsenate and

$\lambda cI b221$				
Experiment	Bacteria	$\frac{\text{Glu}}{\text{TMG}}$	$\frac{\text{As/Az}}{\text{TMG}}$	Ratio
1	S3207	0.007	0.08	11.4
	S3222	0.47	0.91	1.9
2	S3207	0.008	0.0067	8.4
	S3222	0.75	0.83	1.1

Table 2: Replicating the results of Brown et al. for the phage λ

Azide. The experiment is currently being repeated with an increased MOI and a λ host-range mutant that bypasses reversible binding [198]. Subsequently, we will proceed with applying the protocol on other phages.

4.4 Conclusion

In their study, Brown et al. [198] reported the adsorption of the λ phage, which necessitates LamB, is influenced by the metabolic state of the host. Currently, I am in the process of replicating their results. The hypothesis of our study is that this sensitivity to metabolic state of the host could be a prevalent feature among phages. Consequently, the probability of a phage infecting a cell exhibiting reduced metabolism could be an evolutionary trait, potentially determined by the density of host cells in the phage's native habitat. To test this hypothesis, the experimental protocol will be performed with multiple different *E. coli* phage strains, with plans to subsequently examine *Vibrio* phage strains for comparative analysis. Although we are still in the preliminary stages and have not yet obtained definitive results, we anticipate meaningful findings in the forthcoming weeks.

4.5 Project: Do bacteriophages ”decide” on infection based on the host's metabolic condition?

Collaborators: Anastasios Marantos*, Kim Sneppen*, Namiko Mitarai*, Stanley Brown*

Affiliations: *Center for Models of Life, Niels Bohr Institute, University of Copenhagen, Copenhagen, Denmark.

My contribution: I have conceptualized and set the direction of this scientific project. I am conducting the experiments and the data analysis and I will produce figures, and contribute to the writing and editing of the work.

Supervision: I work under the supervision of Prof. Kim Sneppen and co-supervision of Assoc. Prof. Namiko Mitarai.

Publication status: In Progress - This study is ongoing. It's worth noting that this research endeavor necessitated the acquisition of microbiological lab skills that were previously outside my domain of expertise. Prof. Stanley Brown has been helping me learn the necessary microbiology laboratory skills. Therefore a period of training was required. I am currently conducting the experiments. As a result, no manuscript accompanies this chapter.

5 Conclusion

The primary focus of this thesis is to explore the profound effects that challenging conditions exert on the dynamics of phage-bacteria ecosystems.

The chapter on local microbial ecosystems in the ocean's upper layers, unveiled that ecosystem stability and robustness requires specialization in infection network patterns, when there is intense competition for shared limited resources. Notably, even minor deviations from this self-organized specialization have a profound effect on the emergence and survival of slower-growing bacteria . This results in extinction events that can include even the fastest growing strain. The extinction of the fastest growers is driven by the dynamic formation a triplet motif when one phage strain infects both the fastest growing but more susceptible bacterial strain and a slower growing but more resistant strain. The chapter dedicated to Bacillus Subtilis has brought forth a significant revelation: sporulation is triggered not only by nutrient scarcity but also by the presence of viruses. This sporulation mechanism, particularly effective in spatial environments, serves as a collective defense strategy, considerably restricting the expanse of viral plaques. To our knowledge this is the first account of such a mechanism, providing new insights and avenues for research in one of the best studied organisms in Microbiology.

Finally, preliminary experimental observations presented in this study corroborate previous findings of phages exhibiting selectivity based on the host's metabolic state. Particularly, there is significant evidence that λ phage tends to avoid infecting Escherichia coli cells in low metabolic state. The aim is to continue this research on other Escherichia coli to assess the potential for a new layer of sophistication in phage-bacteria interactions.

Overall, the findings presented here serve as both a conclusion to my research activities as a PhD candidate and a starting point for future research in microbial ecology.

References

[1] Madigan M.T., Bender K.S., Buckley D.H., Sattley W. M., and Stahl D.A. *Brock Biology of Microorganisms*. Pearson Education, Inc., Boston, fifteenth edition, 2018.

[2] Woese C.R., Kandler O., and Wheelis M.L. Towards a natural system of organisms: proposal for the domains Archaea, Bacteria, and Eucarya. *Proc Natl Acad Sci USA*, 87(12):4576–4579, 1990.

[3] Alberts B., Johnson A., Lewis J., Morgan D., Raff M., Roberts K., and Walter P. *Molecular Biology of the Cell*. Garland Science, 2014.

[4] Kleckner N., Fisher J.K., M. Stouf, White M.A., Bates D., and Witz G. The bacterial nucleoid: nature, dynamics and sister segregation. *Current Opinion in Microbiology*, 22:127–137, 2014.

[5] Hayes F. Chapter 1 – The Function and Organization of Plasmids. In Casali N. and Presto A., editors, *E. Coli Plasmid Vectors: Methods and Applications*, volume 235 of *Methods in Molecular Biology*, pages 1–5. Humana Press, 2003.

[6] Bardy S.L., Ng S.Y.M., and Jarrell K.F. Prokaryotic motility structures. *Microbiology*, 149(Pt 2):295–304, 2003.

[7] Proft T. and Baker E.N. Pili in Gram-negative and Gram-positive bacteria — structure, assembly and their role in disease. *Cellular and Molecular Life Sciences*, 66(4):613–635, 2009.

[8] Kolenda R., Ugorski M., and Grzymajlo K. Everything You Always Wanted to Know About Salmonella Type 1 Fimbriae, but Were Afraid to Ask. *Frontiers in Microbiology*, 10:1017, 2019.

[9] Nuccio S.P. et al. Evolution of the chaperone/usher assembly pathway: fimbrial classification goes Greek. *Microbiology and Molecular Biology Reviews*, 71(4):551–575, 2007.

[10] Gram H.C. Über die isolierte Färbung der Schizomyceten in Schnitt- und Trockenpräparaten. *Fortschr. Med.*, 2:185–189, 1884.

[11] Romaniuk J.A. and Cegelski L. Bacterial cell wall composition and the influence of antibiotics by cell-wall and whole-cell NMR. *Philosophical Transactions of the Royal Society of London. Series B, Biological Sciences*, 370(1679):20150024, 2015.

[12] Megrian D., Taib N., Witwinowski J., and Gribaldo S. One or two membranes? Diderm firmicutes challenge the Gram-positive/Gram-negative divide. *Molecular Microbiology*, 113(3):659–671, 2020.

[13] Rietschel E.T., Kirikae T., Schade F.U., Mamat U., Schmidt G., Loppnow H., Ulmer A.J., Zähringer U., Seydel U., and Di Padova F. Bacterial endotoxin: molecular relationships of structure to activity and function. *FASEB J*, 8(2):217–25, 1994.

[14] Avila-Calderón E.D., Ruiz-Palma M.D., and Contreras-Rodríguez A. Outer Membrane Vesicles of Gram-Negative Bacteria: An Outlook on Biogenesis. *Frontiers in Microbiology*, 12:557902, 2021.

[15] Black J.G. *Microbiology: Principles and Explorations*. Prentice Hall, 1993.

[16] Christie G. and Setlow P. Bacillus spore germination: Knowns, unknowns and what we need to learn. *Cell Signal*, 74:109729, 2020.

[17] Galperin M.Y. Genome Diversity of Spore-forming Firmicutes. *Microbiology Spectrum*, 1(2):TBS–0015–2012–, 2013.

[18] Setlow P. I will survive: DNA protection in bacterial spores. *Trends Microbiol.*, 15(4):172–180, 2007.

[19] Errington J. and Aart L.T. van der. Microbe Profile: Bacillus subtilis: model organism for cellular development, and industrial workhorse. *Microbiology (Reading)*, 166(5):425–427, 2020.

[20] Dusenbery D.B. *Living at Micro Scale*. Harvard University Press, Cambridge, Massachusetts, 2009.

[21] Yang D.C., Blair K.M., and Salama N.R. Staying in Shape: the Impact of Cell Shape on Bacterial Survival in Diverse Environments. *Microbiology and Molecular Biology Reviews*, 80:187–203, 2016.

[22] Baker-Austin C. and Dopson M. Life in acid: pH homeostasis in acidophiles. *Trends Microbiol*, 15(4):165–171, Apr 2007. Epub 2007 Feb 28.

[23] Colman D.R. et al. The deep, hot biosphere: Twenty-five years of retrospection. *Proceedings of the National Academy of Sciences*, 114(27):6895–6903, 2017.

[24] Schulze-Makuch D., Wagner D., Kounaves S.P., Mangelsdorf K., Devine K.G., de Vera J.P., Schmitt-Kopplin P., Grossart H.P., Parro V., Kaupenjohann M., Galy A., Schneider B., Airo A., Frösler J., Davila A.F., Arens F.L., Cáceres L., Cornejo F.S., Carrizo D., Dartnell L., DiRuggiero J., Flury M., Ganzert L., Gessner M.O., Grathwohl P., Guan L., Heinz J., Hess M., Keppler F., Maus D., McKay C.P., Meckenstock R.U., Montgomery W., Oberlin E.A., Probst A.J., Sáenz J.S., Sattler T., Schirmack J., Sephton M.A., Schloter M., Uhl J., Valenzuela B., Vestergaard G., Wörmer L., and Zamorano P. Transitory microbial habitat

in the hyperarid Atacama Desert. *Proc Natl Acad Sci U S A*, 115(11):2670–2675, 2018. Epub 2018 Feb 26.

[25] Jeong S.W. and Choi Y.J. Extremophilic Microorganisms for the Treatment of Toxic Pollutants in the Environment. *Molecules*, 25(21):4916, 2020.

[26] Whitman W.B., Coleman D.C., and Wiebe W.J. Prokaryotes: the unseen majority. *Proceedings of the National Academy of Sciences*, 95(12):6578–6583, 1998.

[27] Hall B.K. *Strickberger's Evolution: The Integration of Genes, Organisms and Populations*. Jones and Bartlett, Sudbury, Mass., revised edition, 2008.

[28] Imran A., Hakim S., Tariq M., Nawaz M.S., Laraib I., Gulzar U., Hanif M.K., Siddique M.J., Hayat M., Fraz A., and Ahmad M. Diazotrophs for Lowering Nitrogen Pollution Crises: Looking Deep Into the Roots. *Frontiers in Microbiology*, 12:637815, 2021.

[29] Zehr J.P., Jenkins B.D., Short S.M., and Steward G.F. Nitrogenase gene diversity and microbial community structure: a cross-system comparison. *Environmental Microbiology*, 5(7):539–554, 2003.

[30] Kosugi Y., Matsuura N., Liang Q., and Yamamoto-Ikemoto R. Wastewater Treatment using the "Sulfate Reduction, DenitrificationAnammox and Partial Nitrification (SRDAPN)" Process. *Chemosphere*, 256:127092, 2020.

[31] Morel F.M., Kraepiel A.M., and Amyot M. The chemical cycle and bioaccumulation of mercury. *Annual Review of Ecology and Systematics*, 29:543–566, 1998.

[32] Krasner R.I. *The microbial challenge: a public health perspective*. Jones & Bartlett Learning, Burlington, Mass., 2013.

[33] Cohen Y. Bioremediation of oil by marine microbial mats. *International Microbiology*, 5(4):189–193.

[34] McCutcheon J.P. The Genomics and Cell Biology of Host-Beneficial Intracellular Infections. *Annual Review of Cell and Developmental Biology*, 37:115–142, 2021.

[35] Pommerville J.C. *Fundamentals of Microbiology*. Jones and Bartlett, Boston, 10 edition, 2014.

[36] Clark D. *Germs, Genes, & Civilization: how epidemics shaped who we are today*. FT Press, Upper Saddle River, N.J, 2010.

[37] Fleming A. Streptococcal Meningitis treated with Penicillin. *The Lancet*, 242(6267):434–438, 1943.

[38] Twort F.W. An Investigation on the Nature of Ultra-Microscopic Viruses. *The Lancet*, 186(4814):1241–1243, 1915.

[39] d'Herelle F. Sur un microbe invisible antagoniste des bacilles dysenteriques (An invisible microbe that is antagonistic to the dysentery bacillus). *Comptes rendus de l'Academie des Sciences*, 165:373–375, 1917.

[40] Waldor M.K., Friedman D.I., and Adhya S.L., editors. *Phages: Their Role in Bacterial Pathogenesis and Biotechnology*. ASM Press, 2005.

[41] Keen E.C. A century of phage research: bacteriophages and the shaping of modern biology. 37(1), 2015.

[42] Kutter E., Sulakvelidze A., Summers W., Guttman B., Raya R., Brüssow H., Ecology P., and Carlson K. *Bacteriophages: Biology and Applications*. CRC Press, 2004.

[43] Breitbart M. and Rohwer F. Here a virus, there a virus, everywhere the same virus? *Trends in Microbiology*, 13:278–284, 2005.

[44] Yuan Y. and Gao M. Jumbo Bacteriophages: An Overview. *Frontiers in Microbiology*, 8, 2017.

[45] Weitz J.S., Poisot T., Meyer J.R., Flores C.O., Valverde S., Sullivan M.B., and Hochberg M.E. Phage–bacteria infection networks. *Trends in Microbiology*, 21(2):82–91, 2013.

[46] Weitz J.S. *Quantitative Viral Ecology: Dynamics of Viruses and Their Microbial Hosts*. Monographs in Population Biology. Princeton University Press, Princeton, 2015.

[47] Keen E.C., Bliskovsky V.V., Malagon F., Baker J.D., Prince J.S., Klaus J.S., and Adhya S.L. Novel "Superspreader" Bacteriophages Promote Horizontal Gene Transfer by Transformation. *mBio*, 8(1):e02115–16, 2017.

[48] Lekunberri I., Subirats J., Borrego C.M., and Balcázar J.L. Exploring the contribution of bacteriophages to antibiotic resistance. *Environmental Pollution*, 220(Pt B):981–984, 2017.

[49] Sneppen K. *Models of life: Dynamics and regulation in biological systems*. Cambridge University Press, 2014.

[50] Lwoff A. Lysogeny. *Bacteriological reviews*, 17(4):269–337, 1953.

[51] Kourilsky P. Lysogenization by bacteriophage lambda. II. Multiple infection and the lysogenic response. *Mol Gen Genet*, 122(2):183–195, 1973.

[52] Kourilsky P. Lysogenization by bacteriophage lambda. II. Identification of genes involved in the multiplicity dependent processes. *Biochimie*, 56(11-12):1511–1516, 1974.

[53] Kourilsky P. and Knapp A. Lysogenization by bacteriophage lambda. III. Multiplicity dependent phenomena occurring upon infection by lambda. *Biochimie*, 56(11-12):1517–1523, 1974.

[54] Kourilsky P. and Gros D. Lysogenization by bacteriophage lambda. IV. Inhibition of phage DNA synthesis by the products of genes cII and cIII. *Biochimie*, 58(11-12):1321–1327, 1976.

[55] Ptashne M. *A Genetic Switch, Third Edition, Phage Lambda Revisited*. Cold Spring Harbor Laboratory Press, 2004.

[56] Arkin A., Ross J., and McAdams H.H. Stochastic kinetic analysis of developmental pathway bifurcation in phage lambda-infected Escherichia coli cells. *Genetics*, 149(4):1633–1648, 1998.

[57] St-Pierre F. and Endy D. Determination of cell fate selection during phage lambda infection. *Proc Natl Acad Sci U S A*, 105(52):20705–20710, 2008.

[58] Weitz J.S., Mileyko Y., Joh R.I., and Voit E.O. Collective decision making in bacterial viruses. *Biophys J*, 95(6):2673–2680, 2008.

[59] Maslov S. and Sneppen K. Diversity waves in collapse-driven population dynamics. *PLoS computational biology*, 11(9):e1004440, 2015.

[60] Zeng L., Skinner S.O., Zong C., Sippy J., Feiss M., and Golding I. Decision making at a subcellular level determines the outcome of bacteriophage infection. *Cell*, 141(4):682–691, 2010.

[61] Golding I. Infection by bacteriophage lambda: an evolving paradigm for cellular individuality. *Curr Opin Microbiol*, 43:9–13, 2018.

[62] Golding I., Coleman S., Nguyen T.V.P., and Yao T. Decision Making by Temperate Phages. In Bamford D.H. and Zuckerman M., editors, *Encyclopedia of Virology (Fourth Edition)*, pages 88–97. Academic Press, Oxford, fourth edition, 2021.

[63] Salmond G.P. and Fineran P.C. A century of the phage: past, present and future. *Nature Reviews Microbiology*, 13(12):777–786, 2015.

[64] Rostøl J.T. and Marraffini L. (Ph)ighting phages: How bacteria resist their parasites. *Cell Host & Microbe*, 25(2):184–194, 2019.

[65] Smith W.P.J., Wucher B.R., Nadell C.D., and Foster K.R. Bacterial defences: mechanisms, evolution and antimicrobial resistance. *Nature Reviews Microbiology*, 21(8):519–534, 2023.

[66] Abedon S.T. and Yin J. Bacteriophage plaques: theory and analysis. In *Bacteriophages*, pages 161–174. Springer, 2009.

[67] Lotka A.J. *Elements of Physical Biology*. Williams and Wilkins., 1925.

[68] Volterra V. Variazioni e fluttuazioni del numero d'individui in specie animali conviventi. *Memoria della regia accademia nazionale del lincei ser.*, 2:31–113, 1926.

[69] Abedon S. *Bacteriophage Ecology: Population Growth, Evolution, and Impact of Bacterial Viruses*. Cambridge University Press, 01 2008.

[70] Davies N.B., Krebs J.R., and West S.A. *An Introduction to Behavioural Ecology*. Wiley-Blackwell, 4 edition, 2012.

[71] Bergh Ø., Børsheim K.Y., Bratbak G., and Heldal M. High abundance of viruses found in aquatic environments. *Nature*, 340:467–468, 1989.

[72] Bar-On Y.M., Phillips R., and Milo R. The biomass distribution on Earth. *Proc Natl Acad Sci U S A*, 115(25):6506–6511, 2018.

[73] Stratmann T. The ProkaBioDen database, a global database of benthic prokaryotic biomasses and densities in the marine realm. *Nature*, 2022.

[74] Middelboe M., Jorgensen N.O.G., and Kroer N. Effects of viruses on nutrient turnover and growth efficiency of noninfected marine bacterioplankton. *Applied and Environmental Microbiology*, 62(6):1991–1997, 1996.

[75] Suttle C.A. Viruses in the sea. *Nature*, 437:356–361, 2005.

[76] Middelboe M. and Lyck P.G. Regeneration of dissolved organic matter by viral lysis in marine microbial communities. *Aquat Microb Ecol*, 27:187–194, 2002.

[77] Middelboe M. and Jørgensen N.O.G. Viral lysis of bacteria: an important source of dissolved amino acids and cell wall compounds. *Journal of the Marine Biological Association of the United Kingdom*, 86(3):605–612, 2006.

[78] Suttle C.A. Marine viruses - Major players in the global ecosystem. *Nature Reviews Microbiology*, 5:801–812, 2007.

[79] Brussaard C., Wilhelm S., Thingstad F., et al. Global-scale processes with a nanoscale drive: the role of marine viruses. *ISME J*, 2:575–578, 2008.

[80] Lennon J.T. and Martiny J.B.H. Rapid evolution buffers ecosystem impacts of viruses in a microbial food web. *Ecology Letters*, 11(11):1178–1188, 2008.

[81] Weitz J.S. and Wilhelm S.W. Ocean viruses and their effects on microbial communities and biogeochemical cycles. *F1000 Biology Reports*, 4:17, 2012.

[82] Weitz J., Stock C., Wilhelm S., Bourouiba L., Coleman M.L., Buchan A., Follows M., Fuhrman J., Jover L.F., Lennon J., Middelboe M., Sonderegger D., Suttle C., Taylor B.P., Thingstad T., Wilson W.H., and Wommack K.E. A multitrophic model to quantify the effects of marine viruses on microbial food webs and ecosystem processes. *The ISME Journal*, 2015.

[83] Hawley A.K., Nobu M.K., Wright J.J., et al. Diverse Marinimicrobia bacteria may mediate coupled biogeochemical cycles along eco-thermodynamic gradients. *Nat Commun*, 8:1507, 2017.

[84] Eilersen A., Jensen M.H., and Sneppen K. Chaos in disease outbreaks among prey. *Sci Rep*, 10:3907, 2020.

[85] Fuhrman J.A. and Noble R.T. Viruses and protists cause similar bacterial mortality in coastal seawater. *Limnology and oceanography*, 40(7):1236–1242, 1995.

[86] Noble R.T. and Fuhrman J.A. Virus decay and its causes in coastal waters. *Applied and Environmental Microbiology*, 63(1):77–83, 1997.

[87] Wikipedia contributors. Pelagic zone — Wikipedia, the free encyclopedia, 14 July 2023. Online; accessed 10 October 2023.

[88] Wikipedia contributors. Photic zone — Wikipedia, the free encyclopedia, 3 September 2023. Online; accessed 10 October 2023.

[89] Hutchinson G.E. The Paradox of the Plankton. *The American Naturalist*, 95(882):137–145, 1961.

[90] Holt R.D. Predation, apparent competition, and the structure of prey communities. *Theoretical Population Biology*, 12:197–229., 1977.

[91] Wilson J.B. Mechanisms of species coexistence: twelve explanations for Hutchinson's 'Paradox of the Plankton': evidence from New Zealand plant communities. *New Zealand Journal of Ecology*, 13:17–42, 1990.

[92] Thingstad T.F. Elements of a theory for the mechanisms controlling abundance, diversity, and biogeochemical role of lytic bacterial viruses in aquatic systems. *Limnology and Oceanography*, 45, 2000.

[93] Heilmann S., Sneppen K., and Krishna S. Sustainability of Virulence in a Phage-Bacterial Ecosystem. *Journal of Virology*, 84:3016–3022, 2010.

[94] Heilmann S., Sneppen K., and Krishna S. Coexistence of phage and bacteria on the boundary of self-organized refuges. *Proceedings of the National Academy of Sciences of the United States of America*, 109:12828–12833, 2012.

[95] Moebus K. and Nattkemper H. Bacteriophage sensitivity patterns among bacteria isolated from marine waters. *Helgoländer Meeresuntersuchungen*, 34(3):375–385, 1981.

[96] Kauffman K.M., Chang W.K., Brown J.M., Hussain F.A., Yang J., Polz M.F., and Kelly L. Resolving the structure of phage-bacteria interactions in the context of natural diversity. *Nature communications*, 13(1), 372, 2022.

[97] Flores C.O., Valverde S., and Weitz J.S. Multi-scale structure and geographic drivers of cross-infection within marine bacteria and phages. *ISME Journal*, 7:1–13, 2013.

[98] Kauffman K.M., Chang W.K., Brown J.M., Hussain F.A., Yang J., Polz M.F., and Kelly L. Resolving the structure of phage–bacteria interactions in the context of natural diversity. *Nature communications*, 13(1):1–20, 2022.

[99] Haerter J.O., Mitarai N., and Sneppen K. Phage and bacteria support mutual diversity in a narrowing staircase of coexistence. *ISME Journal*, 8(11):2317–2326, 2014.

[100] Darwin C. *On the Origin of Species by Means of Natural Selection, or The Preservation of Favoured Races in the Struggle for Life.* John Murray, London, 1859.

[101] Grinnell J. The origin and distribution of the chestnut-backed chickadee. *The Auk*, 21:364–379, 1904.

[102] Lotka A.J. The growth of mixed populations: Two species competing for a common food supply. *Journal of the Washington Academy of Sciences*, 22(16/17):461–469, 1932.

[103] Gause G.F. The Struggle for Existence. *Soil Science*, 41:159, 1936.

[104] Hardin G. The competitive exclusion principle. *Science*, 131:1292–1297, 1960.

[105] Campbell A. Conditions for the Existence of Bacteriophage. *Evolution*, 15:153–165, 1961.

[106] Levin B.R., Stewart F.M., and Chao L. Resource-Limited Growth, Competition, and Predation: A Model and Experimental Studies with Bacteria and Bacteriophage. *The American Naturalist*, 111:3–24, 1977.

[107] Thingstad T.F., Våge S., Storesund J.E., Sandaa R.A., and Giske J. A theoretical analysis of how strain-specific viruses can control microbial species diversity. *Proceedings of the National Academy of Sciences*, 111(21):7813–7818, 2014.

[108] Marantos A., Mitarai N., and Sneppen K. From kill the winner to eliminate the winner in open phage-bacteria systems. *PLOS Computational Biology*, 18(8):e1010400, 2022.

[109] Jover L.F., Cortez M.H., and Weitz J.S. Mechanisms of multi-strain coexistence in host-phage systems with nested infection networks. *Journal of Theoretical Biology*, 332:65–77, 2013.

[110] Jover L.F., Flores C.O., Cortez M.H., and Weitz J.S. Multiple regimes of robust patterns between network structure and biodiversity. *Scientific Reports*, 5, 2015.

[111] Mitarai N., Marantos A., and Sneppen K. Sustainable diversity of phage-bacteria systems. *Current Opinion in Systems Biology*, 35:100468, 2023.

[112] Seth E.C. and Taga M.E. Nutrient cross-feeding in the microbial world. *Frontiers in microbiology*, 5:350, 2014.

[113] Goldford J.E., Lu N., Bajić D., Estrela S., Tikhonov M., Sanchez-Gorostiaga A., Segrè D., Mehta P., and Sanchez A. Emergent simplicity in microbial community assembly. *Science*, 361(6401):469–474, 2018.

[114] Goyal A. and Maslov S. Diversity, stability, and reproducibility in stochastically assembled microbial ecosystems. *Physical Review Letters*, 120(15):158102, 2018.

[115] Wang Z., Goyal A., Dubinkina V., George A.B., Wang T., Fridman Y., and Maslov S. Complementary resource preferences spontaneously emerge in diauxic microbial communities. *Nature communications*, 12(1):1–12, 2021.

[116] Tilman D. Competition and biodiversity in spatially structured habitats. *Ecology*, 75(1):2–16, 1994.

[117] Yanni D., Márquez-Zacarías P., Yunker P.J., and Ratcliff W.C. Drivers of spatial structure in social microbial communities. *Current biology*, 29(11):R545–R550, 2019.

[118] Beckett S.J. and Williams H.T.P. Coevolutionary diversification creates nested-modular structure in phage–bacteria interaction networks. *Interface focus*, 3(6):20130033, 2013.

[119] Piel D., Bruto M., Labreuche Y., Blanquart F., Goudenège D., Barcia-Cruz R., Chenivesse S., Le Panse S., James A., Dubert J., et al. Phage–host coevolution in natural populations. *Nature Microbiology*, 7(7):1075–1086, 2022.

[120] Morgan A.D., Gandon S., and Buckling A. The effect of migration on local adaptation in a coevolving host–parasite system. *Nature*, 437(7056):253–256, 2005.

[121] Parkes R.J. et al. Deep bacterial biosphere in Pacific Ocean sediments. *Nature*, 371(6496):410–413, 1994.

[122] Hoehler T.M. and Jørgensen B.B. Microbial life under extreme energy limitation. *Nature Reviews Microbiology*, 11(2):83–94, 2013.

[123] Hobbie J.E. and Hobbie E.A. Microbes in nature are limited by carbon and energy: the starving-survival lifestyle in soil and consequences for estimating microbial rates. *Frontiers in Microbiology*, 4, 2013.

[124] Lever M.A. et al. Life under extreme energy limitation: a synthesis of laboratory- and field-based investigations. *FEMS Microbiology Reviews*, 39(5):688–728, 2015.

[125] Merino N. et al. Living at the Extremes: Extremophiles and the Limits of Life in a Planetary Context. *Frontiers in Microbiology*, 10, 2019.

[126] Wörmer L. et al. Microbial dormancy in the marine subsurface: Global endospore abundance and response to burial. *Science Advances*, 5(2), 2019.

[127] Morita R.Y. Bioavailability of energy and its relationship to growth and starvation survival in nature. *Canadian Journal of Microbiology*, 34(4):436–441, 1988.

[128] Morita R.Y. *Bioavailability of Energy and the Starvation State*, pages 1–23. Springer US, Boston, MA, 1993.

[129] Maitra A. and Dill K.A. Bacterial growth laws reflect the evolutionary importance of energy efficiency. *Proceedings of the National Academy of Sciences*, 112(2):406–411, 2015.

[130] Cohen D. Optimizing reproduction in a randomly varying environment. *Journal of Theoretical Biology*, 12(1):119–129, 1966.

[131] Lennon J.T. and Jones S.E. Microbial seed banks: The ecological and evolutionary implications of dormancy, 2011.

[132] Oliver J.D. The viable but non-culturable state in the human pathogen Vibrio vulnificus. *FEMS Microbiology Letters*, 133(3):203–208, 1995.

[133] Evans M.E.K. and Dennehy J.J. Germ banking: bet-hedging and variable release from egg and seed dormancy. *The Quarterly Review of Biology*, 80(4):431–451, 2005.

[134] Bradshaw W.E., Armbruster P.A., and Holzapfel C.M. Fitness Consequences of Hibernal Diapause in the Pitcher-Plant Mosquito, Wyeomyia smithii. *Ecology*, 79(4):1458–1462, 1998.

[135] Caceres C.E. and Tessier A.J. To sink or swim: Variable diapause strategies among Daphnia species. *Limnology and Oceanography*, 49(4, part 2):1333–1340, 2004.

[136] Bodegom van P. Microbial Maintenance: A Critical Review on Its Quantification. *Microbial Ecology*, 53(4):513–523, 2007.

[137] Guppy M. and Withers P. Metabolic depression in animals: physiological perspectives and biochemical generalizations. *Biol. Rev. Camb. Philos. Soc.*, 74:1–40, 1999.

[138] Stevenson L.H. A Case for Bacterial Dormancy in Aquatic Systems. *Microbial Ecology*, 4(2):127–133, sep 1977.

[139] Alvarez C.R. et al. Associations between organic matter fractions and the active soil microbial biomass. *Soil Biology and Biochemistry*, 30(6):767–773, 1998.

[140] Blagodatskaya E. and Kuzyakov Y. Active microorganisms in soil: Critical review of estimation criteria and approaches. *Soil Biology and Biochemistry*, 67:192–211, 2013.

[141] Coates A.R.M., editor. *Dormancy and Low-Growth States in Microbial Disease*. Cambridge Univ. Press, Cambridge, UK, 2003.

[142] Lewis K. Persister cells, dormancy, and infectious disease. *Nature Reviews Microbiology*, 5:48–56, 2007.

[143] Fisher R.A., Gollan B., and Helaine S. Persistent bacterial infections and persister cells. *Nature Reviews. Microbiology*, 15(8):453–464, 2017.

[144] Svenningsen M.S., Veress A., Harms A., et al. Birth and Resuscitation of (p)ppGpp Induced Antibiotic Tolerant Persister Cells. *Sci Rep*, 9:6056, 2019.

[145] Svenningsen M.K., Svenningsen S.L., Sørensen M.A., and Mitarai N. Existence of log-phase Escherichia coli persisters and lasting memory of a starvation pulse. *Life Science Alliance*, 5(2), 2022.

[146] Himeoka Y. and Mitarai N. When to wake up? The optimal waking-up strategies for starvation-induced persistence. *PLOS Computational Biology*, 17(2):1–22, 02 2021.

[147] Kaprelyants A.S., Gottschal J.C., and Kell D.B. Dormancy in non-sporulating bacteria. *FEMS Microbiol. Rev.*, 10:271–285, 1993.

[148] Votyakova T.V., Kaprelyants A.S., and Kell D.B. Influence of Viable Cells on the Resuscitation of Dormant Cells in Micrococcus luteus Cultures Held in an Extended Stationary Phase: the Population Effect. *Applied and Environmental Microbiology*, 60(9):3284–3291, 1994.

[149] Ishiguro K. et al. Real-time monitoring of the metabolic activity of periodontopathic bacteria. *Journal of Microbiological Methods*, 115:22–26, 2015.

[150] Epstein S.S. Microbial awakenings. *Nature*, 457(7233):1083, 2009.

[151] Keynan A. et al. Activation of bacterial endospores. *Journal of Bacteriology*, 88(2):313–318, 1964.

[152] Aanderud Z.T. et al. Resuscitation of the rare biosphere contributes to pulses of ecosystem activity. *Frontiers in Microbiology*, 6:24, 2015.

[153] Dworkin J. and Shah I.M. Exit from dormancy in microbial organisms. *Nature Reviews. Microbiology*, 8(12):890–896, 2010.

[154] Locey K.J., Fisk M.C., and Lennon J.T. Microscale Insight into Microbial Seed Banks. *Frontiers in Microbiology*, 7, 2017.

[155] Bale M.J. et al. The survival of bacteria exposed to desiccation on surfaces associated with farm buildings. *The Journal of Applied Bacteriology*, 75(6):519–528, 1993.

[156] Johnson S.S. et al. Ancient bacteria show evidence of DNA repair. *Proceedings of the National Academy of Sciences*, 104(36):14401–14405, 2007.

[157] Cano R.J. and Borucki M.K. Revival and identification of bacterial spores in 25- to 40-million-year-old Dominican amber. *Science (New York, N.Y.)*, 268(5213):1060–1064, 1995.

[158] Vreeland R.H., Rosenzweig W.D., and Powers D.W. Isolation of a 250 million-year-old halotolerant bacterium from a primary salt crystal. *Nature*, 407(6806):897–900, 2000.

[159] Chesson P. and Warner R.R. Environmental Variability Promotes Coexistence in Lottery Competitive Systems. *The American Naturalist*, 117(6):923–943, 1981.

[160] Cole J.J. Aquatic microbiology for ecosystem scientists: new and recycled paradigms in ecological microbiology. *Ecosystems*, 2:215–225, 1999.

[161] Kalamees R. and Zobel M. The role of the seed bank in gap regeneration in a calcareous grassland community. *Ecology*, 83:1017–1025, 2002.

[162] Chrzanowski T.H. and Simek K. Prey-size selection by freshwater flagellated protozoa. *Limnology*, 35:1429–1436, 1990.

[163] Bryan D., El-Shibiny A., Hobbs Z., Porter J., and Kutter E.M. Bacteriophage T4 Infection of Stationary Phase E. coli: Life after Log from a Phage Perspective. *Frontiers in Microbiology*, 7, 2016.

[164] Shoemaker W.R. and Lennon J.T. Evolution with a seed bank: The population genetic consequences of microbial dormancy. *Evolutionary Applications*, 11(1):60–75, 2018.

[165] González-Casanova A. et al. Strong seed-bank effects in bacterial evolution. *Journal of Theoretical Biology*, 356:62–70, 2014.

[166] Weller C. and Wu M. A generation-time effect on the rate of molecular evolution in bacteria. *Evolution*, 69(3):643–652, 2015.

[167] Gulbudak H. and Weitz J.S. A touch of sleep: biophysical model of contact-mediated dormancy of archaea by viruses. *Proceedings of the Royal Society B: Biological Sciences*, 283(1839):20161037, 2016.

[168] Koopmann B. et al. Fisher-Wright model with deterministic seed bank and selection. *Theoretical Population Biology*, 114:29–39, 2017.

[169] Gestel J. van, Ackermann M., and Wagner A. Microbial life cycles link global modularity in regulation to mosaic evolution. *Nature Ecology & Evolution*, 3(8):1184–1196, 2019.

[170] Lenski R.E. Coevolution of bacteria and phage: Are there endless cycles of bacterial defenses and phage counterdefenses? *Journal of Theoretical Biology*, 108(3):319–325, 1984.

[171] Lenski R.E. and Levin B.R. Constraints on the coevolution of bacteria and virulent phage: a model, some experiments, and predictions for natural communities. *The American Naturalist*, 125(4):585–602, 1985.

[172] Piggot P.J. and Hilbert D.W. Sporulation of Bacillus subtilis. *Curr. Opin. Microbiol.*, 7:579–586, 2004.

[173] Battistuzzi F.U., Feijao A., and Hedges S.B. A genomic timescale of prokaryote evolution: insights into the origin of methanogenesis, phototrophy, and the colonization of land. *BMC Evol Biol*, 4:44, 2004.

[174] Tocheva E.I., Ortega D.R., and Jensen G.J. Sporulation, bacterial cell envelopes and the origin of life. *Nat Rev Microbiol*, 14(8):535–542, 2016.

[175] Nicholson W.L., Munakata N., Horneck G., Melosh H.J., and Setlow P. Resistance of Bacillus Endospores to Extreme Terrestrial and Extraterrestrial Environments. *Microbiology and molecular biology reviews : MMBR*, 64(3):548–572, 2000.

[176] Horneck G., Moeller R., et al. Resistance of bacterial endospores to outer space for planetary protection purposes–experiment PROTECT of the EXPOSE-E mission. *Astrobiology*, 12(5):445–456, 2012.

[177] Setlow P. Mechanisms for the prevention of damage to DNA in spores of Bacillus species. *Annu. Rev. Microbiol.*, 49:29–54, 1995.

[178] Galperin M.Y. et al. Genomic determinants of sporulation in Bacilli and Clostridia: towards the minimal set of sporulation-specific genes. *Environmental Microbiology*, 14(11):2870–2890, 2012.

[179] Losick R. and Stragier P. Crisscross regulation of cell-type-specific gene expression during development in B. subtilis. *Nature*, 355(6361):601–604, 1992.

[180] Setlow P. Spores of Bacillus subtilis: their resistance to and killing by radiation, heat and chemicals. *Journal of Applied Microbiology*, 101(3):514–525, 2006.

[181] Schwartz D.A., Shoemaker W.R., Măgălie A., Weitz J.S., and Lennon J.T. Bacteria-phage coevolution with a seed bank. *The ISME Journal*, 2023.

[182] Schwartz D.A., Lehmkuhl B.K., and Lennon J.T. Phage-encoded sigma factors alter bacterial dormancy. *mSphere*, 7(4):e0029722, August 2022.

[183] Abedon S.T. and Yin J. *Bacteriophage Plaques: Theory and Analysis*, pages 161–174. Humana Press, Totowa, NJ, 2009.

[184] Gabay C. Kishony R. Oppenheim A. Pearl, S. and N.Q. Balaban. Nongenetic individuality in the host–phage interaction. *PLoS Biology*, 6(5):e120, 2008.

[185] Gallet R., Kannoly S., and Wang I. Effects of bacteriophage traits on plaque formation. *BMC Microbiology*, 11(1):181, 2011.

[186] Tzipilevich E., Pollak-Fiyaksel O., Shraiteh B., and Ben-Yehuda S. Bacteria elicit a phage tolerance response subsequent to infection of their neighbors. *EMBO J.*, 41(3):e109247, February 2022.

[187] Schaeffer P., Millet J., and Aubert J.P. Catabolic repression of bacterial sporulation. *Proceedings of the National Academy of Sciences*, 54(3):704–711, 1965.

[188] Li L., Jin J., Hu H., Deveau I.F., Foley S.L., and Chen H. Optimization of sporulation and purification methods for sporicidal efficacy assessment on Bacillus spores. *Journal of Industrial Microbiology and Biotechnology*, 49(4):kuac014, jul 2022.

[189] Kauffman K.M. and Polz M.F. Streamlining standard bacteriophage methods for higher throughput. *MethodsX*, page 159–172, 2018.

[190] Wang X. and Montero Llopis P. Visualizing Bacillus subtilis During Vegetative Growth and Spore Formation. *In: Leake, M. (eds) Chromosome Architecture. Methods in Molecular Biology*, 1431, 2016.

[191] Piggot P.J. and Coote J.G. Genetic aspects of bacterial endospore formation. *Bacteriological reviews*, (40(4)):908–962, 1976.

[192] Aertsen A. and Michiels C.W. Stress and How Bacteria Cope with Death and Survival. *Critical Reviews in Microbiology*, 30:263 – 273, 2004.

[193] Kussell E. and Leibler S. Phenotypic Diversity, Population Growth, and Information in Fluctuating Environments. *Science*, 309(5743):2075–2078, 2005.

[194] Weitz J.S. and Dushoff J. Alternative stable states in host–phage dynamics. *Theoretical Ecology*, 1(1):13–19, 2008.

[195] Wang Z. and Goldenfeld N. Fixed points and limit cycles in the population dynamics of lysogenic viruses and their hosts. *Phys. Rev. E*, 82:011918, Jul 2010.

[196] Kolter R., Balaban N., and Julou T. Bacteria grow swiftly and live thriftily. *Current Biology*, 32(12):R599–R605, 2022.

[197] Meeske A.J., Nakandakari-Higa S., and Marraffini L.A. Cas13-induced cellular dormancy prevents the rise of CRISPR-resistant bacteriophage. *Nature*, 2019.

[198] Brown S., Mitarai N., and Sneppen K. Protection of bacteriophage-sensitive Escherichia coli by lysogens. *Proceedings of the National Academy of Sciences*, 119(14):e2106005119, 2022.

[199] Schwartz M. and Le Minor L. Occurrence of the bacteriophage lambda receptor in some enterobacteriaceae. *J Virol*, 15(4):679–685, Apr 1975.

[200] Oddershede L., Dreyer J.K., Grego S., Brown S., and Berg-Sørensen K. The motion of a single molecule, the lambda-receptor, in the bacterial outer membrane. *Biophys J*, 83(6):3152–3161, Dec 2002.

[201] Winther T., Xu L., Berg-Sørensen K., Brown S., and Oddershede L.B. Effect of energy metabolism on protein motility in the bacterial outer membrane. *Biophys J*, 97(5):1305–1312, Sep 2 2009.

[202] Bæk K.T., Svenningsen S.L., Eisen H., Sneppen K., and Brown S. Single-cell Analysis of ? Immunity Regulation. *Journal of Molecular Biology*, 2003.